NATIONAL ADVISORY COMMITTEE FOR AERONAUTICS

TECHNICAL NOTE 3456

PROPAGATION OF A FREE FLAME IN A TURBULENT GAS STREAM

By William R. Mickelsen and Norman E. Ernstein

Lewis Flight Propulsion Laboratory
Cleveland, Ohio

Washington
July 1955

TABLE OF CONTENTS

NATIONAL ADVISORY COMMITTEE FOR AERONAUTICS

TECHNICAL NOTE 3456

PROPAGATION OF A FREE FLAME IN A TURBULENT GAS STREAM

By William R. Mickelsen and Norman E. Ernstein

SUMMARY

Effective flame speeds of free turbulent flames were measured by photographic, ionization-gap, and photomultiplier tube methods and were found to have a statistical distribution attributed to the nature of the turbulent field. The effective turbulent flame speeds for the free flame were less than those previously measured for flames stabilized on nozzle burners, Bunsen burners, and bluff bodies. The statistical spread of the effective turbulent flame speeds was markedly wider in the lean and rich fuel-air-ratio regions, which might be attributed to the greater sensitivity of laminar flame speed to flame temperature in those regions. Values calculated from the turbulent free-flame-speed analysis proposed by Tucker and the Scurlock-Grover analysis of turbulent flame propagation apparently form upper limits for the statistical spread of free-flame-speed data. Hot-wire anemometer measurements of the longitudinal velocity fluctuation intensity and longitudinal correlation coefficient were made and were employed in the comparison of data and in the theoretical calculation of turbulent flame speed.

INTRODUCTION

The high volumetric heat-release rate required in present-day and future jet-engine combustors has placed an ever-growing emphasis on turbulent combustion research. The theory of turbulent flame propagation is as yet in a formative stage, partly because of the lack of reliable experimental methods for determining the effect of turbulence on the rate of flame propagation. The purpose of the present investigation was to explore a new experimental method believed to approximate more nearly a theoretical, or ideal, flame model than previous methods.

The major portion of experimental data on turbulent flame speeds has been taken in open flames stabilized on Bunsen burners (refs. 1 to 3) or on Mache type burners (refs. 4 and 5). A substantial amount of experimental data has also been obtained from flames confined in a duct

and stabilized on bluff bodies (refs. 6 to 8). Another experimental method consists of measuring the speed of a flame advancing into a turbulent fuel-air mixture flowing through a tube (ref. 9). In general, the definition of turbulent flame speed used in these methods is that given in reference 8:

$$S_T = U \frac{A_a}{\bar{A}} \tag{1}$$

(All symbols are defined in appendix A.) Equation (1) has been used for local measurements by the flame-front angle method and for over-all flame-speed measurements by the flame-area method. These two methods are shown in the following sketches:

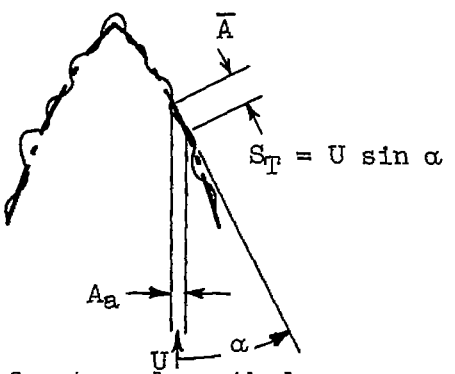

Flame-front angle method

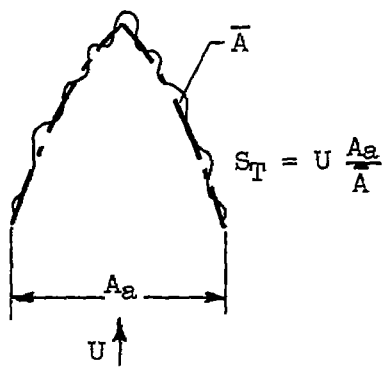

Flame-area method

Turbulent-flame-speed values obtained by these methods may be significantly affected by conditions external to the flame-front proper, such as:

(1) Large fluctuations in instantaneous flame-front position which introduce uncertainty in the determination of mean position in long-time-exposure photographs of stabilized flames (ref. 10)

(2) Existence of "piloting zones" at the rims of Bunsen burners, immediately downstream of bluff bodies, or in the boundary layer of flame tubes which may affect the burning rate of the flames near such zones (refs. 7 and 10)

(3) Large velocity differences between unburned and burned gas flows which may introduce considerable turbulence in stabilized flames (refs. 2, 6, 7, and 11)

(4) Curvature of unburned-gas streamlines at the flame front which may introduce substantial error in flame speeds measured in stabilized flames by the angle method (refs. 7 and 12)

(5) Variations in local flame speeds along the flame envelope which may introduce substantial error in average flame speeds measured by the flame-area method

The objective of this investigation was to determine the effect of turbulence on the growth of a free flame. It was thought that the free flame would not be subject to the complicating conditions present in stabilized flames such as those listed. In addition, the free-flame growth could take place entirely in a homogeneous, isotropic, turbulent field away from boundary layers and bluff-body wakes, thus providing a more nearly fundamental flame model.

The method used in the present investigation is an extension of the "soap-bubble" technique (ref. 13) and consists of the observation of the growth of a free-flame globule as it is carried downstream in a flowing, turbulent, homogeneous mixture of gaseous fuel and air. The flame globule was initiated by a single spark, and its growth was recorded by three separate methods: high-speed motion picture photography, ionization-gap probes, and photomultiplier tube signals.

The flame-globule growth was characterized by an effective turbulent flame speed S_T, which is defined by a mass-balance equation similar to that derived in reference 13:

$$S_T = \frac{\rho_F}{\rho_a} \frac{dr}{dt} \tag{2}$$

Equation (2) can be clarified by the following sketch:

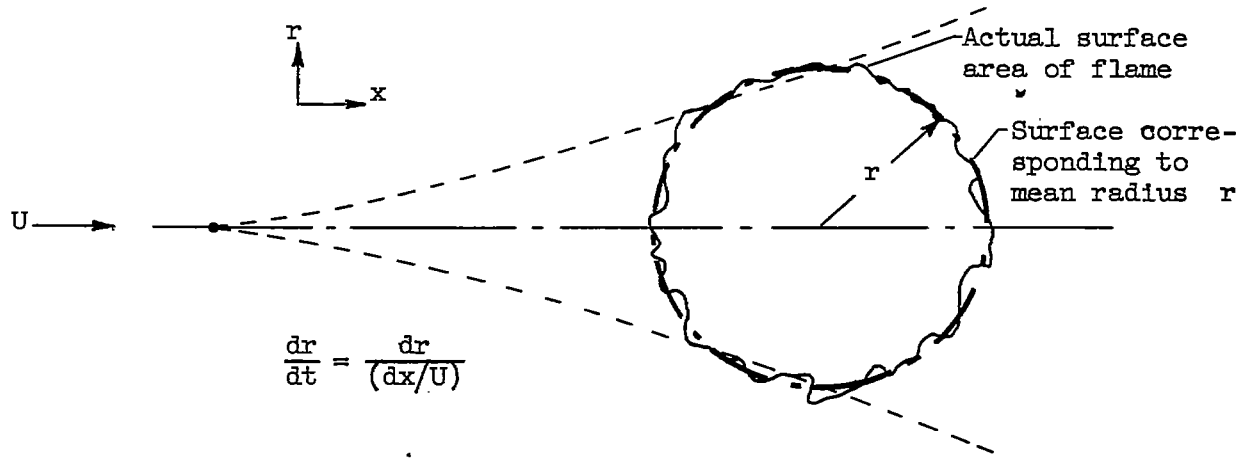

The rate of change of the globule radius was measured over times less than the characteristic time of the turbulence. This means that, on the average, the flame front traveled through less than one turbulent eddy

during the time of observation. In the past, average turbulent flame speeds have generally been measured from photographs having long exposure times compared with the characteristic time of the turbulence.

The experimental work was carried out in two phases. The first phase was initiated and carried out at the NACA Lewis laboratory and is reported in reference 14. (Because of its limited circulation, considerable portions of the work reported in ref. 14 are included in this report.) Turbulent flame-speed measurements were obtained from high-speed motion picture records of the growth of the free-flame globule as it was swept downstream in an enclosed tunnel. The turbulent field was introduced by means of a wire grid placed at the tunnel inlet some distance upstream of the spark-electrode position. The turbulent field was characterized by hot-wire anemometer measurements.

The effective turbulent flame speeds determined by the photographic method varied for runs made under identical fuel-air and mean stream conditions. The variation was concluded to be due to the statistical nature of the turbulent field. Statistical analysis of groups of 30 or more runs made at identical fuel-air and mean stream conditions showed that the data for each group approximated a normal probability distribution. When plotted on the basis of cumulative probability of occurrence, the effective turbulent flame-speed data showed a consistent increase with increasing turbulence intensity.

The second phase of the investigation was carried out in a free jet with a technique whereby the cumulative probability of occurrence of turbulent flame speed could be determined from flame groups consisting of thousands of separate flame globules. This technique utilized ionization-gap probes and counters, which indicated directly the percentage of flames reaching or exceeding any given diameter at a series of stations downstream of the spark electrodes. By this method, flame speeds were measured over a range of fuel-air weight ratios from 0.053 to 0.090 and a range of mean stream velocities from 35 to 142 feet per second at a stream static pressure of 1 atmosphere and a stream static temperature of 85° F. The stream turbulence was varied by the use of three interchangeable grids, and the parameters of the turbulence were measured with constant-temperature hot-wire-anemometer instrumentation.

The investigation was carried out at the Lewis Flight Propulsion Laboratory as a part of the combustion research program.

APPARATUS

Air-Ducting, Wind-Tunnel, and Air-Flow Instrumentation

The air-ducting, wind-tunnel, and air-flow instrumentation used in the first phase of the investigation and reported in reference 14 is shown in figure 1(a). Alterations made to the apparatus for the second phase of the investigation are shown in figure 1(b). The alterations essentially converted the system from an enclosed tunnel to a free jet.

Air supplied from the laboratory air facility was metered with a standard variable-area orifice and controlled with the butterfly and gate valves shown in figure 1. Static pressures and temperatures were measured with conventional manometers and thermocouples.

The ducting approach to the tunnel was designed from principles used in conventional low-turbulence wind tunnels. The transition section was followed by a honeycomb and turbulence-damping screen in the calming section to reduce the turbulence present in the air-supply flow. The entrance to the enclosed tunnel (or free jet) was a nozzle with a contraction ratio of 20, and provisions were made at the tunnel throat for the insertion of turbulence-producing grids. Three grids were used for the investigation, all having a mesh-to-wire diameter ratio of 5. The grid wire diameters were 0.0313, 0.063, and 0.125 inch.

The enclosed-tunnel installation was equipped with an adjustable plug and nozzle by which critical flow could be maintained at the tunnel exit, so that the tunnel flow field could be isolated from pressure disturbances in the laboratory exhaust facility. The free-jet installation was equipped with an exhaust hood into which diluting room air could be drawn in addition to the free-jet flow.

Fuel System

The propane fuel used throughout the investigation had the following composition by liquid volume:

Propane, percent	97.76
Ethane, percent	1.72
Isobutane, percent	.51

The propane fuel system is shown in figure 2 and was identical for both the enclosed-tunnel and free-jet installations. Propane was supplied from a laboratory facility and metered with standard rotameters. Pressure, temperature, and flow controls are shown in figure 2. The propane

was injected into the air stream through a grid having 60 equally spaced 0.040-inch-diameter holes. The injection grid was installed at a station upstream of the calming chamber as shown in figure 1.

Ignition System

The flame-globule ignition system consisted of a pair of spark electrodes protruding into the tunnel stream from opposing walls and an electrical energy source. The spark electrodes used in the enclosed tunnel were carefully streamlined to a fineness ratio of 5 with a thickness tapering from 0.019 inch at the tunnel center to 0.038 inch at the tunnel wall. The spark electrodes used in the free-jet installation were of circular cross section with a diameter tapering from 0.015 inch at the stub tunnel center to 0.075 inch at the stub tunnel wall. The spark-gap spacing was 0.015 and 0.030 inch for the enclosed-tunnel and free-jet installations, respectively. The spark-electrode positions for the two installations are shown in figure 1.

The spark-energy source was of the capacitive type and produced single sparks synchronized with the camera operation in the enclosed-tunnel installation or successive sparks at three per second in the free-jet installation. The spark energy could be varied by changing capacitors.

Flow-Field Instrumentation

In general, the flow-field instrumentation was adaptable to point measurements in either the enclosed-tunnel or free-jet streams. Mean-stream-velocity measurements were made with a conventional pitot-static probe and micromanometer. Fuel-air ratio was measured directly by a mixture analyzer. Stream samples were drawn through a sharp-edged 0.125-inch-inside-diameter sampling probe to the analyzer, which indicated fuel-air ratio directly by the thermal-conductivity-bridge method.

Turbulence measurements were made with constant-temperature hot-wire-anemometer equipment, which is described in appendix B. Sound-pressure levels were measured with a conventional microphone and a sound-pressure-level meter, also described in appendix B.

Free-Flame-Growth Measurement

Photographic instrumentation. - The growth of the free-flame globule was recorded photographically in the enclosed-tunnel installation with the optical system shown in figure 3. The photographic records were

taken with a 16-millimeter Fastax camera operated at approximately 3600 frames per second and located at the end point of the parallel-beam schlieren system. The enclosed-tunnel windows were striation-free plate glass. The light source was a mercury-vapor BH-6 lamp operated with a high-voltage direct-current power supply.

Ionization-gap instrumentation. - The growth of the free-flame globule was measured in the free-jet installation with an ionization-gap probe, a photomultiplier flame sensing unit, and two flame counters. The physical orientation of these instrumentation components is shown in figures 4(a) and (b). The photomultiplier unit and its accompanying flame counter recorded the total number of flames that occurred during any particular run. The ionization-gap probe and its accompanying flame counter recorded the number of flames that grew to a radius of r or greater at the axial station x during any particular run.

The photomultiplier unit consisted of a 931A photomultiplier vacuum tube with a fixed-plate voltage supply. The ionization-gap probe is shown in detail in figures 4(c) and (d). The brass fairing along the probe tip prevented flame seating on the probe both by flame quenching and by elimination of the recirculation zone. Because of the convoluted form of each flame globule, the voltage signal from the ionization gap usually contained multiple peaks, which caused spurious counts in the flame counter. In order to smooth these peaks, resistors, capacitors, and diodes were included in the 360-volt direct-current battery circuit for the ionization gap.

In order to prevent spurious counts arising from small fluctuations in the voltage signal from both the photomultiplier unit and the ionization-gap probe, a long time constant was included in the flame-counter design. These flame counters employed thyratron-controlled relays and solenoids which actuated a mechanical counter. They were designed by C. C. Conger of the Lewis laboratory.

Photomultiplier instrumentation. - Simultaneous measurements of the spark light intensity and ensuing free-flame-globule growth were made in the free-jet installation with the photomultiplier instrumentation shown in figure 5. The photomultiplier unit consisted of a 931A photomultiplier tube with an adjustable-plate voltage supply. Light emitted from the spark and ensuing flame passed through the narrow slit to the photomultiplier unit. The voltage signal from the photomultiplier unit was recorded on 35-millimeter film from an oscilloscope trace. The photomultiplier instrumentation and the assumption required to relate output voltage to flame speed are discussed in appendix C.

PROCEDURE

The test schedule was as follows:

Grid size, in.		Stream velocity, U, ft/sec	Propane-air weight ratio	Distance downstream of grid, x, in.
Wire diam.	Mesh			
Free jet				
0.125	0.625	35 to 105	0.07	15.2 to 16.2
.125	.625	70	.056 to .090	15.2 to 16.2
.063	.313	70	.058 to .084	15.2 to 16.2
.0313	.156	70	.053 to .084	15.2 to 16.2
Enclosed tunnel				
0.125	0.625	35 to 140	0.045 (approx.)	6.3 to 15.3

Enclosed-Tunnel Installation

Room air was supplied to the enclosed tunnel and exhausted at critical flow condition through an exit choke by means of the altitude exhaust facility. Tunnel static pressures and temperatures were measured by manometers and thermocouple rakes as shown in figure 1(a). Fuel was injected into the air stream and metered through a standard rotameter, after which dilution air was admitted downstream of the choke. The tunnel stream velocity was then measured with a pitot-static probe and micromanometer.

The sequential schlieren photographs of the propagation of the free-flame globule in the fuel-air mixture were obtained by actuating a single switch which synchronized the following operations: fuel shut-off (producing a semi-infinite fuel slug); camera start; ignition by a single spark; and camera stop after an appropriate interval.

Free-Jet Installation

An exhaust air-flow rate of approximately 500 pounds per minute was initiated, and dilution air was admitted to the hood. Laboratory pressurized air and propane were admitted into the stub tunnel, after which the fuel-air ratio was adjusted to the desired value by means of a probe and the NACA mixture analyzer; the stream velocity was determined from pitot-tube measurements.

The ionization-gap probe was positioned at a station x downstream of the spark electrodes and at a radial distance r from the tunnel centerline. A series of flame globules was initiated by the ignition system, firing at the rate of three sparks per second. The number of flame globules N_p intercepting the ionization-gap probe and the total number of flame globules ignited N_t were read from instrumentation shown in figure 4(b).

FLOW-FIELD MEASUREMENTS

In order to check the uniformity of the flow field, velocity profiles were measured in both the enclosed-tunnel and free-jet installations. The mean stream velocity for both installations was essentially constant over the core of interest, as shown by figure 6. Similar measurements were made to check the uniformity of the propane-air ratio in both installations. The propane-air ratio was found to be constant over the major portion of the enclosed-tunnel flow field, and typical profiles measured in the free-jet installation are shown in figure 7.

In order to establish the characteristics of the turbulent field, extensive measurements of the turbulence intensity $\sqrt{u^2}$, the spectrum function F, and the correlation coefficient f were made in both the enclosed-tunnel and the free-jet installations. The definitions of these quantities and the instrumentation used to measure them are discussed in appendix B.

Enclosed-Tunnel Turbulence Measurements

Longitudinal turbulence intensity measurements made in the enclosed-tunnel installation are shown in figure 8. The data shown in the figure agree well with the von Kármán data quoted in reference 15 and show a substantial decrease in turbulence intensity from the electrode position ($x/d = 50$) to the end of the flame-growth observation field ($x/d = 122$). Longitudinal intensity profiles measured in the tunnel center plane perpendicular to the observation plane were essentially flat over the core of interest. Turbulent energy spectra were measured in the enclosed-tunnel installation as described in appendix B. The scale of turbulence was estimated by comparison of experimental data with a grid of spectrum density curves based on an exponential form of the longitudinal correlation coefficient $f = \exp(\xi/L_f)$. A typical measured spectrum is shown in figure 9, and the estimated turbulence scales are listed in table I.

Free-Jet Turbulence Measurements

Conversion of the enclosed tunnel to a free jet resulted in an intense sound field originating in the dilution air and exhaust hood and piping. As described in reference 16, velocity fluctuations associated with sound waves contribute to the hot-wire anemometer measurements through the relation

$$\sqrt{\overline{u^2}} = \sqrt{\overline{u_T^2} + \overline{u_s^2}} \qquad (3)$$

with the assumption that no correlation exists between the turbulence and sound velocity fluctuations. In order to determine the applicability of equation (3) in the free jet, longitudinal velocity fluctuation intensities were measured both with and without the intense sound field. These measurements are shown in figure 10 for each of the three turbulence grids used in the investigation. The velocity fluctuation intensity was definitely increased with the presence of the sound field for each of the three turbulence-generating grids.

The sound-pressure level in the free jet was measured with the instrumentation described in appendix B and was found to be 136 decibels, which corresponds to a sound-velocity fluctuation $\sqrt{\overline{u_s^2}}$ of 0.96 foot per second. Values of the sound-velocity fluctuation $\sqrt{\overline{u_s^2}}$ were also calculated from the data of figure 10 by the use of equation (3). These values of $\sqrt{\overline{u_s^2}}$ are compared in table II with the value of $\sqrt{\overline{u_s^2}}$ corresponding to the sound-pressure level of 136 decibels; good agreement is shown in every case.

The kinetic-energy spectrum of the sound field alone is shown in figure 11; it has a generally continuous form with peaks, or periodicities, at 57, 110, 140, 170, 230 to 285, 600 to 870, 1050, 1500, 2400, 3000, 4000 to 5600, and 7000 to 9000 cycles per second. Periodicities observed in the sound spectrum were generally found again in the longitudinal velocity fluctuation energy spectra measured in the free-jet installation, as shown by the typical spectrum in figure 12.

Longitudinal double-velocity correlation coefficients f measured in the free-jet installation are shown in figure 13 for each of the three turbulence-producing grids. The irregular form of the correlation-coefficient curves is attributed to the periodic nature of a considerable portion of the velocity fluctuations. The correlation coefficients were measured by the special methods described in appendix B and are defined by the relation

$$f = \frac{\overline{u_o u_\xi}}{\overline{u^2}} \tag{4}$$

where the symbols are defined by the following vector diagram:

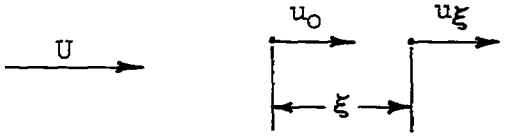

The longitudinal turbulence scale is usually defined by the relation

$$L_f = \int_0^\infty f \, d\xi \tag{5}$$

Because of the periodic nature of the combined turbulence and sound fields, the longitudinal correlation coefficient did not approach zero within the range of measurement. Therefore, equation (5) could not be used to define the turbulence scale. Since the growth of the flame globule was observed over times comparable with $\xi = 0.1$ inch, only the first portions of the correlation curves shown in figure 13 were considered relevant to the experiment. As a part of the calculations involved in the Scurlock-Grover analysis, values of the lateral scale of turbulence L_g were calculated as described in appendix D. These calculated values of L_g are listed in the table included in the RESULTS section of the text.

DETERMINATION OF FLAME SPEED

Fundamental Considerations

The relation between flame speed and free-flame globule-expansion rate is derived in reference 13 for a constant-pressure laminar free flame propagating in a quiescent fuel-air mixture. This relation was obtained by equating the mass flow of the unburned gases entering a flame front of infinitesmal thickness to the mass flow of the burned gases leaving the flame front. In a physical sense, the following equation accounts for both the flame-front motion due to flame propagation and the motion due to thermal expansion of the burned gases:

$$S_T = \frac{\rho_F}{\rho_a} \frac{dr}{dt} \tag{2}$$

The following modification of this equation to account for a finite flame-front thickness δ has been presented in reference 14:

$$S_T = \frac{\rho_F}{\rho_a} \frac{dr}{dt} \left(\frac{r - \delta/2}{r + \delta/2} \right)^2 \tag{6}$$

For this investigation, the thickness of the flame front was considered negligible compared with the radius r so that equation (2) was used to analyze the data. The values of ρ_a, computed from R_a and T_a, were obtained from measurements of tunnel approach-stream flow. The values of ρ_F, computed from R_F and T_F for each fuel-air ratio, were taken from references 17 and 18, respectively. The value of ρ_F/ρ_a varied from 0.12 to 0.14 in the present investigation.

A number of assumptions are necessary to the definition of effective turbulent flame speed as given by equation (2). The definition requires that

(1) The free-flame globule grow uniformly in all radial directions

(2) The combustion proceed in a constant pressure field

(3) The flame globule be swept downstream at the stream velocity

(4) No circumferential flow exist about the flame globule

(5) Variations in spark energy not affect the globule propagation rate

The validity of the assumptions was established by special tests described later in this section.

Photographic Method

Photographic data obtained in the enclosed tunnel were analyzed by projecting the 16-millimeter motion picture film record of each flame-globule expansion onto a film viewer. A typical photographic record is shown in figure 14(a). The outline of each globule was traced in order to permit planimetering its area and calculating a mean radius. The mean radius was plotted against time for each flame globule of the sequence, as shown in figure 14(b). The slope of a straight line faired through such a series of experimental points is dr/dt. The effective turbulent flame speed was then calculated by multiplying dr/dt by the expansion factor ρ_F/ρ_a as shown in equation (2).

From sets of 30 or more flame speeds obtained in this manner for identical fuel-air-flow conditions, the cumulative probability of occurrence of flames having these flame speeds was calculated. In order to illustrate the statistical nature of these data, the turbulent flame speeds of a typical set of data have been plotted against cumulative probability of occurrence in figure 14(c). Each data point represents the effective flame speed of a single free flame. Cumulative probability of occurrence is defined as the percentage of flames having flame speeds greater than a given value.

Ionization-Gap Method

In order to obtain a set of turbulent flame speeds for a particular condition of turbulent approach-stream intensity and fuel-air ratio in the free-jet installation, the ionization-gap probe was positioned consecutively at two stations $x = 15.2$ and 16.2 inches, as outlined diagrammatically in figure 15. For each chosen position r, at least 1000 flames N_t were ignited. The ionization-gap counter recorded the number of flames N_p intercepting the probe. The ratio N_p/N_t was the cumulative probability of a flame globule having a radius at least as great as that indicated by the probe setting r. The ratio N_p/N_t was then plotted on probability coordinates against r and a curve was faired through each of the two sets of data as shown in figure 16. The difference Δr was obtained from the curves for the cumulative probabilities of 2, 20, 50, 80, and 98 percent. Equation (2) was then employed to determine the flame speeds corresponding to the five probability percentages.

Photomultiplier Method

The photomultiplier method was used to obtain values proportional to the effective flame speed. The method essentially consists of measuring the free-flame globule-growth rate along the axial diameter of the globule. The method is described in the APPARATUS section and in appendix C. The instrumentation is shown in figure 5.

Verification of Experimental Method

The discussion of equation (2) in a preceding section included a number of assumptions necessary to the derivation of the equation. Since equation (2) essentially expresses the experimental method used in the investigation, the assumptions were verified by tests that are described in the following paragraphs.

Uniformity of globule growth. - Photographic data of the flame-globule growth in the enclosed tunnel were analyzed to determine whether the globules had preferential growth directions. This analysis was made by measuring globule diameters (see fig. 17) at four angles of rotation from the tunnel axis. While each globule had different growth rates along the four diameters, no consistent relation between growth rate and direction was found. This observation supports the use of a mean radius in the photographic method of flame-speed measurement, the use of a single radial direction in the ionization-gap method, and the use of a single diameter in the photomultiplier method of flame-growth observation.

Pressure pulsations. - In order to determine whether the fluctuations in flame-globule-growth rates, illustrated by figure 14(b), were due to pressure fluctuations in the enclosed tunnel, data as shown in figure 17 were inspected for possible phase relations between the fluctuations in growth rate along the four diametral directions. Since no frequency-phase relation was found from these data, it was concluded that pressure fluctuations were not responsible for the fluctuations in globule-growth rate. Additional measurements with a wall-mounted pressure pickup indicated the absence of significant pressure pulsations in the enclosed tunnel.

Axial velocity of flame globule. - The effect of buoyancy of the hot flame globule on its axial velocity was determined by measuring the distance from the spark electrodes to the globule center on each frame of photographic sequences such as shown in figure 14(a). The axial velocities calculated from such measurements agreed closely in all cases with the measured stream velocity, which indicated that the buoyancy effect was negligible.

Unburned-gas motion. - As shown by equation (2), the rate of thermal expansion of the flame globule is from 7 to 8 times as great as the effective turbulent flame speed. In order to determine whether the unburned-gas motion caused by this thermal expansion was purely radial (from the globule center), simultaneous oscillograph records were made in the free-jet installation with the ionization-gap probe and a shielded hot-wire anemometer probe as shown by the typical oscillograph and probe position diagram in figure 18. The ionization-gap trace indicated the flame-globule passage, and the anemometer trace was proportional to the instantaneous stream velocity. Inspection of 60 such records indicated no axial change in mean stream velocity and therefore no circumferential flow of unburned gases about the sphere. The marked decrease in amplitude of velocity fluctuations at the time of flame-globule passage is interpreted as being due to the radial translation of the free-jet stream core by the thermal expansion of the flame globule.

Effect of spark energy. - In order to determine the effect of spark energy on the flame-globule growth, two series of runs were made in the free-jet installation under identical stream and fuel conditions but with spark source energies differing by a factor of 2.5. As shown in figure 19, cumulative probabilities of flame-globule sizes were measured at a series of axial positions with the ionization-gap instrumentation for the two spark source capacitors of 0.0004 and 0.0010 microfarads. The data of figure 19 show an increase in initial flame-globule size, but no change in turbulent flame speed between the axial positions $x = 15.2$ and 16.2 inches.

Effect of spark light intensity. - Additional information on the relation between the spark characteristics and the flame-globule growth was obtained with the photomultiplier instrumentation shown in figure 5. With this instrumentation, oscillographs were obtained in a free-jet installation showing spark light intensity and flame light intensity as a function of time for 151 consecutive flame globules at constant mean stream and fuel conditions. Typical oscillographs obtained by this method are shown in figure 20. As shown in appendix C, the portion of the trace due to the spark light intensity was proportional to spark current, and statistical analysis of the magnitudes of the peak spark light intensity indicated that this parameter approximated a normal probability distribution. The flame speed of the globule was taken as proportional to the slope of the portion of the oscillograph trace due to flame light intensity, as discussed in appendix C.

The group of 151 consecutive runs are shown in figure 21, in which peak spark light intensity is plotted against flame speed for each particular flame globule. The statistical correlation coefficient for this data was determined with Pearson's product moment formula (ref. 19) and was found to have an absolute value of $|0.17|$ for a possible range of zero to $|1.0|$. The low value of the statistical correlation coefficient is interpreted to indicate that variations in spark current had no effect on turbulent flame speed.

Additional verification of statistical variation of turbulent flame propagation. - The cumulative probability of occurrence of slopes measured from the series of 151 photomultiplier oscillographs is shown in figure 22. The statistical distribution of flame speeds measured by this method is interpreted as additional proof of the randomness of the phenomena.

Validity of common origin assumption. - The ionization-gap method, described earlier in this section, assumes that all flame globules have a common origin point, as shown in figure 15. In order to determine the error introduced by this assumption, "origin points" were measured from the series of 151 photomultiplier traces by

extrapolating the slope of the flame light intensity trace to the time axis, as shown in figure 20. The origin points showed a statistical deviation in position, and the theoretical error introduced into flame speeds determined by the ionization-gap method was calculated to be ±2.5 percent or less, within one standard deviation of origin position. The error in flame speed due to shift in origin point is small compared with the deviations in flame speed actually measured by the photographic (fig. 14(c)), the ionization-gap, and the photomultiplier tube methods (fig. 22).

Precision of Data

Ionization-gap measurements. - Each data point plotted as cumulative probability against flame radius, such as shown in figure 16, represents information from at least 1000 flames. As shown in reference 20, samples consisting of 1000 flames would have the following accuracy in the cumulative probability value:

Cumulative probability, percent	Possible error, percent
50	±5
20	±7
2	±29

The possible errors listed correspond to 1.28 standard deviations of the error distribution and therefore should hold 80 percent of the time. The general consistency of the data throughout the lower probability region such as shown in figure 16 seems to justify greater confidence in the low cumulative probability range than that shown in the preceding table.

The reliability of the curves faired through the plotted experimental data, such as presented in figure 16, may be estimated from the deviation of data points from the fitted curves.

The greatest divergence was found in results for the 0.125-inch-diameter screen. For the 98-percent probability level, the maximum data scatter from a faired curve was 20 percent; for the 50-percent level, 7.8 percent; and for the 2-percent level, 3 percent. The maximum scatter for the 0.063-inch-diameter screen was 5.3 percent at 98-percent probability, and for the 0.0313-inch-diameter screen, it was 13 percent at the 98-percent level.

As discussed earlier in this section, the value of flame temperature used in the equation for turbulent flame speed was a calculated theoretical value. It may be of interest to note that flame temperature has a much greater effect on the laminar flame speed than on the calculation leading to effective turbulent flame speed. As shown by reference 21, a decrease of theoretical adiabatic flame temperature from 4000° to 3900° R would result in a laminar flame speed decrease of 43 percent. In contrast, this change in flame temperature would cause only a 2.5-percent decrease in the turbulent flame speed calculated from the equation

$$S_T = \frac{\rho_F}{\rho_a} \frac{dr}{dt} \tag{2}$$

It appears, then, for the purpose of this investigation, that the effect of a small error in actual flame temperature is negligible in calculating the density ratio.

Other sources of inaccuracy may be found in the instrumentation and equipment. The positioning of the ionization-gap probe involved an error not exceeding 0.5 percent. Measurement of the fuel-air ratio was accurate within 2 percent. Flow measurements were made with a precision of 3 percent. For the measurements characterizing the turbulence parameters, an estimated value of ±5 percent is suggested for the probable limit of error.

Photomultiplier method. - A treatment of the sources of error present in flame-speed measurement by the photomultiplier method is presented in appendix C.

Photographic method. - In addition to the errors introduced by the equipment and instrumentation, sources of error peculiar to the photographic method must be considered. Such factors as adjustment of the projected image to one-to-one correspondence, timing, optical resolution, and scale factor are all considered significant and have been thoroughly treated in reference 22, which assigns a relative maximum error of 10 percent to the photographic-reduction technique.

RESULTS

Effective turbulent flame speeds were measured in the enclosed-tunnel and free-jet installations over a range of propane-air and turbulence conditions as shown in the following table:

Grid size, in.		Stream velocity, U, ft/sec	Longitudinal velocity fluctuation intensity, $\sqrt{\overline{u^2}}$, ft/sec	Lateral turbulence scale, L_g, in.	Propane-air weight ratio	Distance downstream of grid, x, in.
Diam.	Mesh					
Free jet						
0.125	0.625	35 to 105	1.18 to 2.60	0.0645	0.07	15.2 to 16.2
.125	.625	70	1.69	.0645	.056 to .09	15.2 to 16.2
.063	.313	70	1.34	.0587	.058 to .084	15.2 to 16.2
.0313	.156	70	1.17	.0437	.053 to .084	15.2 to 16.2
Enclosed tunnel						
0.125	0.625	35 to 140	0.81 to 3.51	0.08 to 0.13	0.045 (approx.)	6.3 to 15.3

The lateral turbulence scales L_g for the enclosed tunnel were obtained from the values of L_f shown in table I by using equation (B7) of appendix B. The values of L_g for the free jet were obtained by fitting an exponential curve to the lateral correlation coefficient g as described in appendix D. Both methods for evaluation of L_g are based on the assumption of isotropy, which was not proven because of the lack of turbulence measurements in the lateral direction.

The effective turbulent flame speeds, plotted in figure 23, were measured in the free-jet installation at a fixed propane-air ratio of 0.07 over a range of mean stream velocities with the 0.125-inch wire diameter by 0.625-inch mesh turbulence-generating grid. The data are plotted as a function of longitudinal velocity fluctuation intensity $\sqrt{\overline{u^2}}$ with cumulative probability as a parameter. Since turbulence measurements were made at only one stream velocity, and since the sound-pressure level was independent of stream velocity, the data of table II and the following equation were employed to calculate the longitudinal velocity fluctuation intensity:

$$\sqrt{\overline{u^2}} = \sqrt{\left[U\left(\frac{\sqrt{\overline{u_T^2}}}{U}\right)\right] + \overline{u_s^2}} \qquad (7)$$

3637

The turbulence intensity $\left(\sqrt{\overline{u_T^2}}/U\right)$ was assumed constant throughout the range of stream velocity U (see ref. 15), and $\overline{u_s^2}$ corresponded to the measured sound-pressure level of 136 decibels.

Effective turbulent flame speeds measured in the enclosed-tunnel installation at a fixed propane-air ratio of approximately 0.045 are plotted in figure 24 as a function of the longitudinal velocity fluctuation intensity $\sqrt{\overline{u^2}}$ with cumulative probability as a parameter. The data show a consistent increase of effective turbulent flame speed with velocity fluctuation intensity. These data were obtained downstream of the 0.125-inch wire diameter by 0.625-inch mesh grid over a range of stream velocities from 30 to 140 feet per second. As shown by the data of figure 8, the decay of the turbulence intensity was quite severe over the range of interest (x/d = 50 to 122). A turbulence intensity of $\left(\sqrt{\overline{u_T^2}}/U\right) = 0.027$ was taken as a representative value and assumed constant to obtain values of $\sqrt{\overline{u^2}}$ over the stream-velocity range.

The effects of propane-air ratio and turbulence scale on the propagation rate of the free flame were investigated in the free-jet installation by measuring the turbulent flame speed downstream of the three turbulence-generating grids over a range of propane-air ratio from 0.053 to 0.090. (The variations in turbulence scale are listed in the table at the beginning of this section.) These data are shown in figure 25 along with a dashed line representing laminar flame-speed data reported in reference 21. Turbulent flame speeds from the enclosed tunnel are included in figure 25(a) and were evaluated by interpolating the data of figure 24 at a velocity fluctuation intensity equal to that of the free-jet data in figure 25(a).

DISCUSSION

Measurements of Present Investigation

A discussion of the effect of turbulence on flame propagation is generally conceded to rest on the principles of turbulent motion set forth by Taylor in reference 23. These principles are summarized in the equation relating the mean displacement X of a fluid particle from its original position to two parameters of the turbulent field:

$$D = \frac{1}{2}\frac{\overline{dX^2}}{dt} = \overline{u^2}\int_0^t \mathscr{R}\, dt \qquad (8)$$

where D is the turbulent diffusion coefficient in the x-direction, X is the particle displacement in the x-direction, and $\mathscr{R}$ is the Lagrangian double-velocity correlation coefficient defined by the relation

$$\mathscr{R} = \frac{\overline{u_o u_t}}{\sqrt{\overline{u_o^2}}\sqrt{\overline{u_t^2}}} \tag{9}$$

It is of particular importance to note that the turbulence parameters in equation (8) are both mean values, and that instantaneous, local particle displacements depend on the statistical deviations about those mean values. It is suggested that the fluid particle displacements have a statistical distribution about the mean much the same as the statistical variation of velocity fluctuations in the turbulence. Such variations in particle displacements would be particularly noticeable when observed over times less than the characteristic time of the turbulence, as is the case in the present investigation.

A statistical variation in the particle displacement X would probably cause variations in the speed of flames where flame wrinkling was controlling; a statistical distribution of the turbulent diffusion coefficient D would also probably cause variations in the flame speed where the diffusion process affects turbulent flame propagation. As a consequence of this statistical distribution of turbulence velocity and correlation coefficients, particular free flames might encounter conditions especially favorable and therefore have high propagation rates, while others might be subjected to conditions that would reduce their rate of growth. This picture of statistical variation is consistent with the data of the present investigation shown in figures 23 to 25 and also agrees with observations of stabilized flames that show a wide brush of flame fronts.

The effect of flame temperature on laminar flame speed has been reported in references 21 and 24, wherein it is shown that small changes in flame temperature result in large changes in laminar flame speed. In particular, reference 24 shows that this dependence of laminar flame speed on flame temperature is of greater magnitude in the lean and rich regions. The lower portions of the flame-speed probability band in figure 25 generally show decreases in the ratio of the turbulent to the laminar flame speed S_T/S_L in the lean and rich fuel-air regions. This decrease is consistent with the effect of flame temperature if the lower portion of the probability band is considered to represent flames that have encountered turbulent conditions sufficiently violent to decrease the flame temperature by diffusive action.

Comparison of figures 25(a), (b), and (c) shows that greater portions of the flame-speed band fall below the laminar flame speed as the grid size becomes smaller. As shown by figure 13, decreases in the grid size reduce the mean turbulent eddy size. Since the effect of the turbulence is thought to be increasingly diffusive in character as the turbulence scale decreases, this trend might be due to an increasing proportion of flames having temperatures less than the adiabatic value as the turbulence scale becomes smaller.

Comparison with Data from Other Investigations

A comparison of the data of the present investigation with those of references 4, 8, 9, and 22 is presented in figure 26. In order to obtain a basis for comparison, the data are plotted with the ratio of turbulent to laminar flame speed S_T/S_L against longitudinal velocity fluctuation intensity $\sqrt{\overline{u^2}}$. The turbulent flame speeds measured in a Mache (nozzle) type burner (ref. 4), a Bunsen burner (ref. 8), and a flame tube (ref. 9) fall above those measured by the free-flame method in references 14 and 22 and in the present investigation. It should be noted that the S_T/S_L data from the present investigation are plotted against the longitudinal velocity fluctuation intensity, which includes the contributions from both turbulence and sound. A better agreement with the data of other investigations could be obtained by plotting the ratio S_T/S_L against the velocity fluctuation intensity $\sqrt{\overline{u_T^2}}$ due to turbulence alone. This procedure is questionable, since the sound-velocity fluctuations may have an appreciable effect on turbulent flame speed when coupled with turbulence, and also because the magnitude of the sound field in the other investigations is unknown. The abscissas of figure 26 may be converted to turbulence intensity by the use of equation (3) and the data of table II.

The effect of fuel-air ratio on turbulent flame speed of free flames is shown in figure 27, in which the data from the free-flame experiment reported in reference 22 are compared with those of the present investigation. The data from the present investigation shown in figure 27 were taken 15.2 to 16.2 inches downstream of the 0.125-inch wire diameter by 0.625-inch mesh grid, while the data from reference 22 were taken 14 to 18 inches downstream of a 0.125-inch wire diameter by 0.500-inch mesh grid. The grid sizes and axial distances are close enough so that the turbulence scales were roughly equal. Because of a large difference in stream velocity, the two sets of data were taken under widely different velocity fluctuation intensities. Both sets of data show a general trend of decreasing turbulent to laminar flame-speed ratio in the lean and rich fuel-air-ratio regions. The considerable

deviation from mean values exhibited by the data of reference 22 substantiates the statistical deviation of turbulent flame speed noted in the present investigation.

Comparison of Data with Various Theories

The current prevailing concept of turbulent flame propagation is based on references 25 and 26, wherein the proposals are made that (1) small-scale turbulence (of the order of the flame-front thickness) increases the local flame propagation rate because of increased diffusion rates, and (2) large-scale turbulence increases the over-all flame propagation rate by wrinkling the flame with attendant increased flame-front area. Although it is well known that a turbulent field contains a statistical distribution of "eddy sizes," the complexity of the problem has dictated the assumption of either the large- or small-scale case.

The basic concept proposed by Shelkin (ref. 26) for the large-scale case is that the wrinkling of the flame front might be approximated by cones having a base proportional to the turbulence scale and a height proportional to the turbulence intensity. This concept has been supported experimentally by Hottel and coworkers in reference 1.

Turbulent flame speeds measured in flames stabilized on bluff bodies in high-velocity fuel-air streams led Scurlock and coworkers to postulate the concept of flame-generated turbulence (refs. 6 and 7). Theoretical analyses to account for flame-generated turbulence were proposed by Karlovitz and coworkers (ref. 2) and by Scurlock and Grover (ref. 11), but neither analysis conforms to all existing experimental data. A recent analysis by Tucker (ref. 27) predicts that little, if any, turbulence would be generated by free flames with small surface deformations.

Since the Shelkin equation is not only of historical interest but is also used as a basis for the Scurlock-Grover theory, the data of the present investigation are compared with the Shelkin equation in figure 28, wherein the ratio S_T/S_L is plotted as a function of longitudinal velocity fluctuation intensity for four cumulative probabilities. The data include flame speeds measured with each of the three turbulence-generating grids and are all for the constant fuel-air weight ratio of 0.07 (figs. 23 and 25). The Shelkin equation was correlated with the data at each value of cumulative probability by the method of least squares. This correlation was accomplished by determining the constant B in the Shelkin equation as follows:

$$\frac{S_T}{S_L} = \left(1 + B \frac{\overline{u^2}}{S_L^2}\right)^{1/2} \tag{10}$$

3637

The value of the constant B was estimated to be unity by Shelkin but varies from 0.867 for the cumulative probability of 2 percent to 0.220 for the cumulative probability of 80 percent. The value of the constant B is shown in figure 28 for each of the cumulative probabilities. The data scatter about the Shelkin equation but show some agreement with the Shelkin theory. A curve plotted through the data obtained with the 0.125-inch grid does not follow the shape of the Shelkin curve, however.

The theoretical expression for turbulent flame speed presented by Tucker in reference 27 was obtained by a wave analysis of the effect of a low-intensity turbulent field on an infinitesmally thin flame front having convolutions, or wrinkles, of low slope. The final equation shows no effect of turbulence correlation coefficient and is, in the present notation,

$$\frac{S_T}{S_L} = 1 + C(\tau)\frac{\overline{u^2}}{S_L^2} \tag{11}$$

where $C(\tau)$ is a function of the ratio $\tau = T_F/T_a$. The analysis includes the assumption that the second-order terms $(\overline{u^2}/S_L^2)^2$ are negligible, that the flame temperature and laminar flame speed are dependent only on fuel-air ratio, and that the diffusive action of turbulence is negligible.

In order to obtain a comparison with the present data, the Tucker analysis was extrapolated well beyond its intended limit of the ratio $(\overline{u^2}/S_L)$. The data of the present investigation compare well with the Tucker analysis in the low velocity fluctuation intensity region as shown in figure 29, but falls below the theory in the higher intensity range, where the theory cannot be expected to hold. A further comparison of the turbulent flame-speed data with the Tucker analysis is made in figure 30, wherein the ratio S_T/S_L is plotted against fuel-air weight ratio. These data are for each of the three turbulence-generating grids and were taken at the same mean stream velocity. The data in each figure fall below the theory, but, with the exception of the enclosed-tunnel data (fig. 30(a), fuel-air ratio, 0.045), follow the general trend of the Tucker analysis in the upper portion of the cumulative probability band. These data suggest that the analysis might be taken as the limiting value of turbulent flame speed for the turbulence conditions specified in the figures.

The turbulent flame-speed data are also compared with the Scurlock-Grover analysis (ref. 11) in figures 29 and 30. This analysis assumes that the flames proceed locally at the laminar rate S_L, but that the

over-all flame speed S_T is increased because of flame-front wrinkling caused by turbulence. The geometrical model is similar to Shelkin's, except that the wrinkle height is assumed to be positively affected by turbulent motion and negatively affected by local flame propagation. The analysis also accounts for flame-generated turbulence caused by velocity and density gradients across the flame front.

Flame-generated turbulence has been neglected in a modified Scurlock-Grover analysis, which was used in the present investigation and is discussed in appendix D. The measured correlation coefficients, as shown in figure 13, were used in the analysis, in contrast to the exponential forms assumed in the Scurlock-Grover report (ref. 11) and the comparison with free-flame data made in reference 22. The analysis predicted that the turbulent flame speed had not yet reached its full value at the axial stations of measurement (x = 15.2 and 16.2 in.). Therefore, values of S_T/S_L were calculated from the theory for flame-growth times corresponding to both stations and are shown in figures 29 and 30.

The data of the present investigation fall below the values of S_T/S_L predicted by the modified Scurlock-Grover analysis but follow the theory fairly well in the upper portion of the probability band. The data follow the Scurlock-Grover analysis more closely for the largest turbulence scale (fig. 30(a)), and the agreement becomes progressively worse as the turbulence scale becomes smaller (figs. 30(b) and (c)). This type of relation may be due to an increasing diffusive action of the turbulence as the scale becomes smaller, as discussed previously in this section.

The data agree more closely with the Scurlock-Grover analysis than with the Tucker theory in the lean and rich fuel-air-ratio regions. This probably is due to the increasing $\sqrt{\overline{u^2}}/S_L$ in those regions that tend to exceed the limits of the assumptions made in the Tucker analysis discussed in a preceding paragraph.

In summary, values from both the Tucker and the Scurlock-Grover analyses seem to form an upper limit to the data of the present investigation.

CONCLUSIONS

From the results of the investigation, the following conclusions are made:

1. The propagation rate of a free flame in a turbulent field with intense random sound-velocity fluctuations is a statistical variable having a probability of occurrence band bounded by a zero propagation rate and possibly an upper propagation rate well above the laminar flame speed.

2. The propagation rate of a free turbulent flame is substantially less than those previously measured for stabilized flames.

3. The statistical spread of free-flame propagation rates is markedly wider in both the lean and rich fuel-air-ratio regions.

4. Values calculated from the Tucker analysis for free-flame propagation rates apparently form an upper limit for the statistical spread of free-flame propagation rates in the regions where the velocity fluctuation intensity is low.

5. Values calculated from the modified Scurlock-Grover analysis apparently form an upper limit for the statistical spread of free-flame propagation rate.

Lewis Flight Propulsion Laboratory
National Advisory Committee for Aeronautics
Cleveland, Ohio, April 25, 1955

APPENDIX A

SYMBOLS

The following symbols are used in this report:

A	cross-sectional area
$\overline{A}$	smoothed time-average surface area of turbulent flame
a	local speed of sound, ft/sec
B	constant in Shelkin equation
C	constant
D	turbulent diffusion coefficient, sq ft/sec
d	wire diameter of turbulence-producing grid, in.
$\overline{E}$	d-c voltage, v
$\sqrt{\overline{E^2}}$	rms of a-c complex wave voltage, v
F	longitudinal energy spectrum density function, sec
f	longitudinal double-velocity correlation coefficient
g	lateral double-velocity correlation coefficient
i	hot-wire current at stream conditions, amp
K	gain of decade amplifier
L_f	longitudinal scale of turbulence, in.
L_g	lateral scale of turbulence, in.
$\mathscr{L}$	Lagrangian scale of turbulence, in.
N	number of flame globules
n	frequency, cps
R	gas constant
$\mathscr{R}$	Lagrangian double-velocity correlation coefficient

r	radial distance from tunnel axis, in.
S	flame speed, ft/sec
SPL	sound-pressure level, db
T	temperature, ^{o}R
t	time, sec
U	mean stream velocity, ft/sec
u	longitudinal velocity fluctuation, ft/sec
v,w	lateral velocity fluctuations, ft/sec
X	fluid particle displacement due to turbulent motion, ft
x	distance downstream of turbulence-producing grid, in.
y	distance from tunnel wall, in.
α	angle, deg
β	power band width of wave analyzer, cps
δ	flame-front thickness, ft
ξ	spatial separation of velocity vectors comprising correlation coefficient, in.
ρ	density, lb/cu ft
σ	one standard deviation
τ	ratio of flame temperature to unburned gas temperature, T_F/T_a
φ	equivalence ratio, (fuel-air ratio)/(stoichiometric fuel-air ratio)
Ω	hot-wire resistance at stream conditions, ohms

Subscripts:

a	ambient, or approach stream
F	flame
f	pertaining to correlation coefficient f

g	pertaining to correlation coefficient g
L	laminar
n	pertaining to a frequency interval
o	no-flow condition in anemometry, or reference point in space or time double-velocity correlation coefficients
P	pertaining to number of flames of a given radius or greater
s	sound
T	turbulent
t	total, or time
ξ	at a distance ξ from zero position

APPENDIX B

TURBULENCE AND SOUND INSTRUMENTATION AND ANALYSIS

Theoretical Background

Turbulent fields are generally defined by the two parameters intensity and correlation coefficient. The turbulence intensity is defined as the rms value of the turbulent velocity fluctuations $\sqrt{\overline{u^2}}$, $\sqrt{\overline{v^2}}$, and $\sqrt{\overline{w^2}}$. The double-velocity correlation coefficient may be represented by a second-order tensor which for a homogeneous, isotropic field of turbulence can be reduced to two components as shown in reference 28. These two components are the longitudinal and lateral double-velocity correlation coefficients defined as follows:

Longitudinal: $$f = \frac{\overline{u_o u_\xi}}{\overline{u^2}} \qquad \text{(B1)}$$

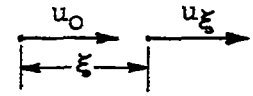

Lateral: $$g = \frac{\overline{v_o v_\xi}}{\overline{v^2}} \qquad \text{(B2)}$$

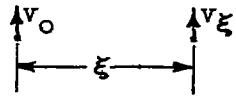

where f and g are the longitudinal and the lateral correlation coefficients, respectively, u is turbulent velocity fluctuation, ξ is the spatial separation between the points of measurement of the u, and the bar signifies a long time average.

Longitudinal and lateral turbulence scales have been defined by the relations

$$L_f = \int_0^\infty f \, d\xi \qquad \text{(B3)}$$

$$L_g = \int_0^\infty g \, d\xi \qquad \text{(B4)}$$

These scales are intended to represent a mean turbulent eddy size, and for homogeneous, isotropic turbulence may be related through the equation (ref. 28)

$$f + \frac{\xi}{2}\frac{\partial f}{\partial \xi} = g \qquad \text{(B5)}$$

which, by integration, becomes

$$L_f + \frac{1}{2}\int_0^\infty \xi \frac{\partial f}{\partial \xi}\, d\xi = L_g \tag{B6}$$

For the commonly observed exponential form of $f = \exp\left(\frac{\xi}{L_f}\right)$, equation (B6) becomes

$$L_f = 2L_g \tag{B7}$$

Taylor has shown in reference 29 that the one-dimensional turbulence energy spectral density function F is the Fourier transform of the longitudinal correlation coefficient f:

$$f = \int_0^\infty F \cos \frac{2\pi n x}{U}\, dn \tag{B8}$$

where F is defined by the relations

$$\overline{u^2} = \int_0^\infty \overline{u_n^2}\, F\, dn \tag{B9}$$

and

$$\int_0^\infty F\, dn = 1 \tag{B10}$$

where $\overline{u^2}$ represents the total kinetic energy in longitudinal direction, and $\overline{u_n^2}$ represents the kinetic energy contained in the frequency interval n to $n + dn$.

Hot-Wire Anemometry

The constant-temperature hot-wire anemometry equipment is shown diagrammatically in figure 31, and for the most part has been described in references 16 and 30. The equation relating the rms voltage $\sqrt{\overline{E_t^2}}$ measured by the average square computer to the turbulence intensity has been discussed in reference 16 and is as follows:

$$\sqrt{\overline{u^2}} = \frac{4iU}{(2K)\,\Omega\,(i^2 - i_o^2)}\sqrt{\overline{E_t^2}} \tag{B11}$$

The spectrum density function F was measured from the tape-recorder play-back signal by the following equation which is given in reference 16:

$$F = \frac{\overline{E_n^2}}{\beta \overline{E_t^2}} \tag{B12}$$

where $\overline{E_n^2}$ is the square of the rms voltage reading of the wave analyzer.

The double-velocity correlation coefficient f was determined from a double-channel magnetic tape recording of the instantaneous voltage signal from the hot-wire anemometer. The double-channel tape was played back into a double correlation computer which electronically performed the instantaneous multiplication of velocity fluctuations indicated in equation (B1). The variable separation ξ between velocity vectors was attained by the use of a movable and a fixed play-back head. The separation ξ between the velocity vectors was equal to the separation between the heads multiplied by the ratio of the stream velocity to the tape speed. The double correlation computer was designed by D. F. Berg and C. C. Conger of the Lewis laboratory. The equivalence of the correlation coefficient measured by this method and by the two-probe method was proven as a part of a research program conducted by J. C. Laurence of the Lewis laboratory.

Sound-Field Instrumentation

The sound instrumentation consisted of a standard microphone and sound-level meter from which sound-pressure level could be determined. The microphone signal was also impressed on the wave analyzer to obtain the sound kinetic energy spectrum through equation (B12). The relation between sound-pressure level SPL and sound-velocity fluctuations $\sqrt{\overline{u_s^2}}$ has been given in reference 31 (for simple harmonic waves) as

$$SPL = 20 \log \left(\rho_a \sqrt{\overline{u_s^2}} \right) + 74 \tag{B13}$$

APPENDIX C

PHOTOMULTIPLIER INSTRUMENTATION

Relation Between Flame Light Intensity and Flame Speed

Assumptions. - The conditions assumed in relating flame light intensity as indicated by the voltage output of a photomultiplier tube to the surface area of a flame are treated in reference 32. They may be summarized as follows: 3637

(1) It is postulated that, if a point source of light is increased to a finite size but the distance from the light source to the detector is constant and large in comparison with the maximum dimension of the flame, the light flux impinging on the detector will obey the inverse square law. Under this condition, a change in the surface area of the flame will produce an approximately linear change in the flux intensity registered by the detector.

(2) The flame must consist of a homogeneous cloud of nonabsorbing emitters.

If the propagation of a free-flame globule moving in a gas stream at stream velocity is observed by a detector through a long slit placed axially with respect to globule travel, some additional requirements are:

(3) The detector has an essentially flat light response over the entire field of view.

(4) The slit is narrow enough in relation to flame-globule diameter to approximate a diameter of the projected spheroid.

(5) The flame-globule center must not suffer any appreciable radial displacement from the tunnel centerline.

(6) The flame globule must not have a preferential growth direction.

(7) The flame temperature must be constant for all the flame globules.

Conditions (1) and (4) were met by suitable placement and dimensioning of the apparatus. For condition (3), it was determined that the photomultiplier unit had a maximum light response error of 5 percent over the total light acceptance angle. Photographic evidence obtained in the preliminary phase of the investigation indicated satisfactory fulfillment of requirements (5) and (6). Assumption (7) has been previously treated in the section of the DISCUSSION entitled Measurements of Present Investigation.

Description of apparatus. - A 931A type photomultiplier having an adjustable-plate voltage power supply was mounted in a light-tight box behind a 0.25-inch-diameter aperture. This detector unit was positioned in an enclosed tunnel 4 feet from the free-jet stub tunnel, as shown in figure 5. The detector aperture was centrally located with respect to the slit in the machined aluminum plate, which replaced an upper portion of one wall of the stub tunnel. The voltage output of the photomultiplier was amplified and fed to an oscilloscope. Oscillograms were taken by high-speed, continuous motion picture technique.

Oscillograms. - As shown in figure 20, the oscillograph trace of the ignition and growth of a single flame consists of two portions, a spark light amplitude decay curve and a flame light amplitude growth curve whose slope at any point is equal to the change of diameter of the flame globule with time, governed by the considerations listed previously. This slope $2dr/dt$ is proportional to turbulent flame speed S_T as given by equation (2).

Relation Between Spark Light Intensity and Spark Current

Standring and Looms (ref. 33), using short-duration sparks produced by a lightly damped oscillatory current, have shown that the light emitted by a given spark gap depends on the current in the gap and its time variation.

In order to determine the effect of a long-duration, direct-current pulsed spark on the current - spark light relation, an auxiliary investigation was undertaken in collaboration with Clyde C. Swett, Jr. The spark production and recording apparatus is fully described in reference 34. The photomultiplier detector apparatus was as described previously except that the detector unit was mounted at one end of a rectangular tube 2 feet in length. The field of view of the photomultiplier tube was limited by a 0.0625- by 2-inch aperture in the other end of the tube. A Polaroid Land camera was used to make oscillograms.

A series of oscillograms was taken of sparks ignited in still air and in an air stream having a velocity of 50 feet per second. Spark duration was about 600 microseconds, spark energy was of the order of 17 millijoules, and peak spark current approximated 0.23 amperes. A comparison of spark light amplitude-time curves with the current-time curves obtained in the apparatus designed by Swett showed a marked similarity of shape between the sets. It was concluded from this information that, at least for a first-order approximation, spark light intensity was roughly proportional to spark current.

APPENDIX D

CALCULATION OF FLAME SPEED FROM SCURLOCK-GROVER ANALYSIS

The basic equation in the Scurlock-Grover theory (ref. 11) is obtained by assuming that the increase of flame speed is due to the wrinkling of the flame front in the form of right circular cones, so that

$$\frac{S_T}{S_L} = \frac{A_T}{A_L} = \left[1 + C_1 \left(\frac{\overline{X^2}}{L_g^2}\right)\right]^{1/2} \tag{D1}$$

where $\sqrt{\overline{X^2}/L_g^2}$ is assumed proportional to the ratio of cone height to base diameter and C_1 is a constant taken equal to 4. The mean square particle displacement is assumed to depend on three effects:

(1) Turbulent mixing, which increases the flame-front area

(2) Laminar flame propagation, which decreases the flame-front area

(3) Flame-generated turbulence, which increases the turbulent mixing

The first effect on $\overline{X^2}$ is given by

$$\frac{\overline{dX_T^2}}{dt} = 2\,\overline{u^2} \int_0^t \mathscr{R}\, g_t\, dt \tag{D2}$$

where $\mathscr{R}$ is the Lagrangian correlation coefficient and g_t is the Eulerian correlation coefficient. The second effect is given by

$$\frac{d\sqrt{\overline{X_L^2}}}{dt} = C_2\, S_L \left\{\left[1 + C_1 \left(\frac{\overline{X_T^2}}{L_g^2}\right)\right]^{1/2} - 1\right\} \tag{D3}$$

where C_2 is a constant taken equal to 1/4. The combination of the first two effects is then

$$\frac{d\sqrt{\overline{X^2}}}{dt} = \frac{1}{2\sqrt{\overline{X_T^2}}} \frac{d\,\overline{X_T^2}}{dt} - \frac{d\sqrt{\overline{X_L^2}}}{dt} \tag{D4}$$

Since the Lagrangian correlation coefficient cannot be measured directly, Scurlock and Grover assumed it to be of the form given in reference 15:

$$\mathscr{R} = \exp\left(-\frac{\sqrt{\overline{u^2}}\,t}{\mathscr{L}}\right) \tag{D5}$$

where $\mathscr{L}$ is the Lagrangian scale of turbulence and was assumed to be equal to $1/2\ L_g$. In the present analysis, $\mathscr{R}$ was assumed to be equal to f, through the independent variable transformation $\xi = \sqrt{\overline{u^2}}\,t$. Isotropy was assumed, so that g was obtained from f through the relation (ref. 28)

$$g = f + \frac{\xi}{2}\frac{df}{d\xi} \tag{D6}$$

The correlation coefficient g_t was then obtained from the independent variable transformation $\xi = S_L t$. The turbulence scale L_g was calculated by matching the curve $\exp(\xi/L_g)$ to the g plot previously calculated from f by equation (D6).

All integrations and differentiations were done graphically, and the calculation procedure followed the following order:

(1) Calculate g from equation (D6).

(2) Transform $f(\xi)$ to $\mathscr{R}(\xi/\sqrt{\overline{u^2}})$.

(3) Transform $g(\xi)$ to $g_t(\xi/S_L)$.

(4) Calculate

$$\frac{d\,\overline{X_T^2}}{dt} = 2\,\overline{u^2}\int_0^t \mathscr{R}\,g_t\,dt$$

(5) Calculate

$$\overline{X_T^2} = \left[\int_0^t \left(\frac{\overline{dX_T^2}}{dt}\right)dt\right]^{1/2}$$

(6) Calculate

$$\frac{d\sqrt{\overline{X_L^2}}}{dt} = \frac{S_L}{4}\left\{\left[1 + 4\left(\frac{\sqrt{\overline{X_T^2}}}{L_g}\right)^2\right]^{1/2} - 1\right\}$$

(7) Calculate

$$\frac{d\sqrt{\overline{X^2}}}{dt} = \frac{1}{2\sqrt{\overline{X_T^2}}} \frac{d\,\overline{X_T^2}}{dt} - \frac{d\sqrt{\overline{X_L^2}}}{dt}$$

(8) Calculate

$$\sqrt{\overline{X^2}} = \int_0^\infty \left(\frac{d\sqrt{\overline{X^2}}}{dt}\right) dt$$

(9) Calculate

$$\frac{S_T}{S_L} = \frac{A_T}{A_L} = \left[1 + 4\left(\frac{\overline{X^2}}{L_g^2}\right)\right]^{\frac{1}{2}}$$

As mentioned in the DISCUSSION section, flame-generated turbulence has been assumed negligible, and the final form of the Scurlock-Grover theoretical equation was as given above.

REFERENCES

1. Hottel, H. C., Williams, G. C., and Levine, R. S.: The Influence of Isotropic Turbulence on Flame Propagation. Fourth Symposium (International) on Combustion, The Williams & Wilkins Co. (Baltimore), 1953, pp. 636-644.

2. Karlovitz, Béla, Denniston, D. W., Jr., and Wells, F. E.: Investigation of Turbulent Flames. Jour. Chem. Phys., vol. 19, no. 5, May 1951, pp. 541-547.

3. Bollinger, Lowell M., and Williams, David T.: Effect of Reynolds Number in Turbulent-Flow Range of Flame Speeds of Bunsen-Burner Flames. NACA Rep. 932, 1949. (Supersedes NACA TN 1707.)

4. Wright, F. H.: Measurements of Flame Speed and Turbulence in a Small Burner. Prog. Rep. No. 3-21, Jet Prop. Lab., C.I.T., June 6, 1950.

5. Bowditch, F. W.: Some Effects of Turbulence on Combustion. Fourth Symposium (International) on Combustion, The Williams & Wilkins Co. (Baltimore), 1953, pp. 674-682.

6. Scurlock, A. C.: Flame Stabilization and Propagation in High-Velocity Gas Streams. Meteor Rep. 19, Fuels Res. Lab., M.I.T., May 1948. (Contract NOrd 9661.)

7. Williams, G. C., Hottel, H. C., and Scurlock, A. C.: Flame Stabilization and Propagation in High Velocity Gas Streams. Third Symposium on Combustion and Flame and Explosion Phenomena, The Williams & Wilkins Co. (Baltimore), 1949, pp. 21-40.

8. Wohl, Kurt, Shore, L., von Rosenberg, H., and Weil, C. W.: The Burning Velocity of Turbulent Flames. Fourth Symposium (International) on Combustion, The Williams & Wilkins Co. (Baltimore), 1953, pp. 620-635.

9. Leason, D. B.: Turbulence and Flame Propagation in Premixed Gases. Fuel, vol. XXX, no. 10, Oct. 1951, pp. 233-238; discussion, pp. 238-239.

10. Caldwell, Frank R., Ruegg, Fillmer W., and Olsen, Lief D.: Combustion in Moving Air. Paper presented at meeting SAE and Air Transport, (New York City), Apr. 13-15, 1948.

11. Scurlock, A. C., and Grover, J. H.: Propagation of Turbulent Flames. Fourth Symposium (International) on Combustion, The Williams & Wilkins Co. (Baltimore), 1953, pp. 645-658.

12. Ball, George A.: Combustion Aerodynamics - A Study of a Two-Dimensional Flame. Dept. Eng. Sci. and Appl. Phys., Harvard Univ., July 1951. (Army Ord. Dept. Contract W19-020-ORD-6509.)

13. Stevens, F. W.: A Constant Pressure Bomb. NACA Rep. 176, 1923.

14. Mickelsen, William R.: The Propagation of a Free Flame Through a Turbulent Gas Stream. M. S. Thesis, Case Inst. Tech., 1953.

15. Dryden, Hugh L.: A Review of the Statistical Theory of Turbulence. Quart. of Appl. Math., vol. 1, no. 1, Apr. 1943, pp. 7-42.

16. Mickelsen, William R., and Laurence, James C.: Measurement and Analysis of Turbulent Flow Containing Periodic Flow Fluctuations. NACA RM E53F19, 1953.

17. Hottel, H. C., Williams, G. C., and Satterfield, C. N.: Thermodynamic Charts for Combustion Processes, Pt. II. John Wiley & Sons, Inc., 1949.

18. Anon.: Annual Program Report. Proj. Squid, U.S. Navy, U.S. Army, Jan. 1, 1949.

19. Worthing, Archie G., and Geffner, Joseph: Treatment of Experimental Data. John Wiley & Sons, Inc., 1943, p. 275.

20. Lusser, Robert: A Study of Methods for Achieving Reliability of Guided Missiles. Tech. Rep. No. 75, U.S. Naval Air Missile Test Center, July 10, 1950.

21. Dugger, Gordon L.: Effect of Initial Mixture Temperature on Flame Speed of Methane-Air, Propane-Air, and Ethylene-Air Mixtures. NACA Rep. 1061, 1952. (Supersedes NACA TN's 2170 and 2374.)

22. Bolz, R. E., and Burlage, H., Jr.: The Influence of Turbulence on Flame Propagation Rates. (To be published in Jet Prop.)

23. Taylor, G. I.: Diffusion by Continuous Movements. Proc. London Math. Soc., vol. 20, 1922, pp. 196-212.

24. Botha, J. P., and Spalding, D. B.: The Laminar Flame Speed of Propane/Air Mixtures with Heat Extraction from the Flame. Proc. Roy. Soc. (London), ser. A, vol. 225, no. 1160, Aug. 6, 1954, pp. 71-95.

25. Damköhler, Gerhard: The Effect of Turbulence on the Flame Velocity in Gas Mixtures. NACA TM 1112, 1947.

26. Shelkin, K. I.: On Combustion in a Turbulent Flow. NACA TM 1110, 1947.

27. Tucker, Maurice: Interaction of a Free Flame Front with a Turbulence Field. NACA TN 3407, 1955.

28. von Kármán, Theodore, and Howarth, Leslie: On the Statistical Theory of Isotropic Turbulence. Proc. Roy. Soc. (London), ser. A, vol. 164, Jan. 21, 1938, pp. 192-215.

29. Taylor, G. I.: The Spectrum of Turbulence. Proc. Roy. Soc. (London), ser. A, vol. 164, Feb. 18, 1938, pp. 476-490.

30. Laurence, James C., and Landes, L. Gene: Auxiliary Equipment and Techniques for Adapting the Constant-Temperature Hot-Wire Anemometer to Specific Problems in Air-Flow Measurements. NACA TN 2843, 1952.

31. Morse, Philip M.: Vibration and Sound. Second ed., McGraw-Hill Book Co., Inc., 1948.

32. Clark, Thomas P., and Bittker, David A.: A Study of the Radiation from Laminar and Turbulent Open Propane-Air Flames as a Function of Flame Area, Equivalence Ratio, and Fuel Flow Rate. NACA RM E54F29, 1954.

33. Standring, W. G., and Looms, J. S. T.: Light Output from a Spark "Point Source". Nature, vol. 165, no. 4192, Mar. 4, 1950, p. 358.

34. Swett, Clyde C., Jr.: Effect of Gas Stream Parameters on the Energy and Power Dissipated in a Spark and on Ignition. Third Symposium on Combustion and Flame and Explosion Phenomena, The Williams & Wilkins Co. (Baltimore), 1949, pp. 353-361.

TABLE I. - SUMMARY OF LONGITUDINAL TURBULENCE SCALES

[Estimated from longitudinal energy spectra in enclosed-tunnel installation. Mean stream velocity, 50 ft/sec; static pressure, 26 in. Hg abs; static temperature, 540° R. Comparative values calculated through the isotropic turbulence relation $L_f = 2L_g$ from lateral scale of turbulence data reported in ref. 15.]

Distance downstream of grid, x, in.	Longitudinal scale of turbulence, L_f, in.	
	Present investigation	Ref. 15
6.3	0.16	----
9.3	.21	----
12.3	.25	0.17
15.3	.25	.21

TABLE II. - COMPARISON OF VELOCITY FLUCTUATIONS IN TURBULENT STREAM WITH AND WITHOUT INTENSE SOUND FIELD

[Velocity fluctuations measured along duct axis. Measured value of sound-pressure level, 136 db; stream velocity, 68.5 ft/sec.]

Grid size, in.		Distance downstream of turbulence-producing grid, x, in.	Stream velocity fluctuations, ft/sec		Calculated values of sound field		Measured values of sound field	
Diam.	Mesh.		With sound field, $\sqrt{\overline{u^2}}$	Without sound field, $\sqrt{\overline{u_T^2}}$	$\sqrt{\overline{u_s^2}} = \sqrt{\overline{u^2} - \overline{u_T^2}}$, ft/sec	Sound-pressure level, db	$\sqrt{\overline{u^2}}$, ft/sec	Sound-pressure level, db
0.125	0.625	3	1.81	1.40	1.15	137.5	0.96	136
		4	1.75	1.32	1.15	137.5	.96	136
0.063	0.313	3	1.32	0.926	0.94	135.5	0.96	136
		4	1.41	.892	1.10	137.0	.96	136
0.0313	0.156	3	1.12	0.688	0.89	135.0	0.96	136
		4	1.22	.619	1.05	136.5	.96	136

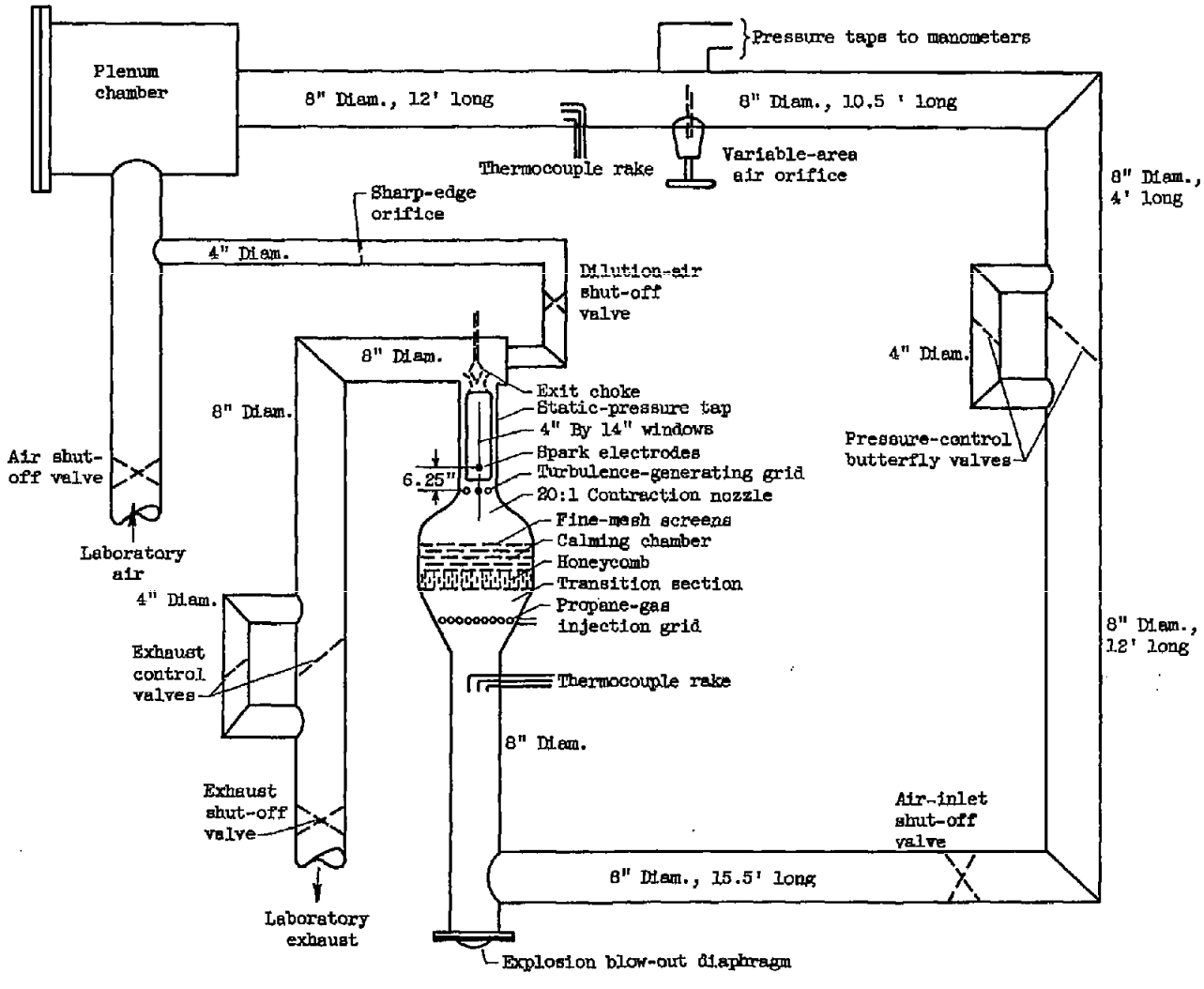

(a) Enclosed-tunnel installation.

Figure 1. - Air-ducting, wind-tunnel, and mean air-flow instrumentation.

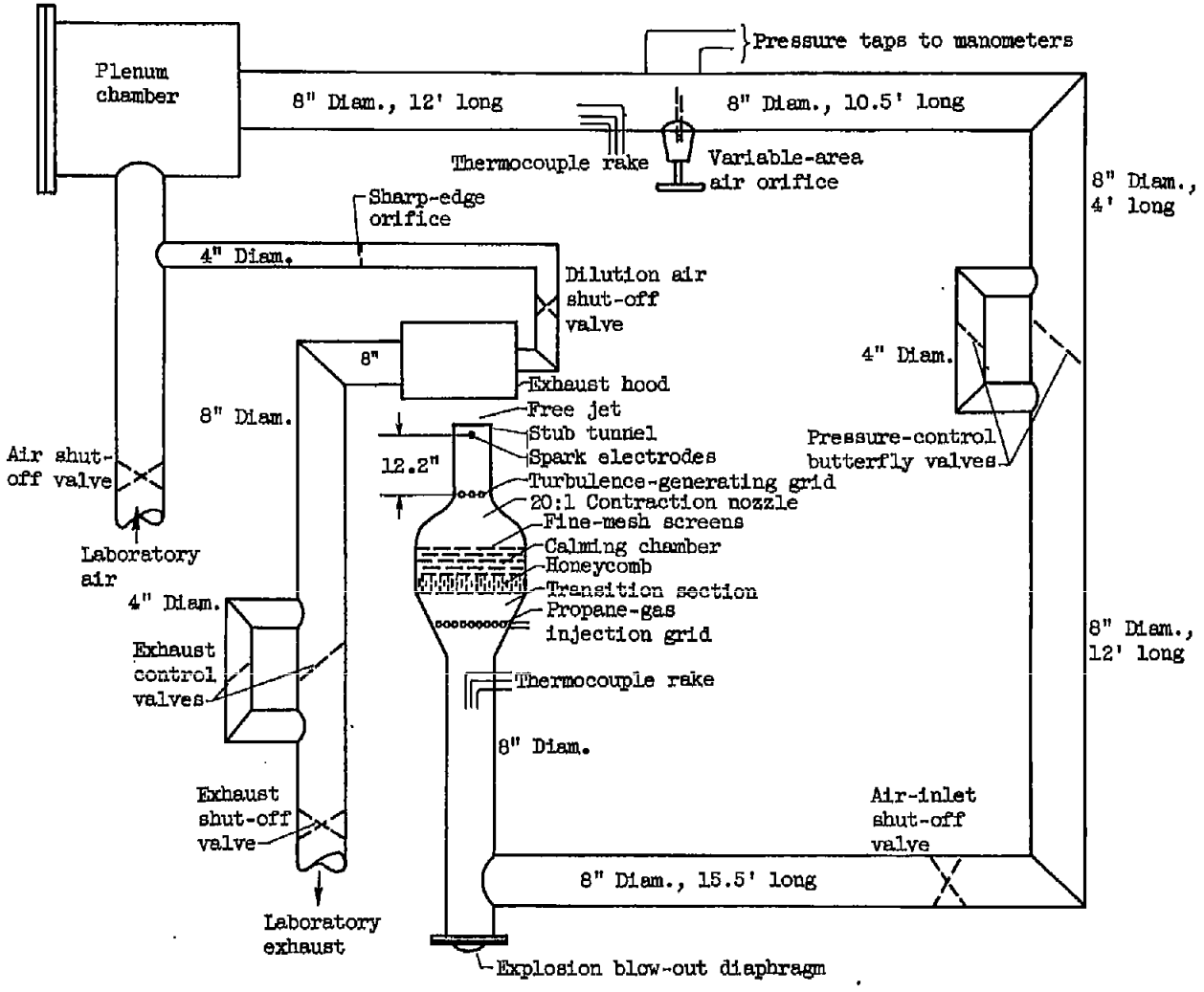

(b) Free-jet installation.

Figure 1. - Concluded. Air-ducting, wind-tunnel, and mean air-flow instrumentation.

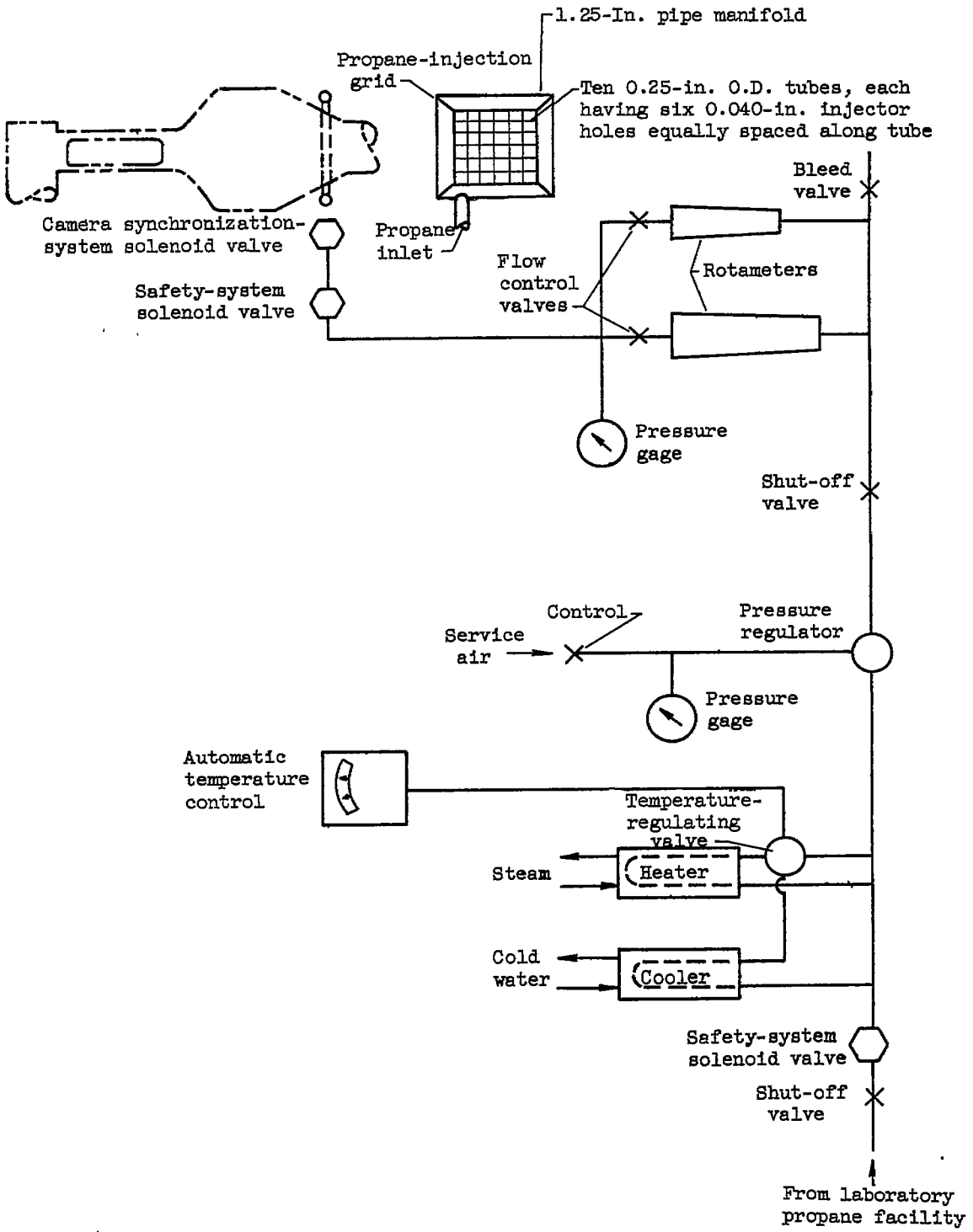

Figure 2. - Fuel system.

Figure 3. - Photographic instrumentation for measurement of free-flame growth in enclosed-tunnel installation.

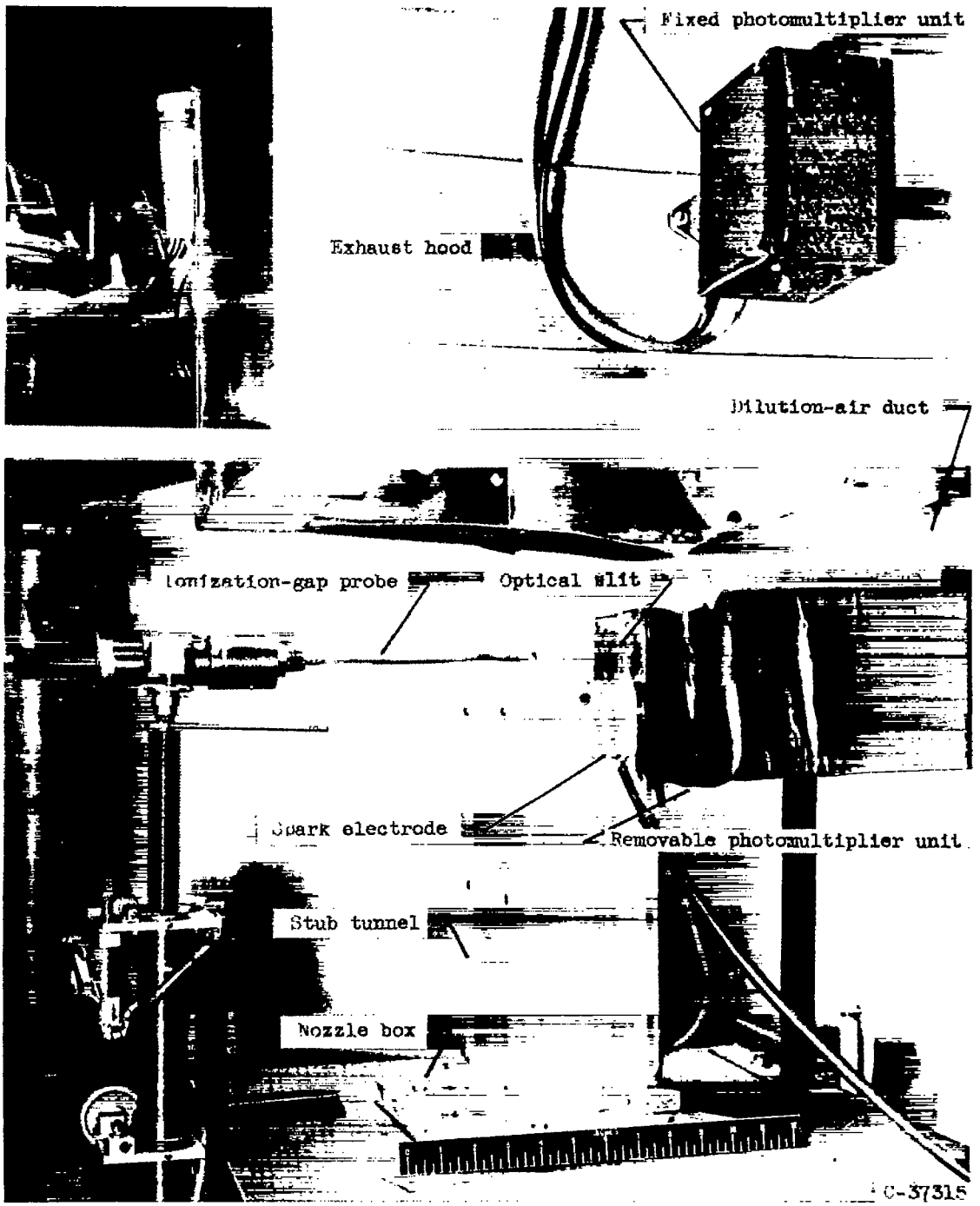

3637

(a) Over-all view of installation.

Figure 4. - Ionization-gap instrumentation for measurement of free-flame growth in free-jet installation.

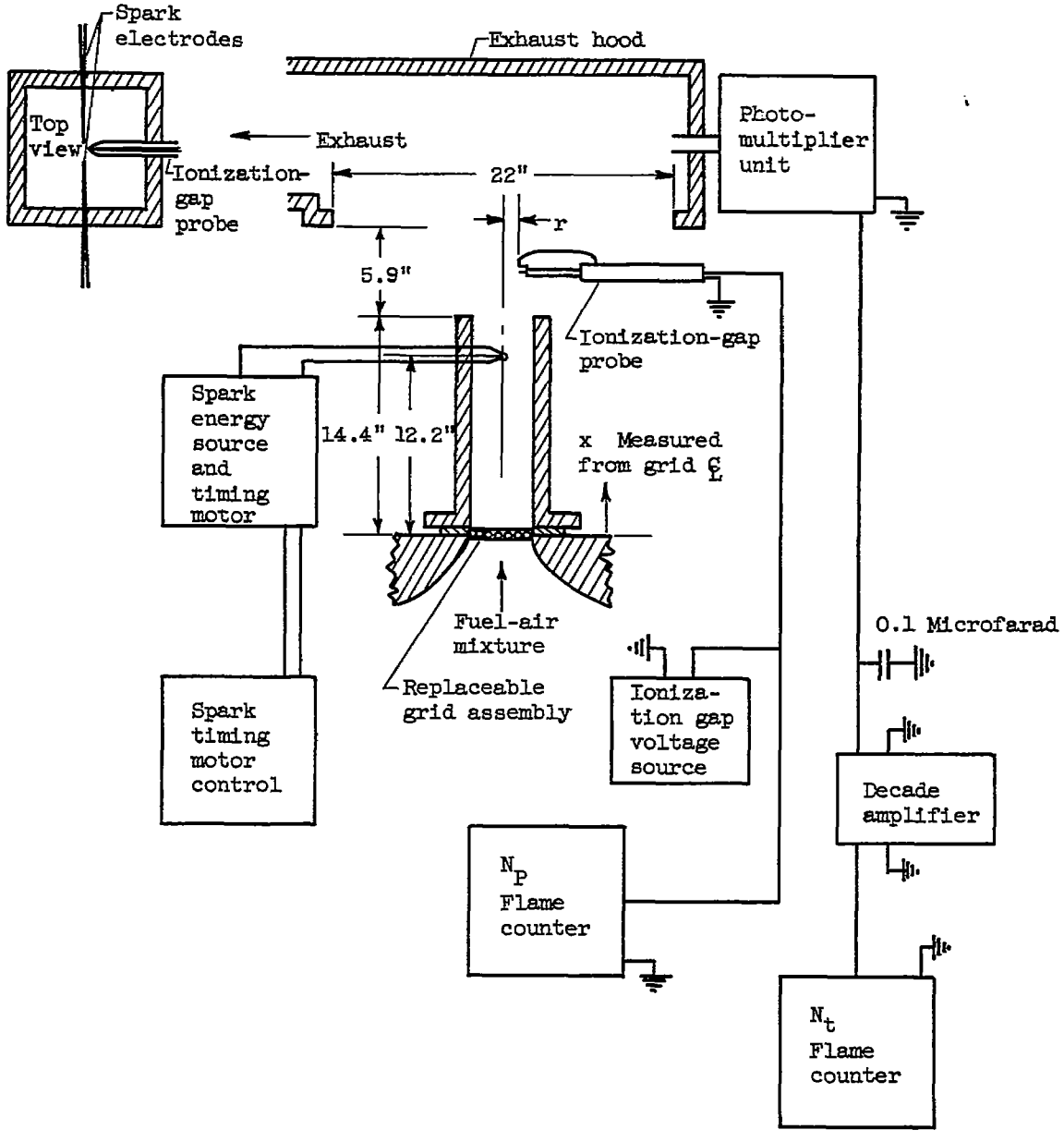

(b) Instrumentation

Figure 4. - Continued. Ionization-gap instrumentation for measurement of free-flame growth in free-jet installation.

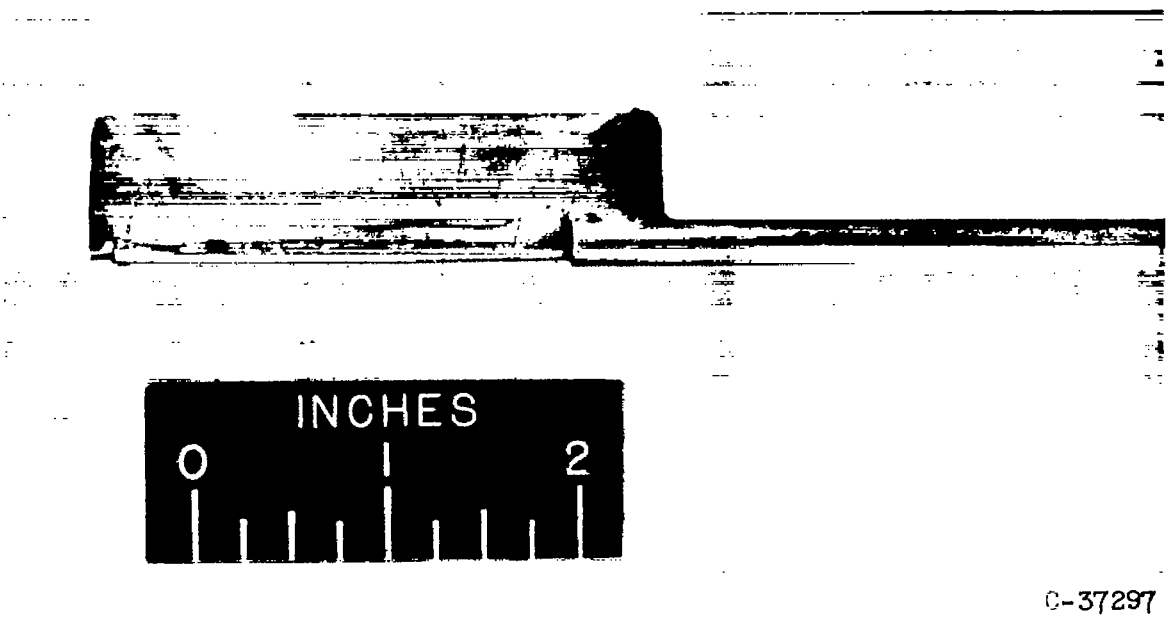

3637

(c) Ionization-gap probe.

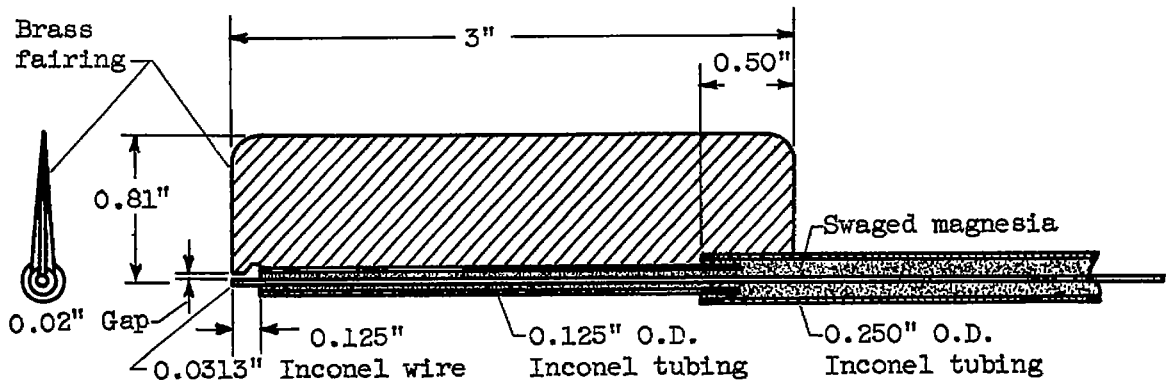

(d) Construction details of ionization-gap probe.

Figure 4. - Concluded. Ionization-gap instrumentation for measurement of free-flame growth in free-jet installation.

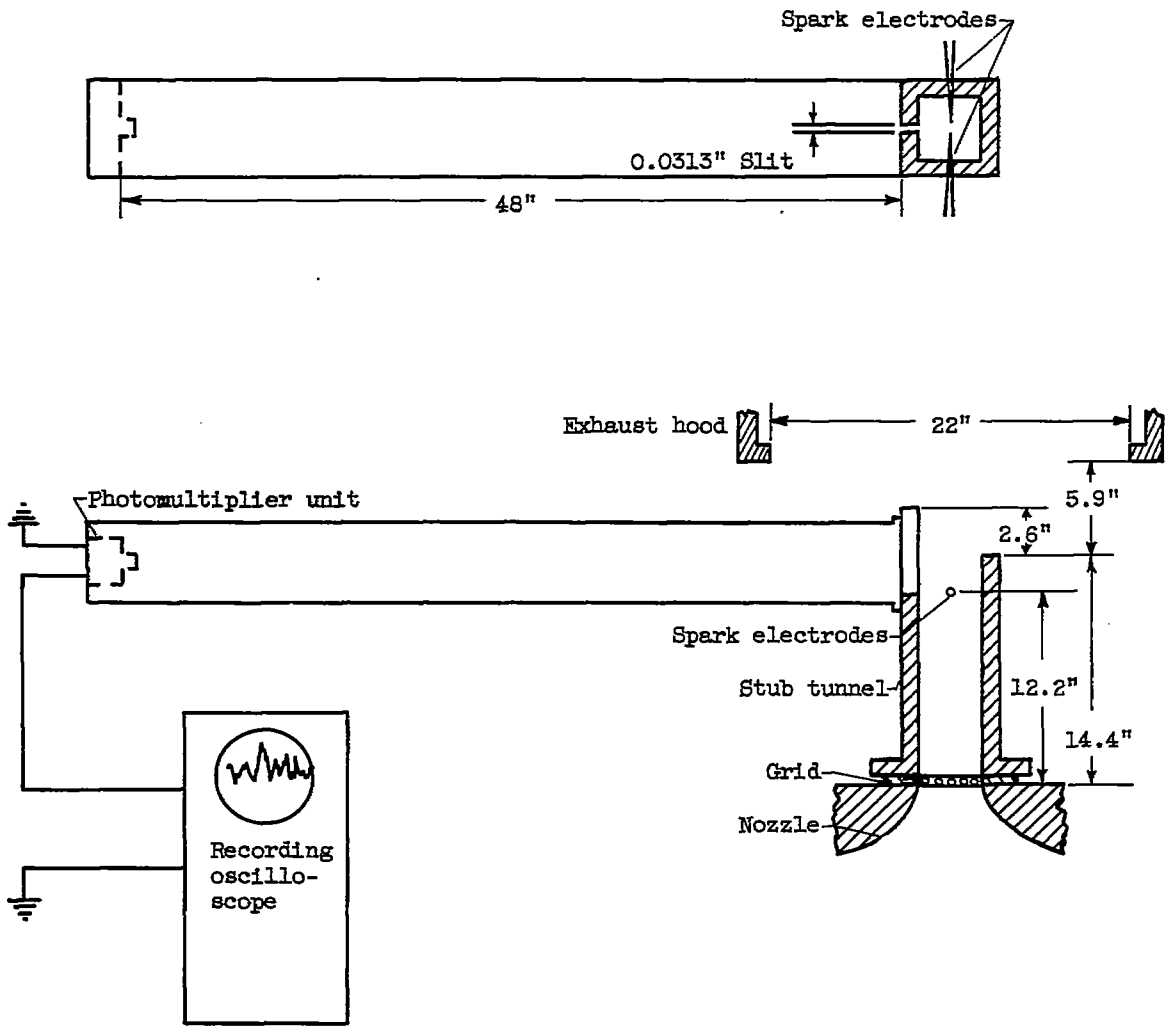

Figure 5. - Photomultiplier instrumentation for simultaneous measurement of free-flame growth and spark light intensity.

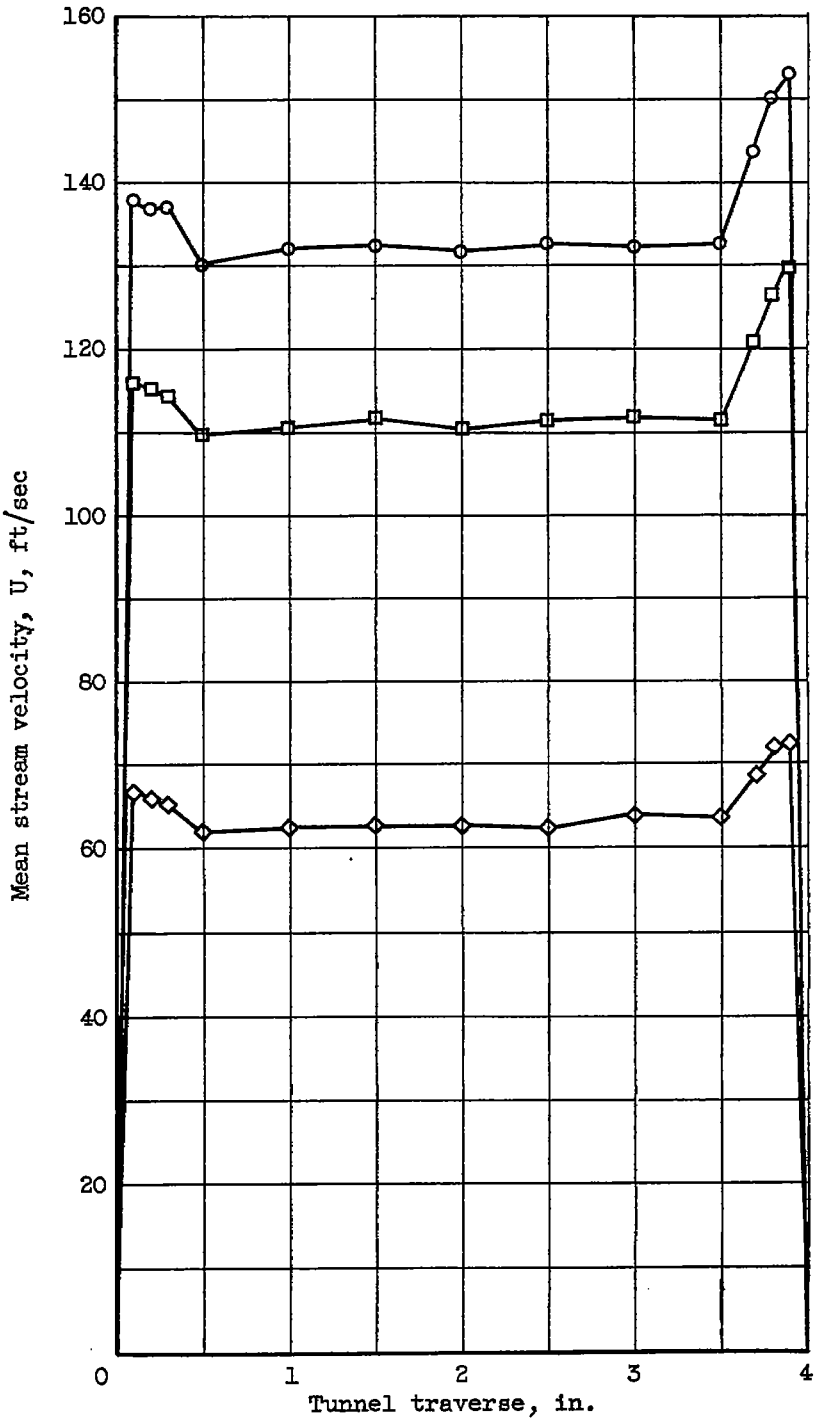

(a) Enclosed-tunnel installation. Measured 10.75 inches downstream of grid of 0.125-inch-diameter wire by 0.625-inch mesh.

Figure 6. - Typical mean stream velocity profiles.

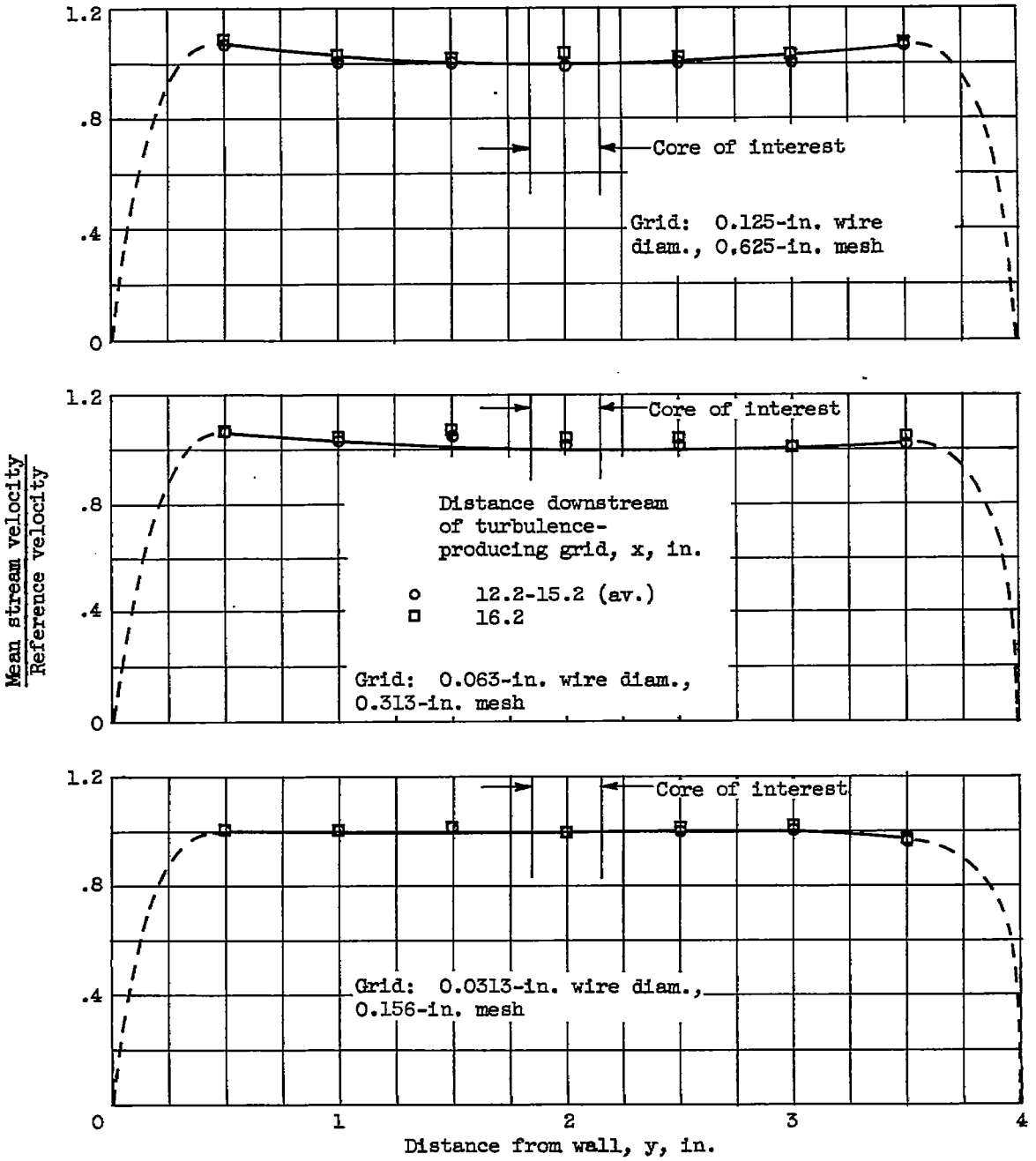

(b) Free-jet installation. Reference velocity equals velocity at $y = 0.5$ inch and $x = 1.0$ inch downstream of spark electrodes.

Figure 6. - Concluded. Typical mean stream velocity profiles.

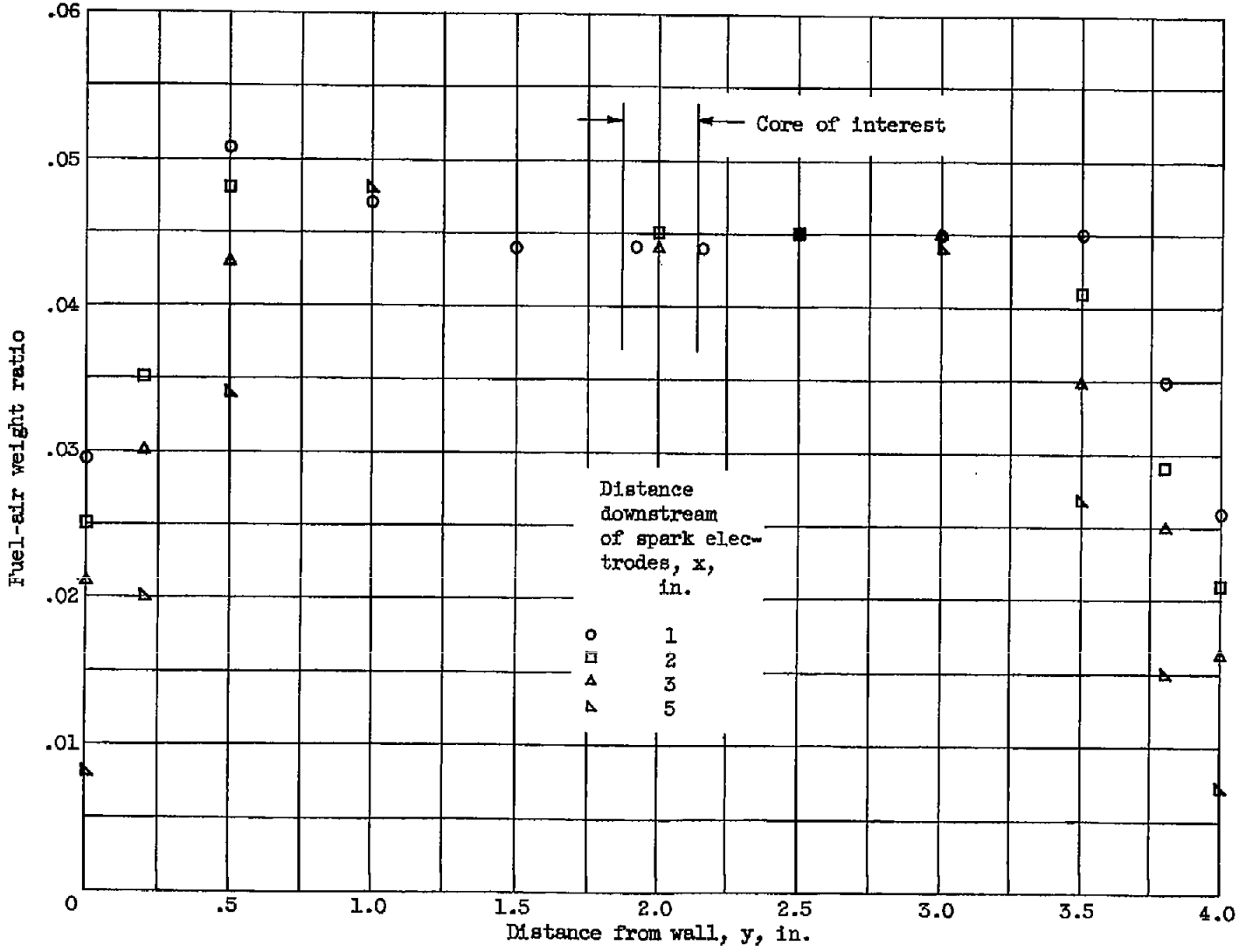

Figure 7. - Typical fuel-air-ratio profiles in free-jet installation.

Figure 8. - Longitudinal turbulence intensity measured in enclosed-tunnel installation.

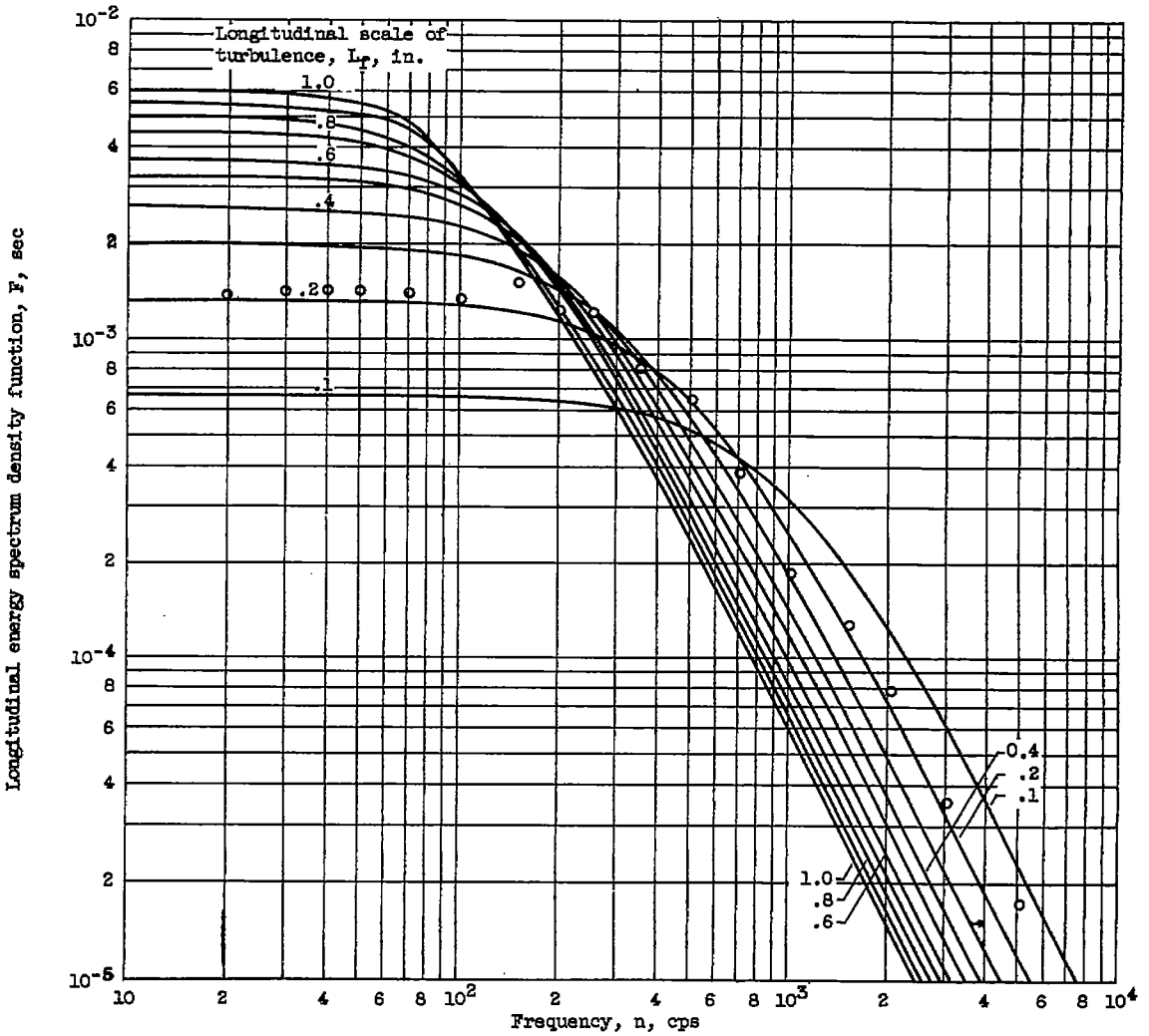

Figure 9. - Typical longitudinal energy spectrum of turbulence in enclosed-tunnel installation. Mean stream velocity, 50 feet per second.

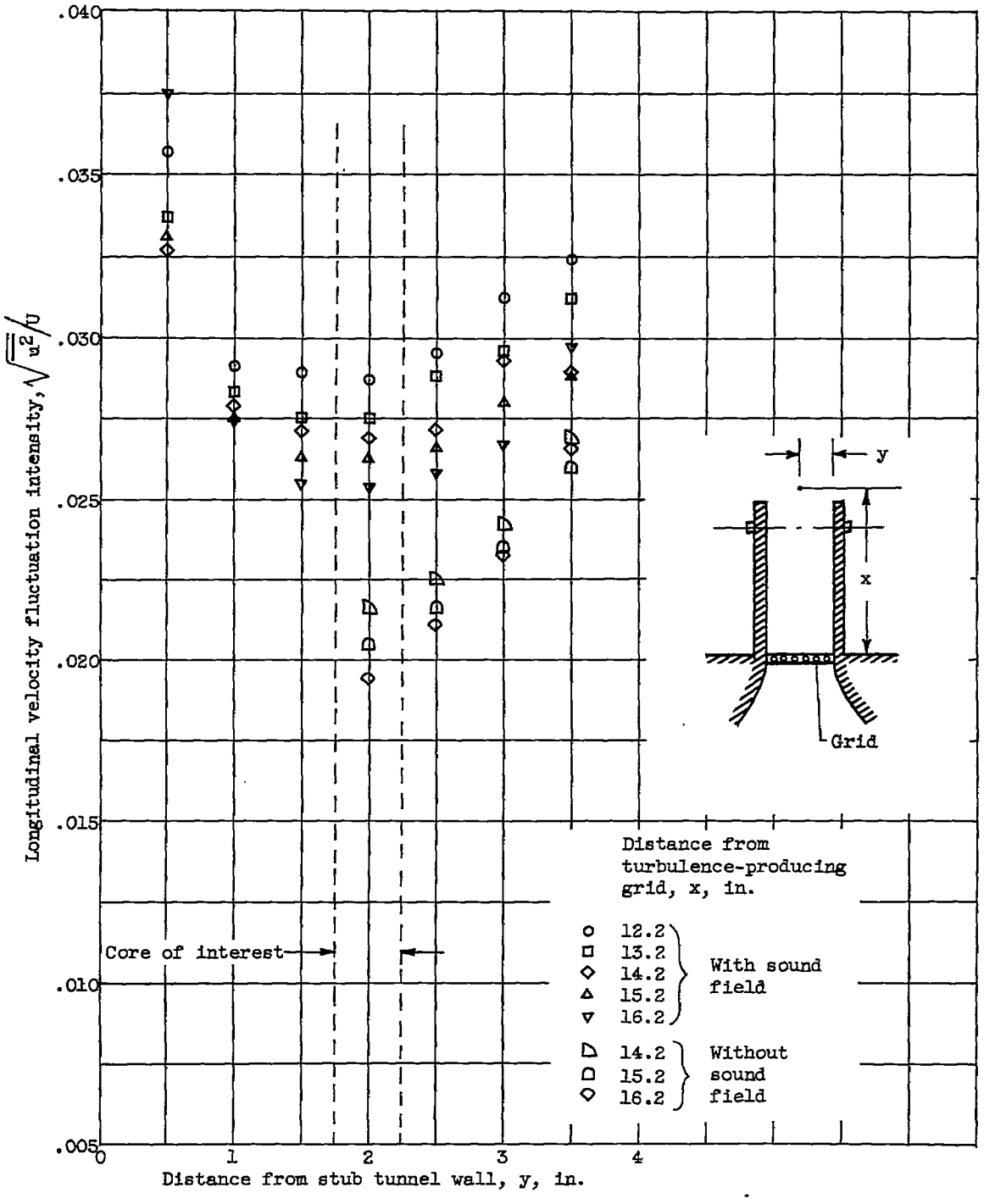

(a) Grid: 0.125-inch wire diameter, 0.625-inch mesh.

Figure 10. - Longitudinal velocity fluctuation intensity in free-jet installation.

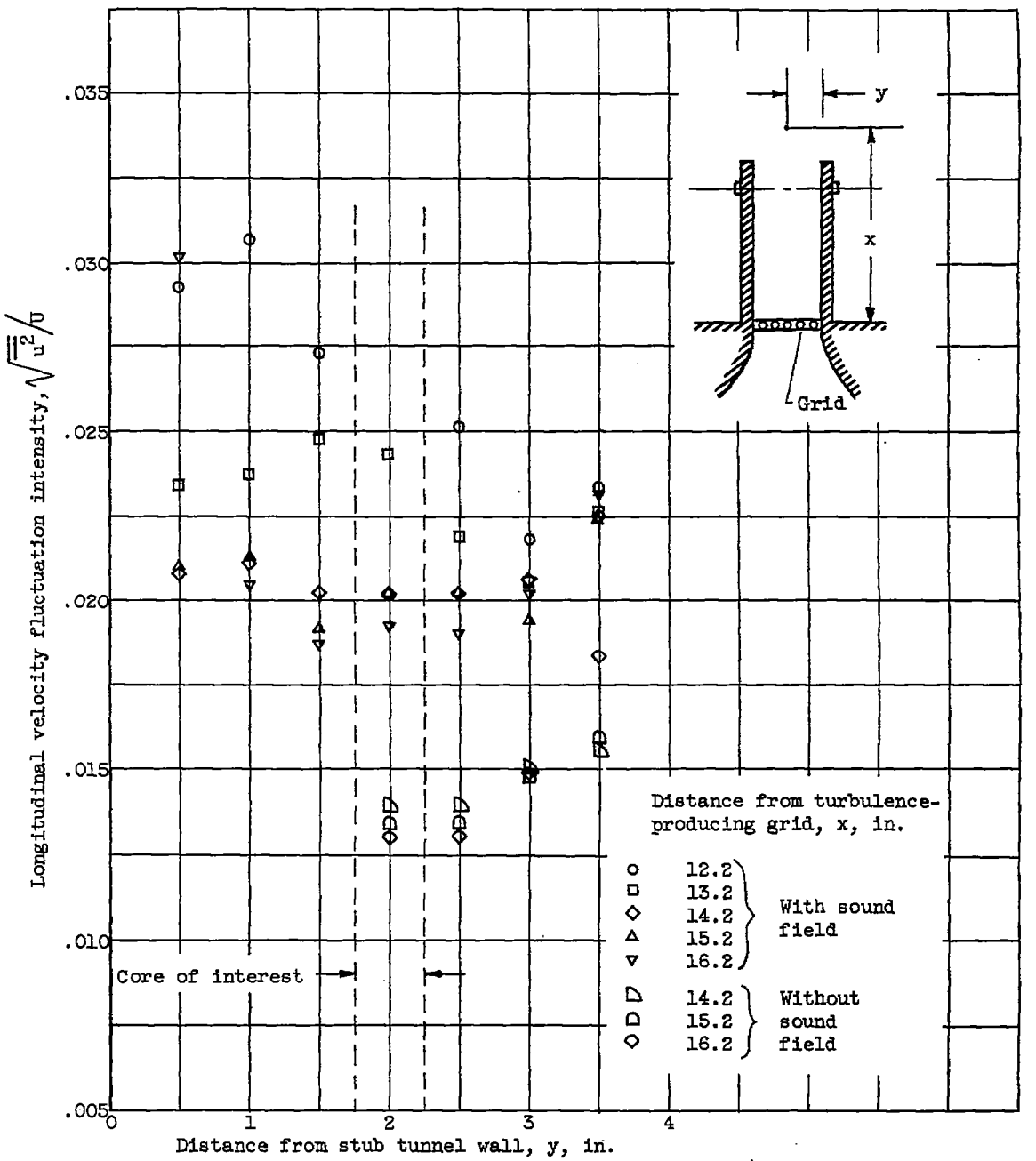

(b) Grid: 0.063-inch wire diameter, 0.313-inch mesh.

Figure 10. - Continued. Longitudinal velocity fluctuation intensity in free-jet installation.

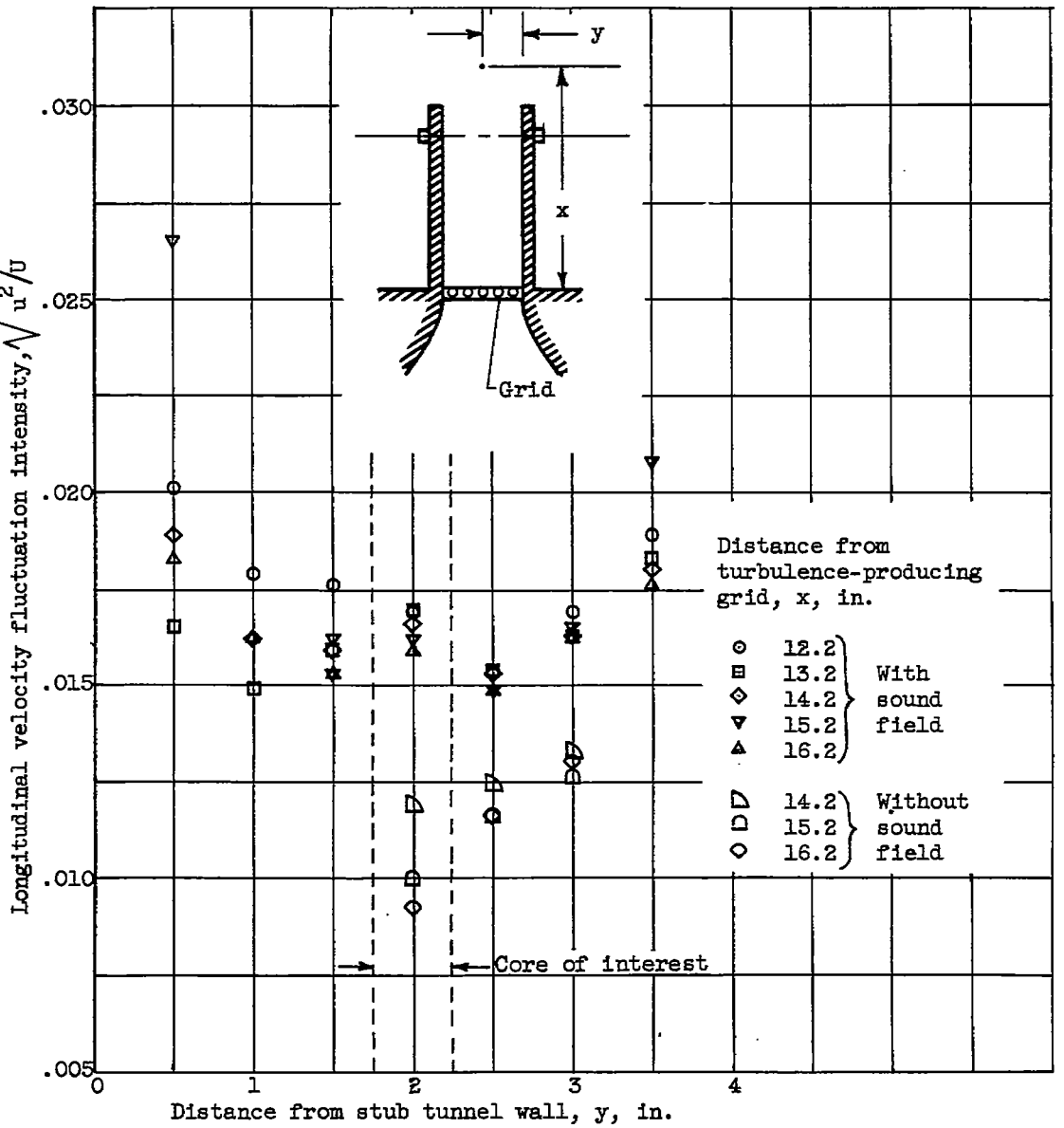

(c) Grid: 0.0313-inch wire diameter, 0.156-inch mesh.

Figure 10. - Concluded. Longitudinal velocity fluctuation intensity in free-jet installation.

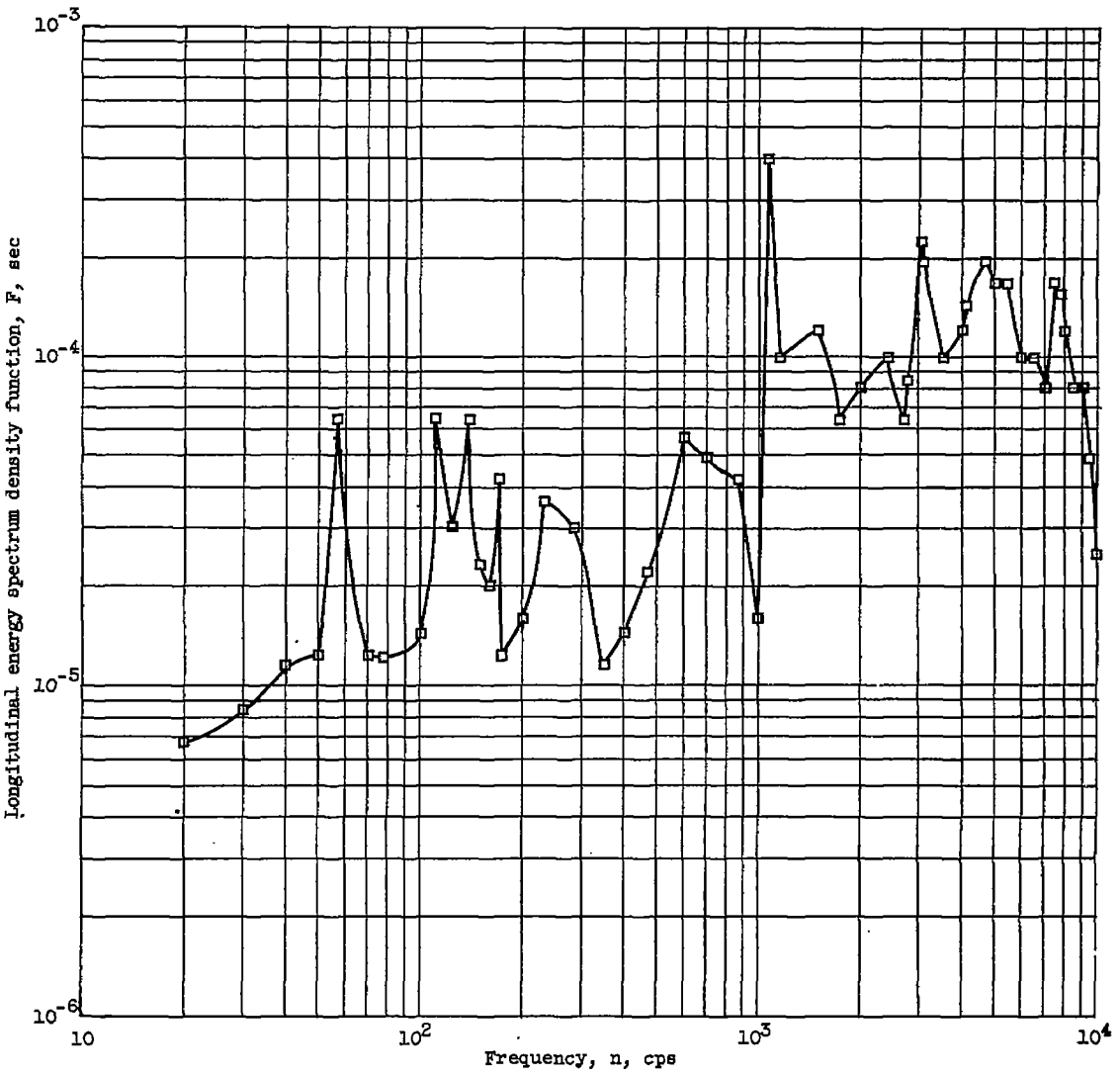

Figure 11. - Longitudinal kinetic-energy spectrum of free-jet sound field.

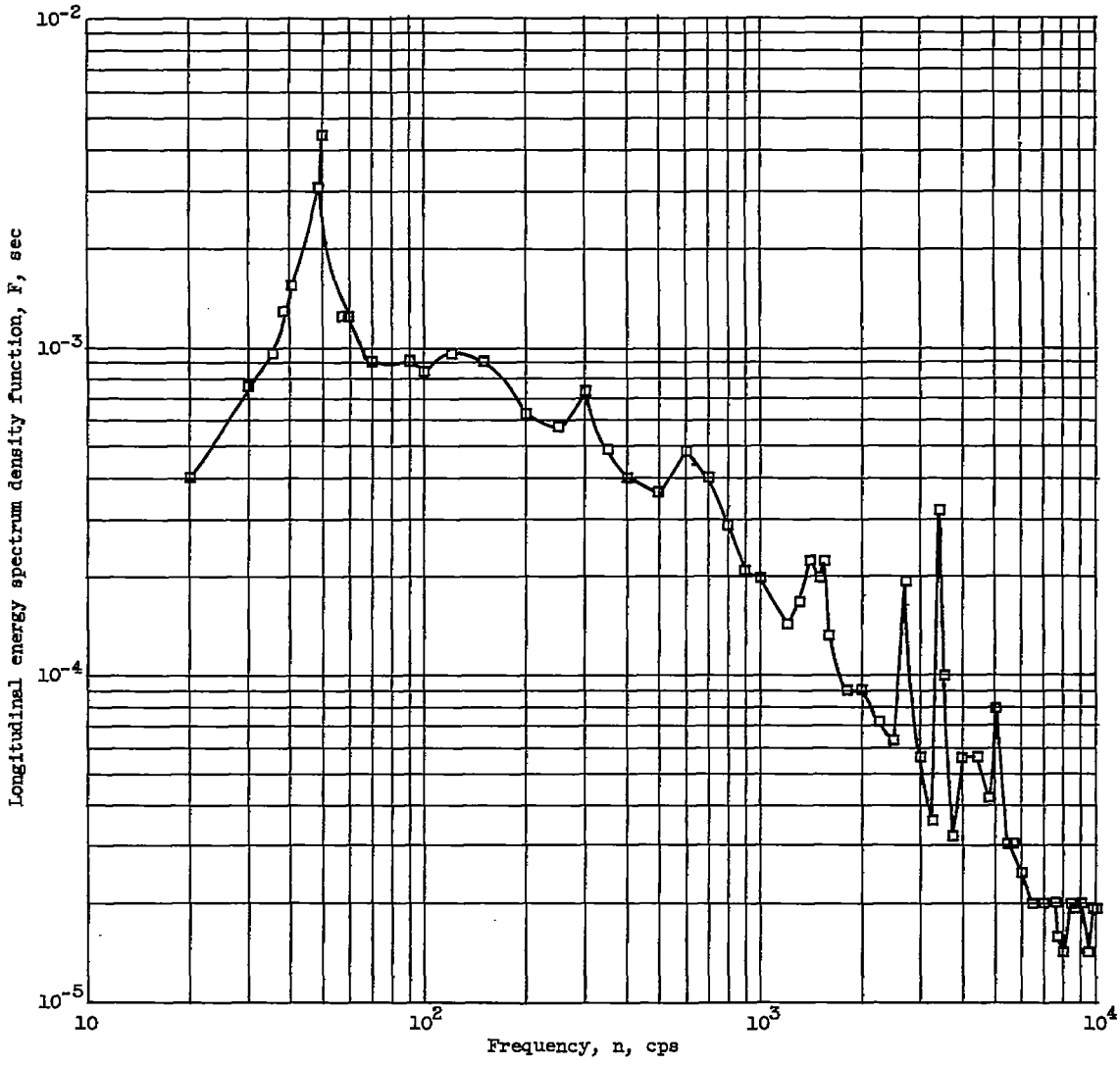

Figure 12. - Typical longitudinal velocity fluctuation energy spectrum measured in free-jet installation. Grid: 0.125-inch wire diameter, 0.625-inch mesh; distance downstream of spark electrodes, 4 inches; mean stream velocity, 68.5 feet per second; static pressure, 29 inches of mercury absolute; static temperature, 545° R.

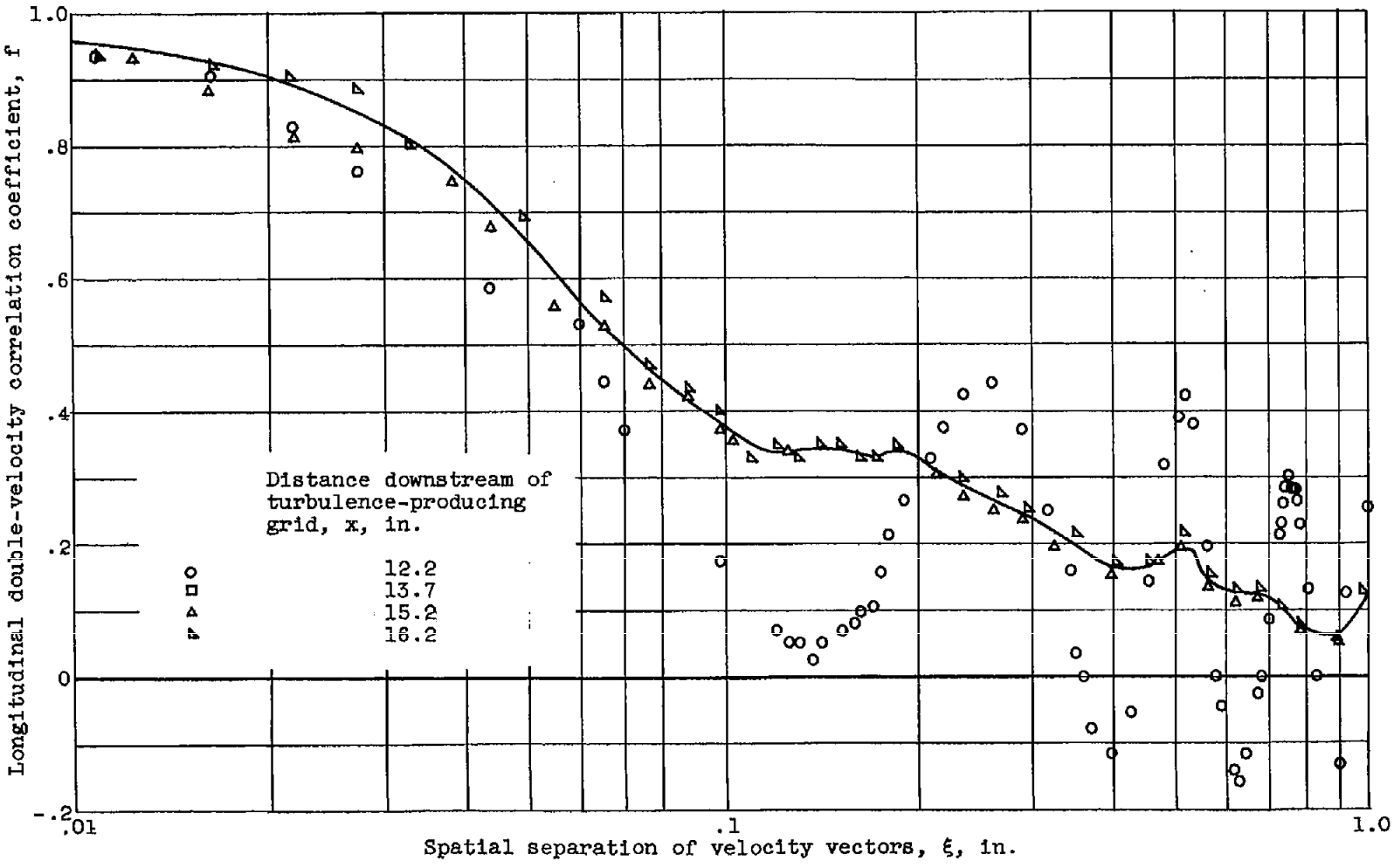

(a) Grid: 0.125-inch wire diameter, 0.625-inch mesh.

Figure 13. - Longitudinal double-velocity correlation coefficients measured in free-jet installation. Mean stream velocity, 68.5 feet per second.

(b) Grid: 0.063-inch wire diameter, 0.313-inch mesh.

Figure 13. - Continued. Longitudinal double-velocity correlation coefficients measued in free-jet installation. Mean stream velocity, 68.5 feet per second.

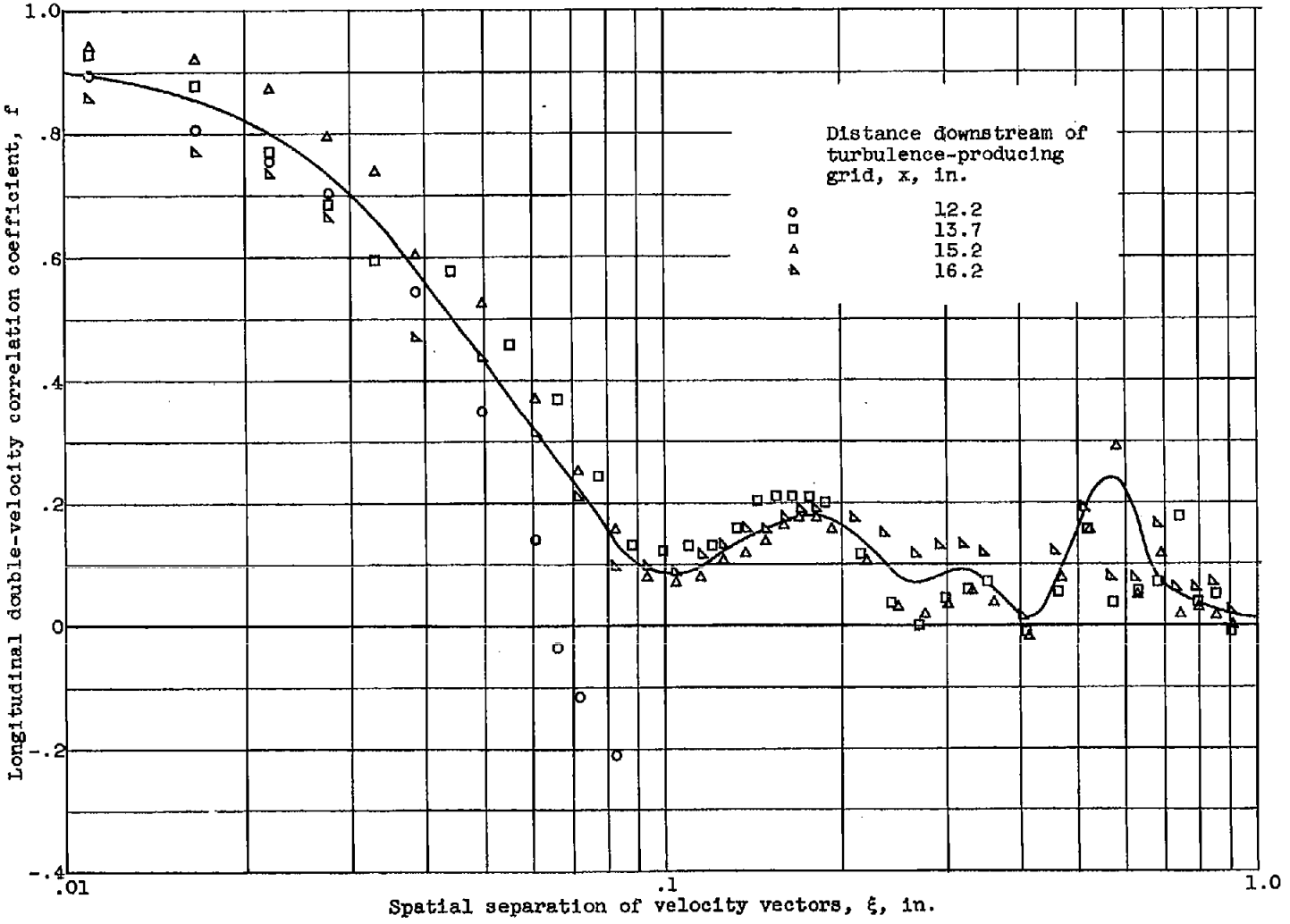

(c) Grid: 0.0313-inch wire diameter, 0.153-inch mesh.

Figure 13. - Concluded. Longitudinal double-velocity correlation coefficients measured in free-jet installation. Mean stream velocity, 68.5 feet per second.

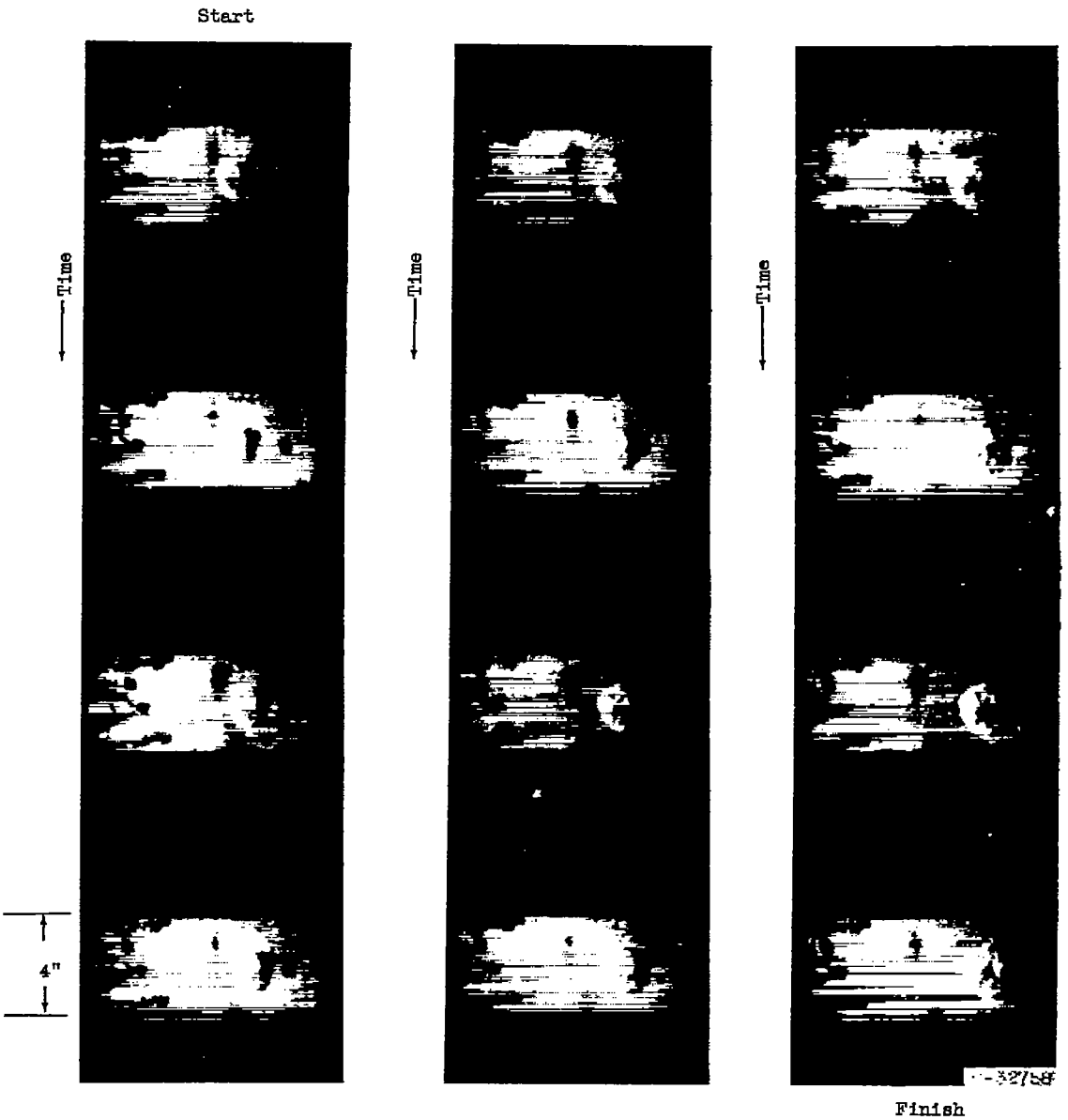

(a) Typical photographic record. Film speed, approximately 3600 frames per second.

Figure 14. - Typical turbulent flame-speed data from enclosed-tunnel installation.

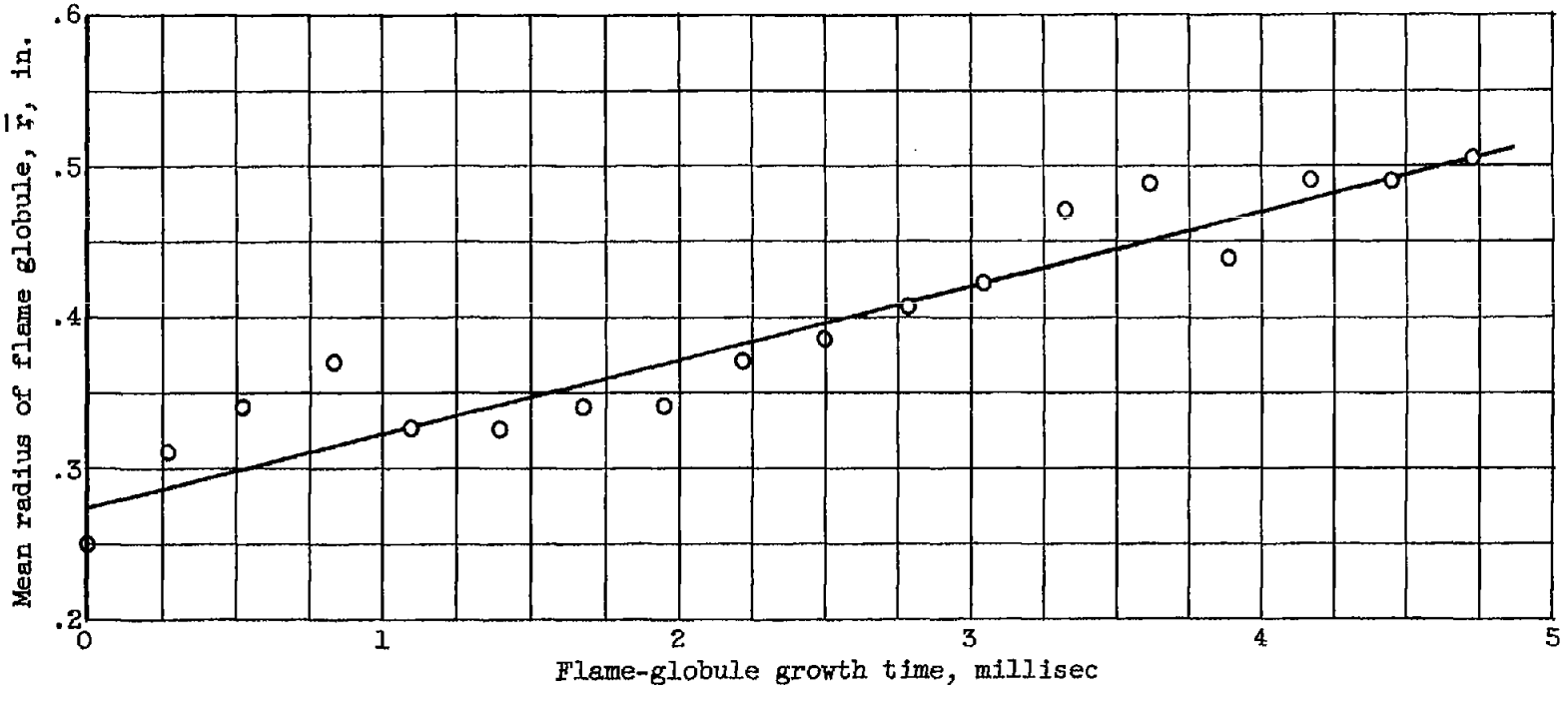

(b) Flame-globule expansion history.

Figure 14. - Continued. Typical turbulent flame-speed data from enclosed-tunnel installation.

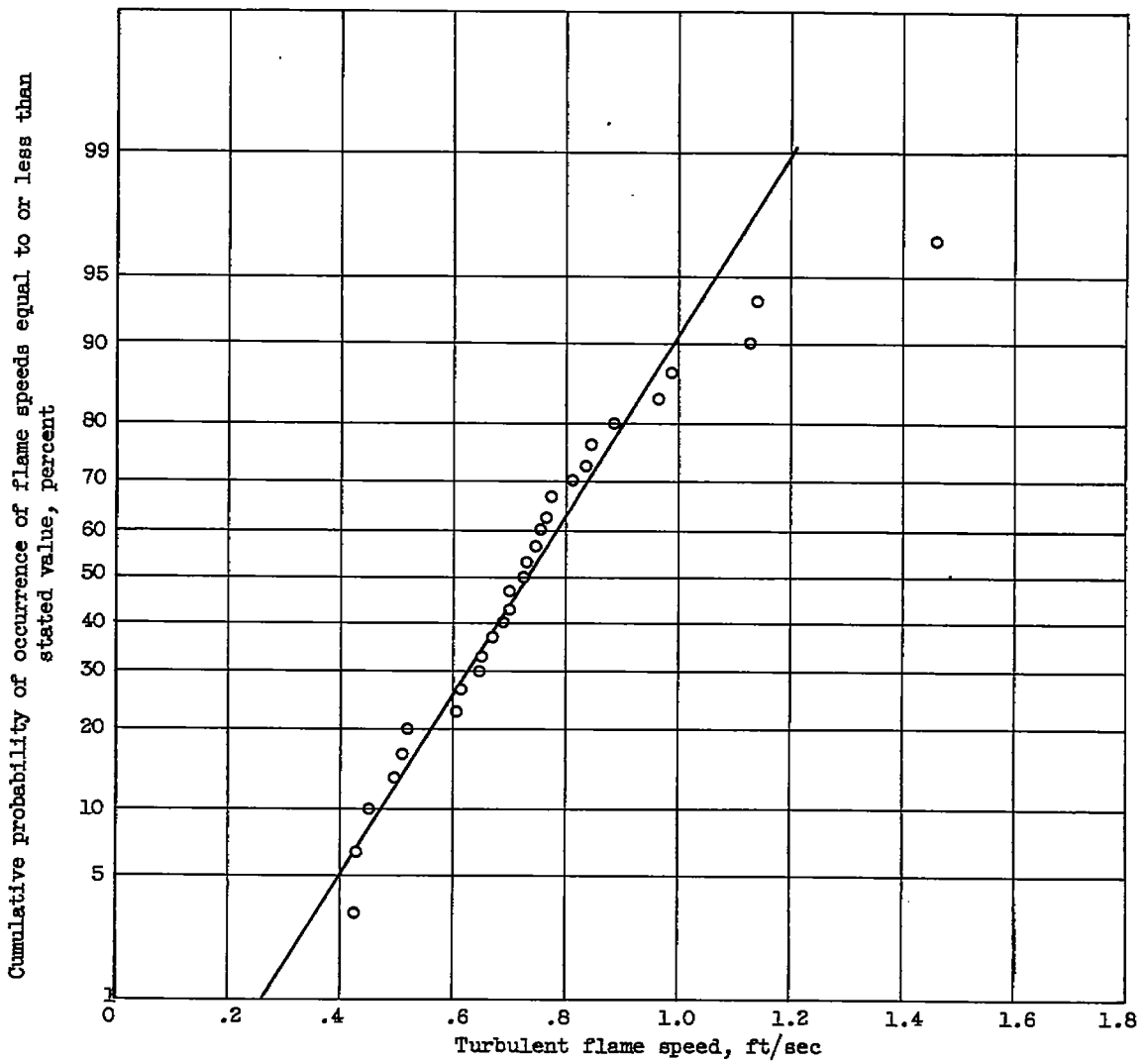

(c) Cumulative probability of turbulent flame speed. Mean stream velocity, 60 feet per second; propane-air ratio, approximately 0.045 by weight; static pressure, 26 inches of mercury absolute; temperature, 540° R.

Figure 14. - Concluded. Typical turbulent flame-speed data from enclosed-tunnel installation.

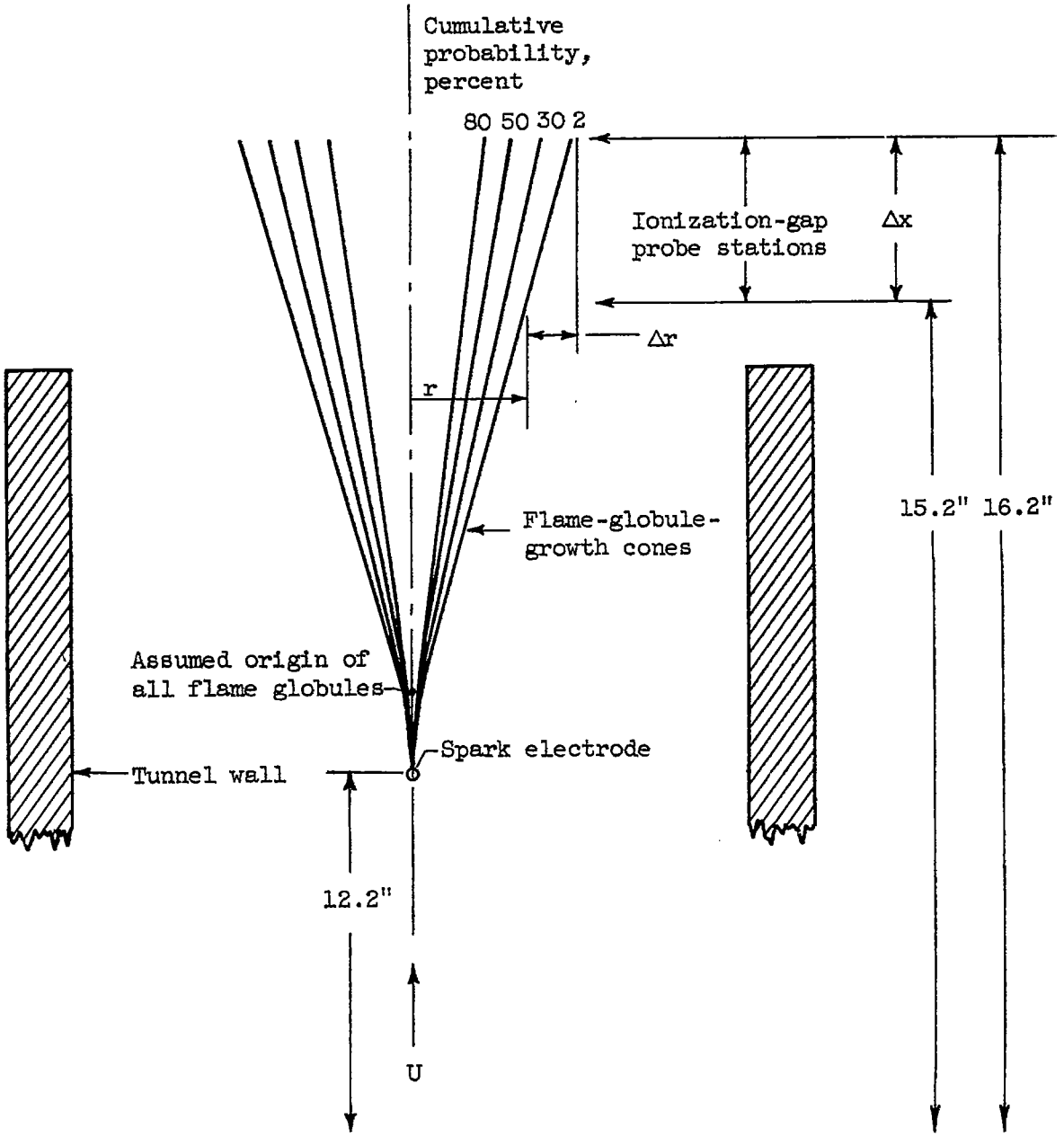

Figure 15. - Flame-globule-growth measurement with ionization-gap instrumentation. $S_T = \frac{\Delta r}{\Delta x/U} \frac{R_a T_a}{R_F T_F}$.

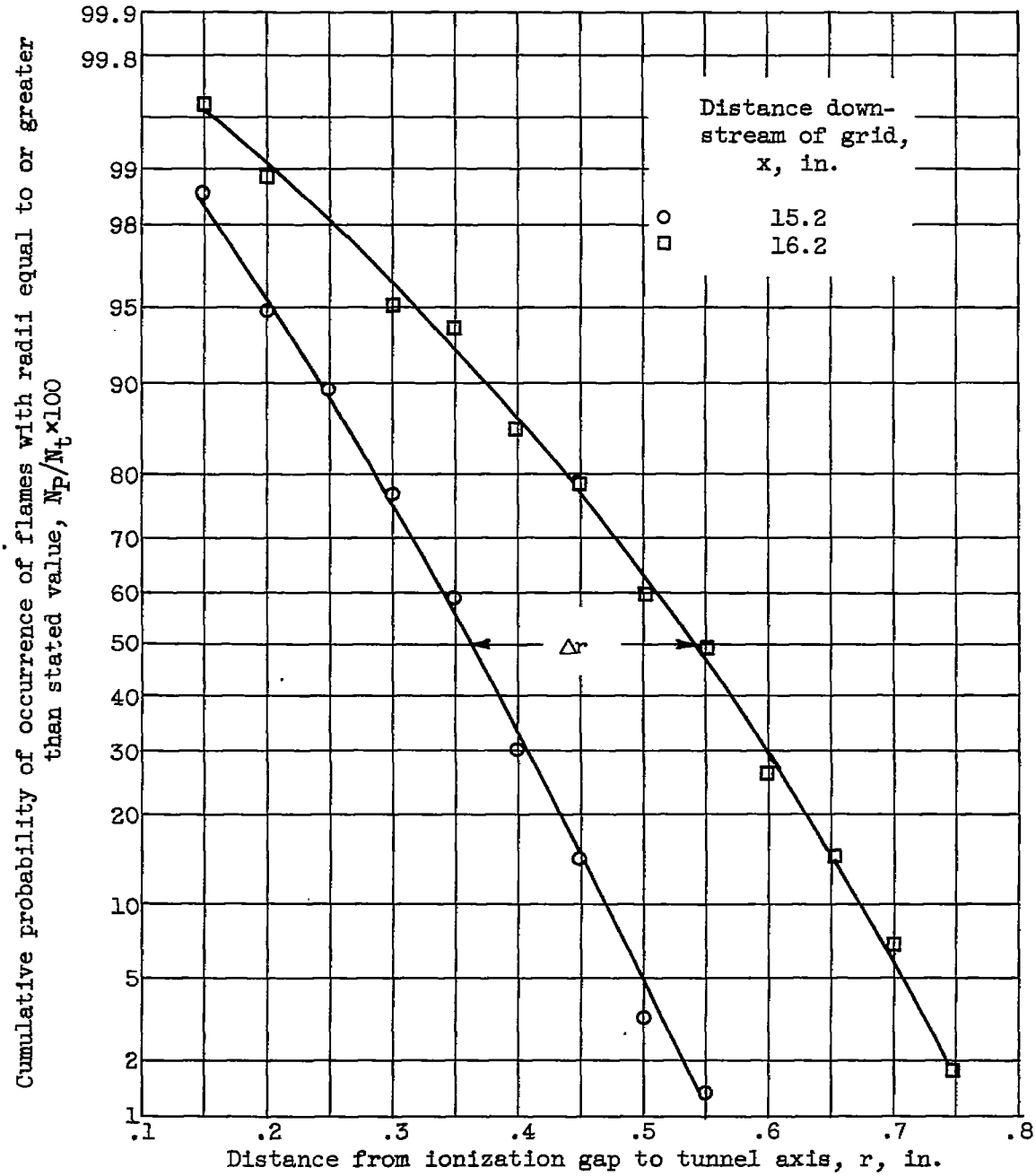

(a) Fuel-air ratio, 0.056; mean stream velocity, 68.3 feet per second.

Figure 16. - Typical cumulative probability of flame-globule size measured with ionization-gap instrumentation in free-jet installation. Grid: 0.125-inch wire diameter, 0.625-inch mesh; static pressure, 29.3 inches of mercury absolute; static temperature, 545° R.

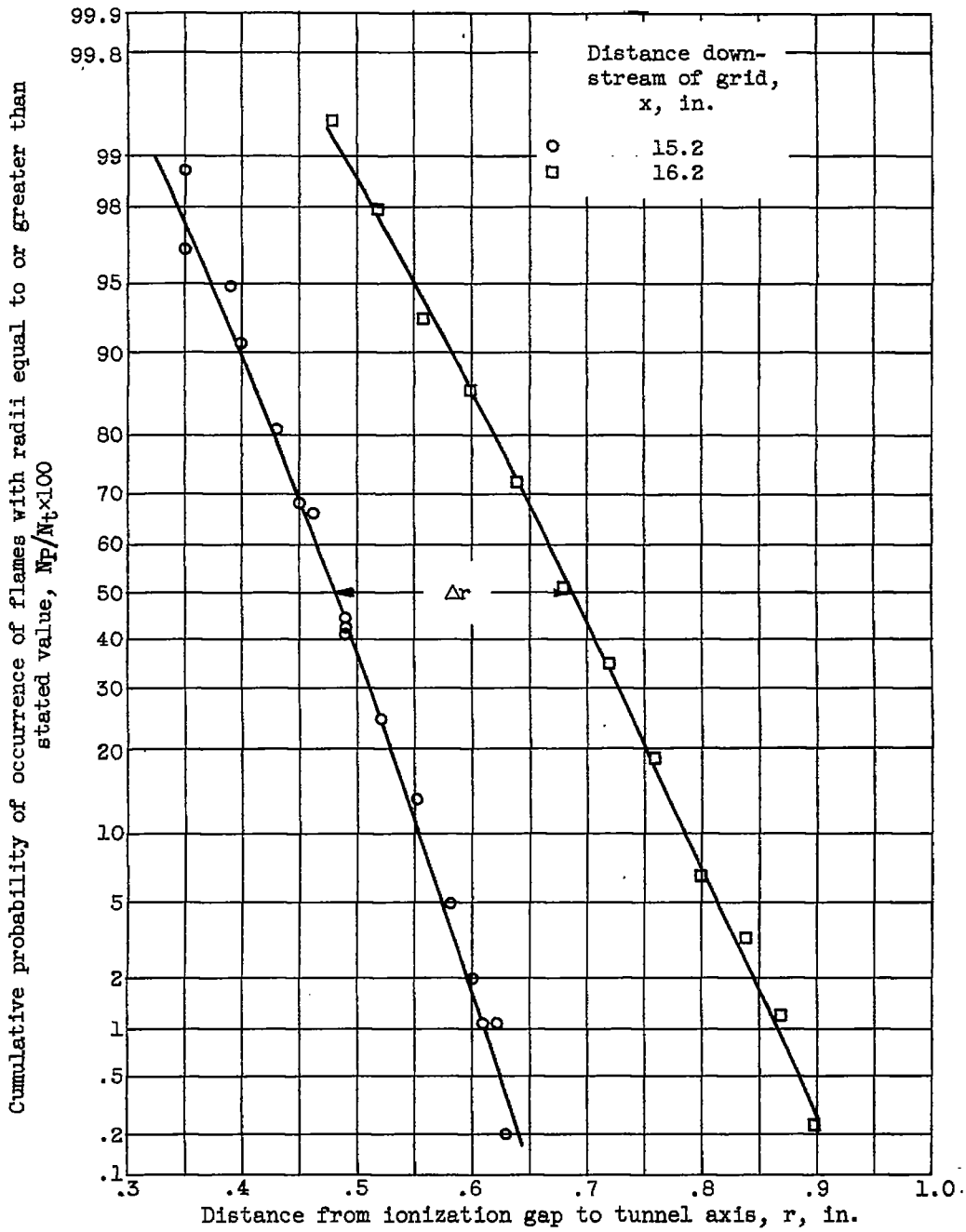

(b) Fuel-air ratio, 0.070; mean stream velocity, 69.6 feet per second.

Figure 16. - Concluded. Typical cumulative probability of flame-globule size measured with ionization-gap instrumentation in free-jet installation. Grid: 0.125-inch wire diameter, 0.625-inch mesh; static pressure, 29.3 inches of mercury absolute; static temperature, 545° R.

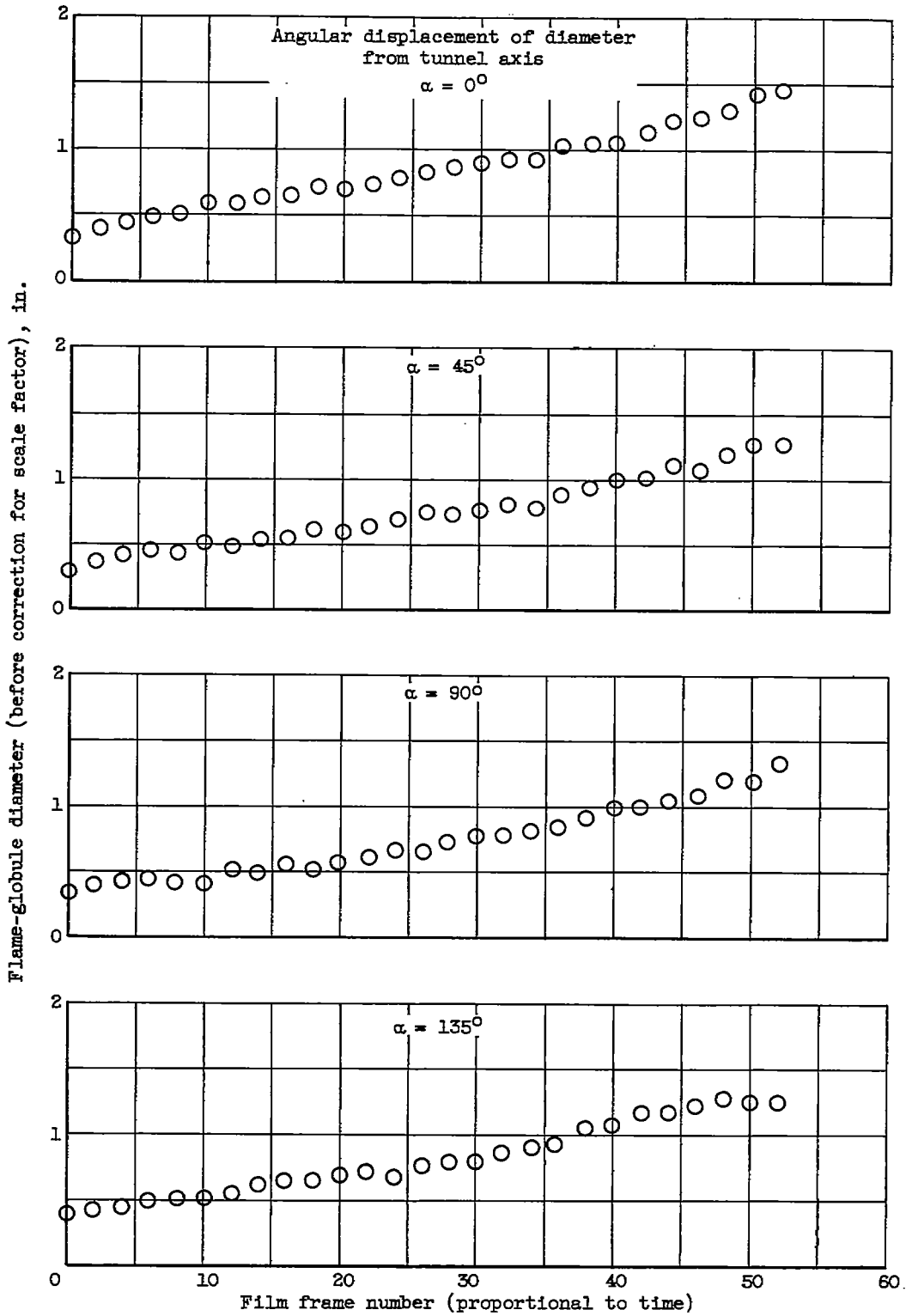

Figure 17. - Typical flame-globule diameter histories measured in enclosed-tunnel installation.

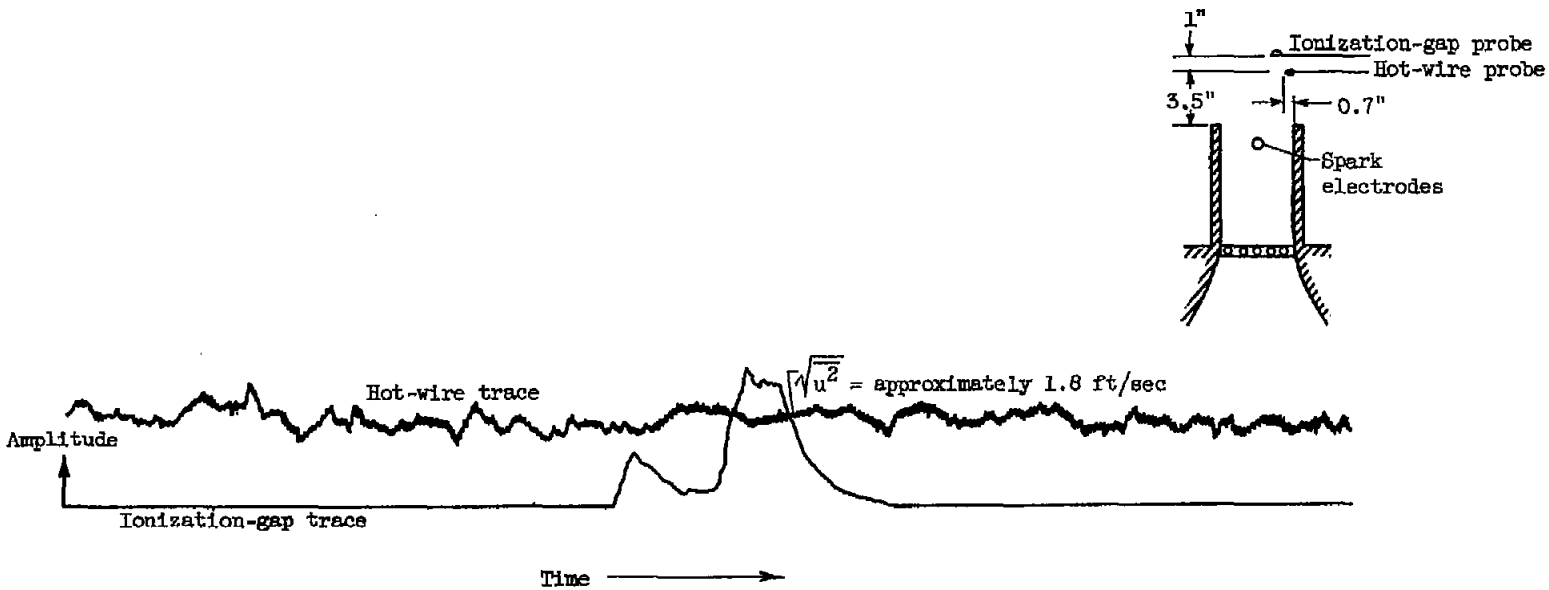

Figure 18. - Typical oscillograph of ionization-gap and hot-wire signals in free-jet stream at time of flame-globule passage. Grid: 0.125-inch wire diameter, 0.625-inch mesh; stream velocity, 70 feet per second; static pressure, 29 inches of mercury absolute; temperature, 80° F.

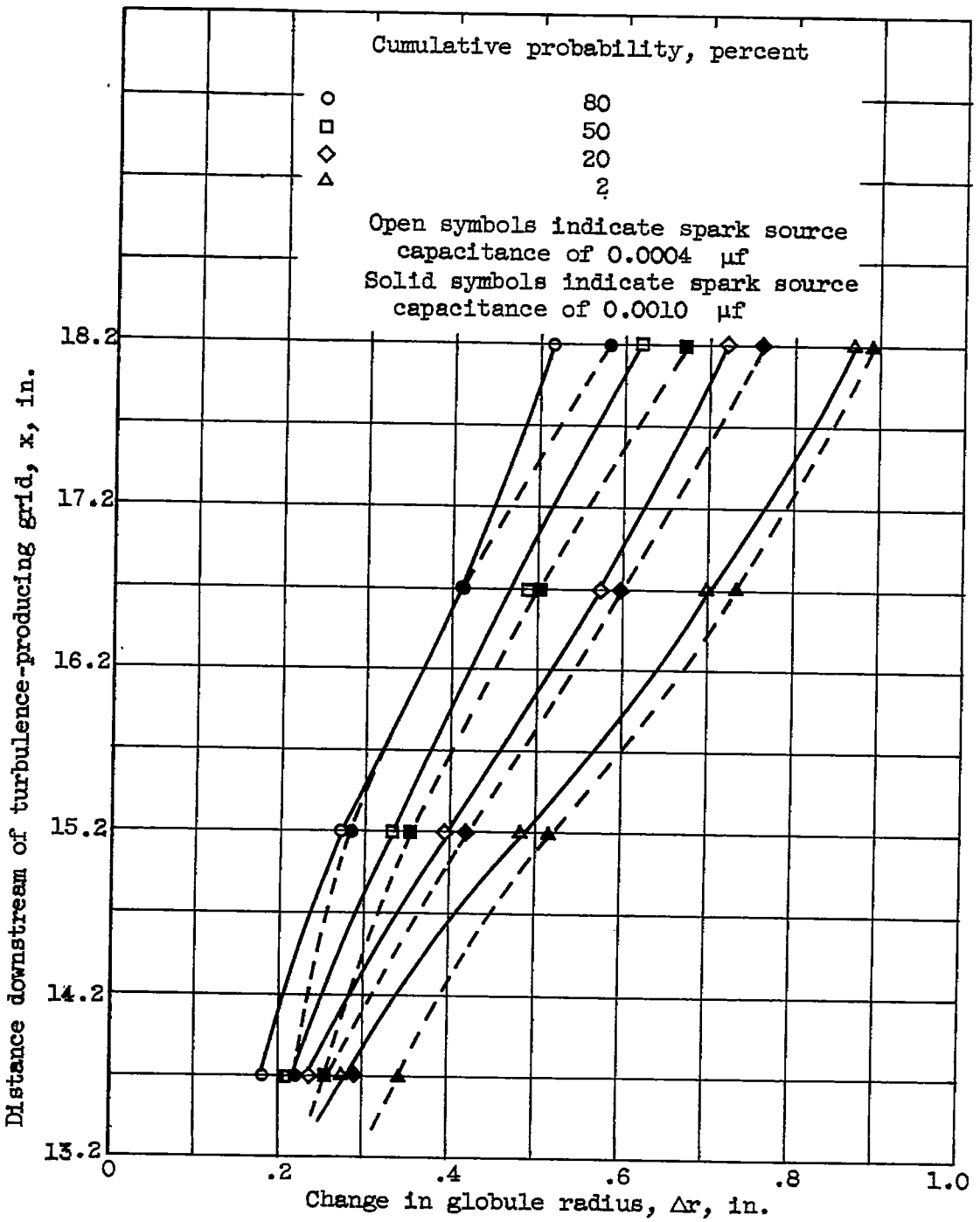

Figure 19. - Effect of spark source energy on flame-globule growth.

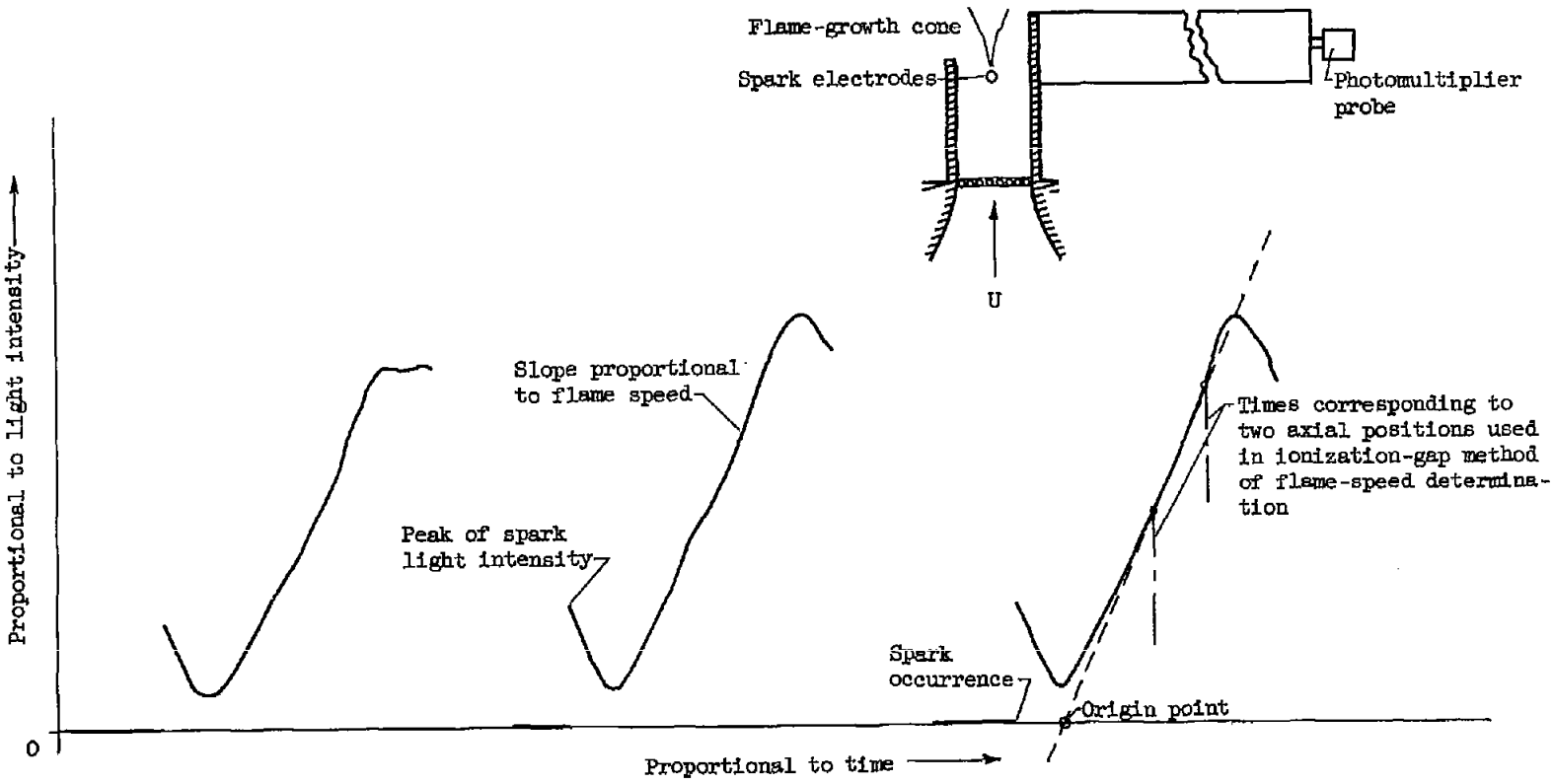

Figure 20. - Typical oscillographs of photomultiplier probe trace depicting spark occurrence and growth of flame globule in free-jet stream.

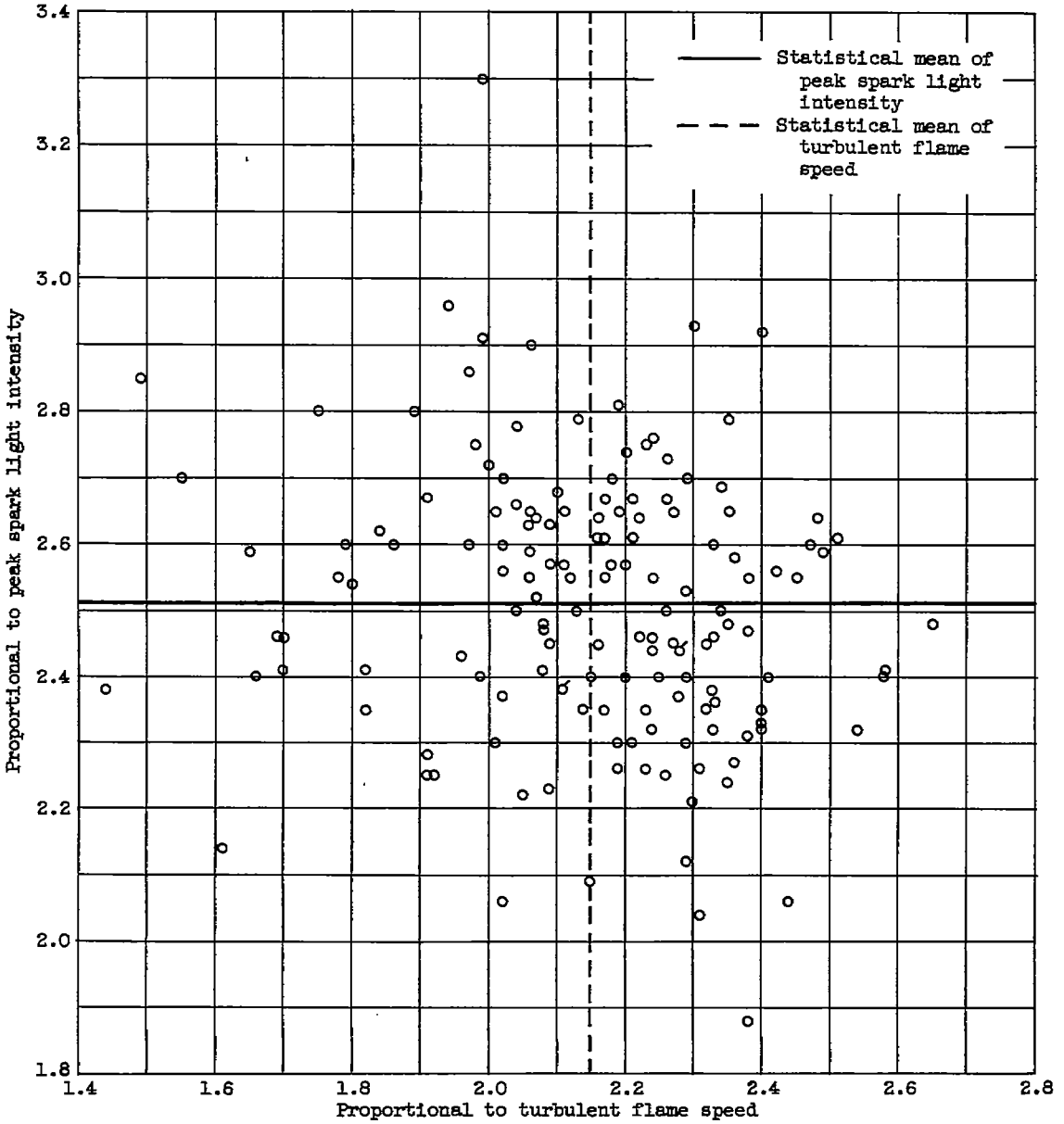

Figure 21. - Correlation between spark light intensity and turbulent flame speed for 151 consecutive flame globules at identical mean stream and fuel conditions.

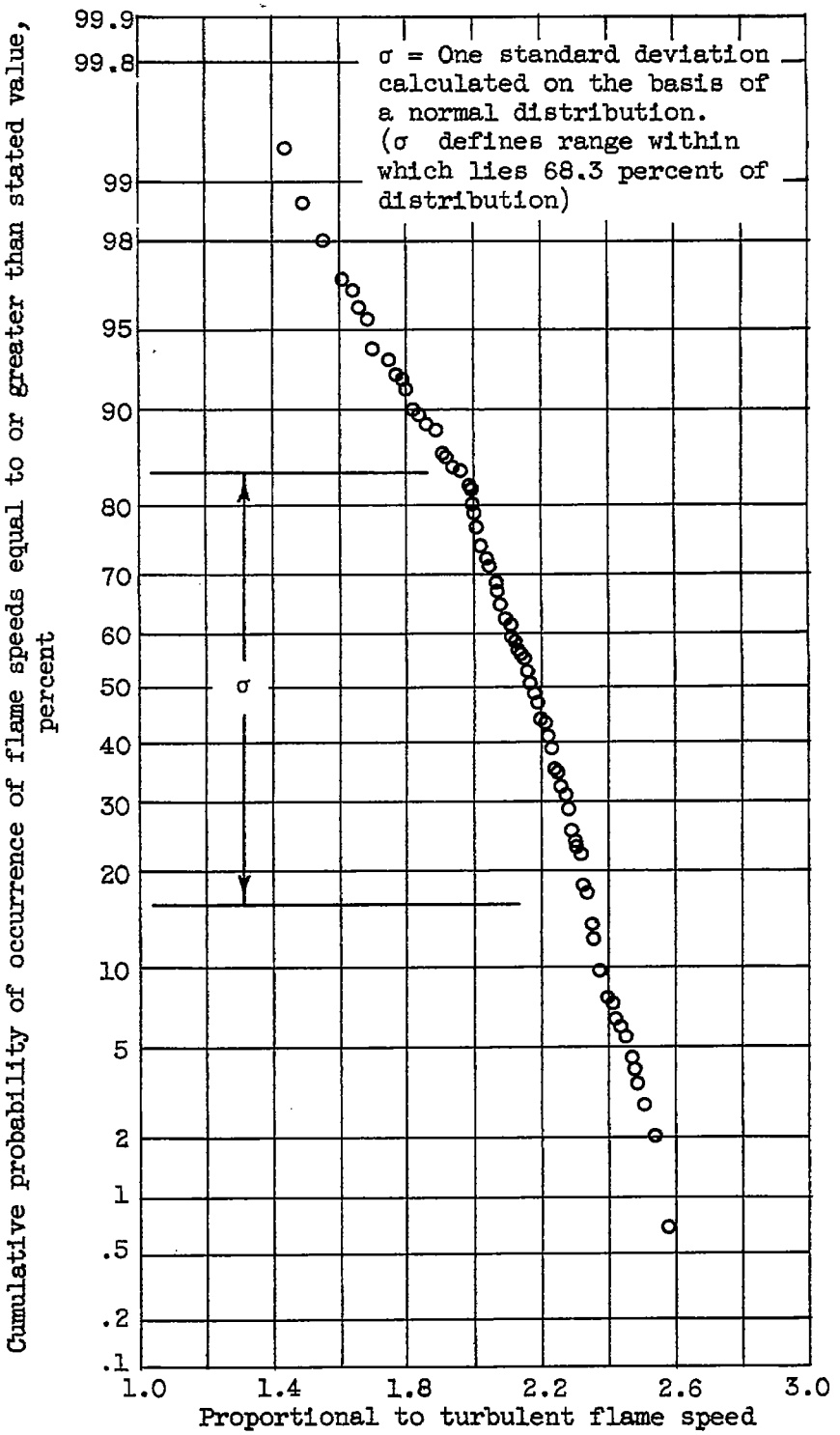

Figure 22. - Statistical variation of flame speed as determined from photomultiplier oscillograms.

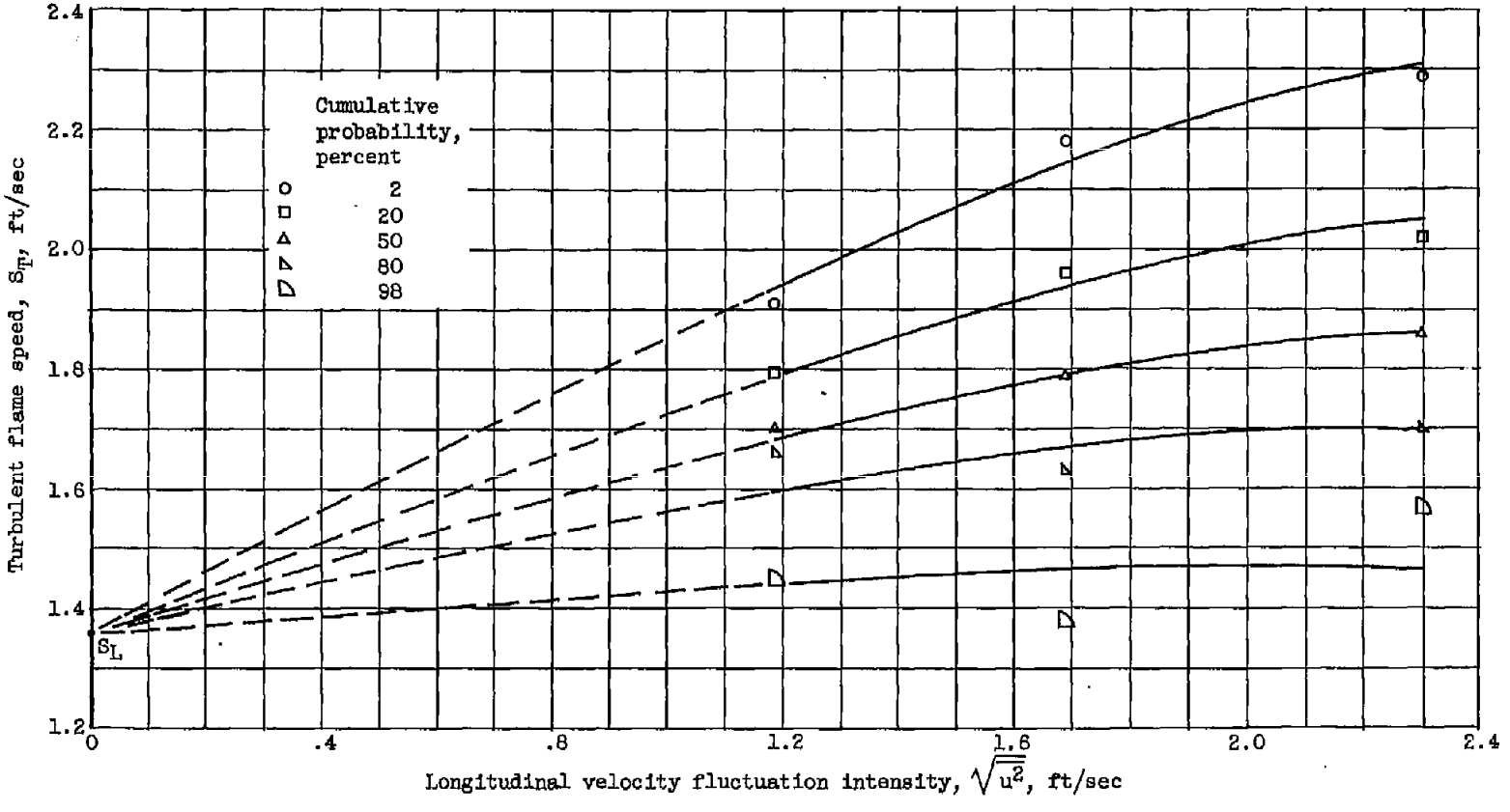

Figure 23. - Turbulent flame speed as a function of longitudinal velocity fluctuation intensity with cumulative probability of occurrence as a parameter. Propane-air weight ratio, 0.070; stream static temperature, 545° R; static pressure, 29.3 inches of mercury absolute; grid: 0.125-inch wire diameter, 0.625-inch mesh; free-jet installation.

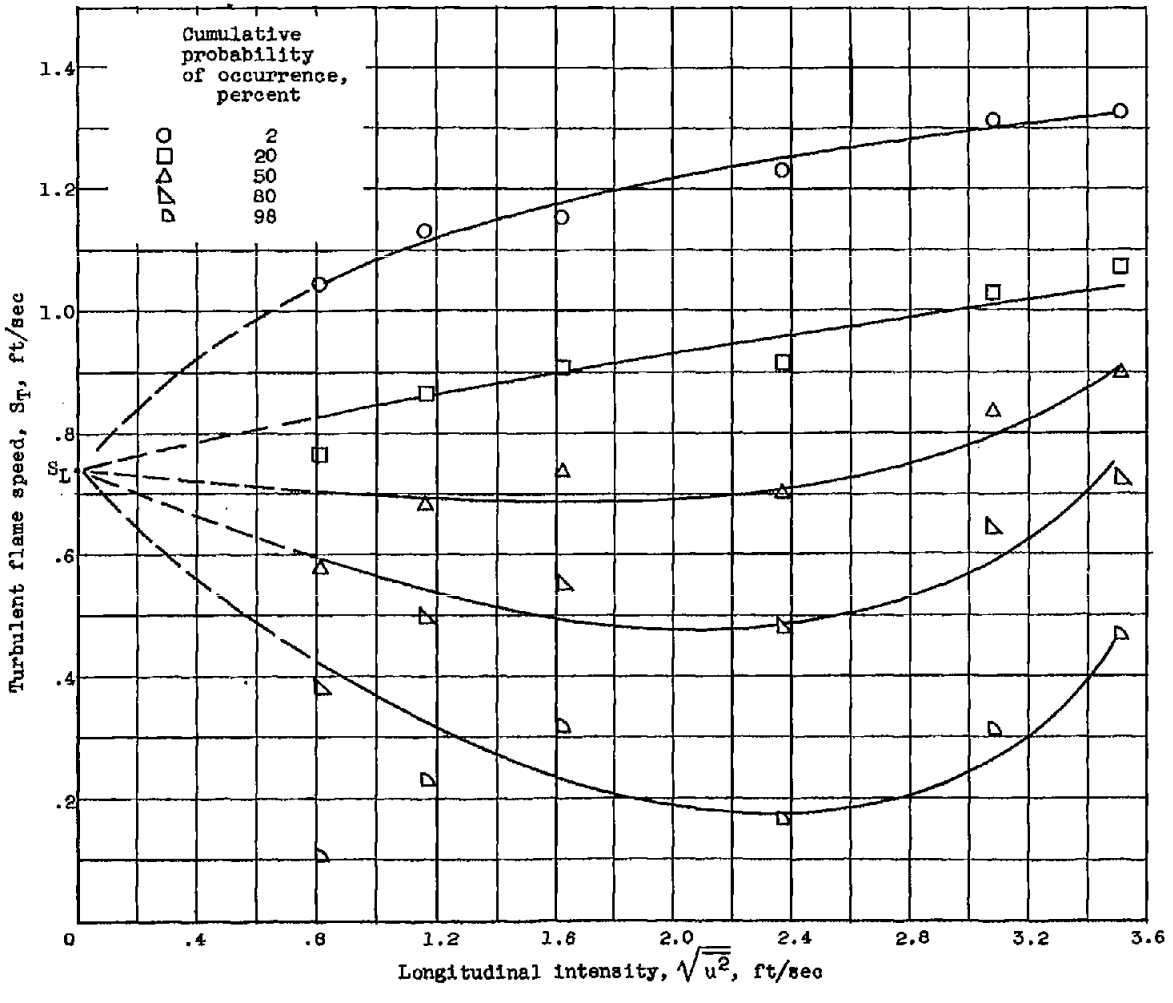

Figure 24. - Turbulent flame speed as a function of turbulence intensity. Propane-air weight ratio, approximately 0.045; stream temperature, 540° R; static pressure, 28 inches of mercury absolute; enclosed-tunnel installation; grid: 0.125-inch wire diameter, 0.625-inch mesh.

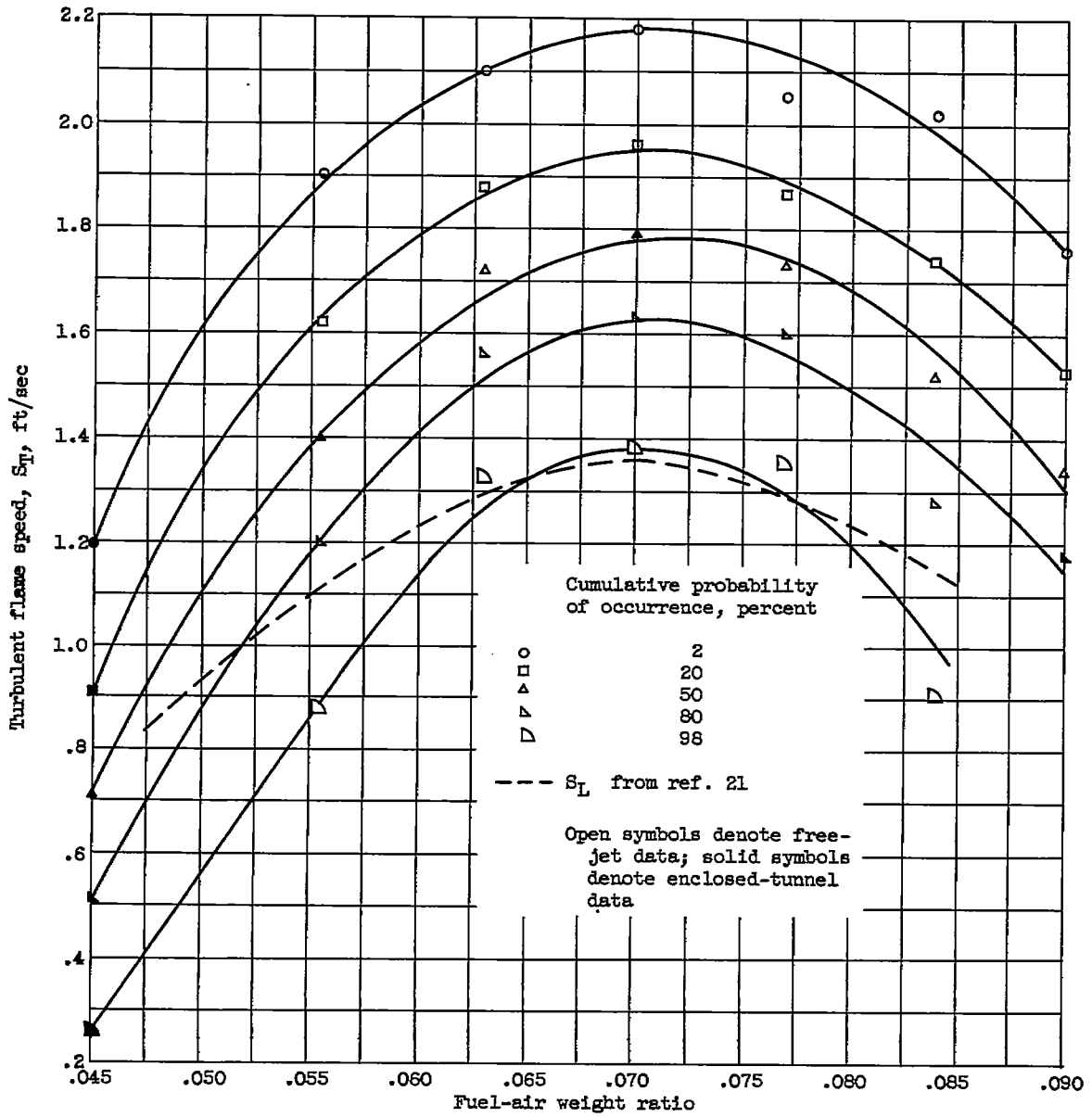

(a) Grid: 0.125-inch diameter, 0.625-inch mesh.

Figure 25. - Turbulent flame speed as function of fuel-air ratio with cumulative probability of occurrence as parameter. Mean stream velocity, 70 feet per second; stream static pressure, 1 atmosphere; static temperature, 85° F.

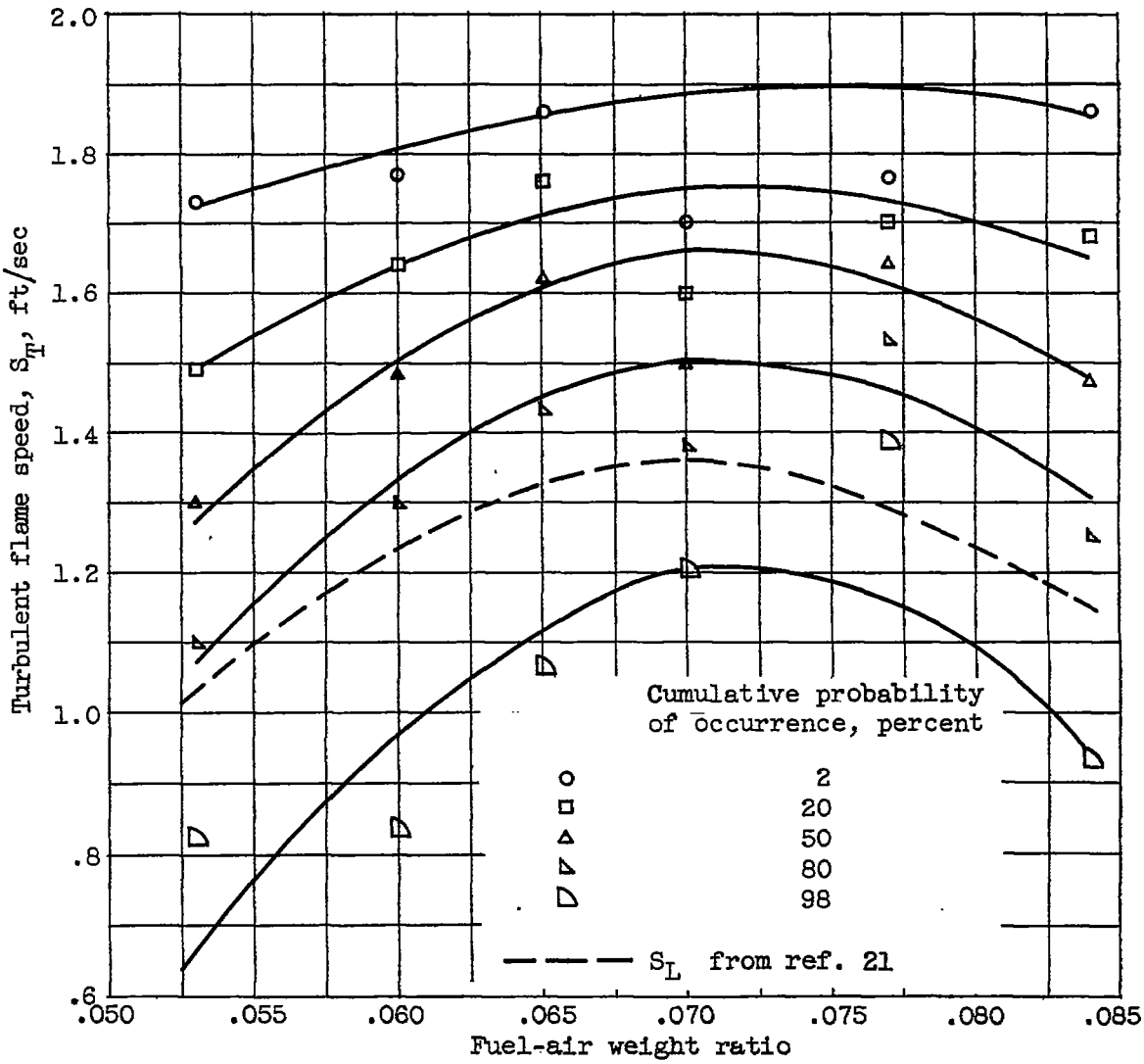

(b) Grid: 0.063-inch diameter, 0.313-inch mesh.

Figure 25. - Continued. Turbulent flame speed as function of fuel-air ratio with cumulative probability of occurrence as parameter. Mean stream velocity, 70 feet per second; stream static pressure, 1 atmosphere; static temperature, 85° F.

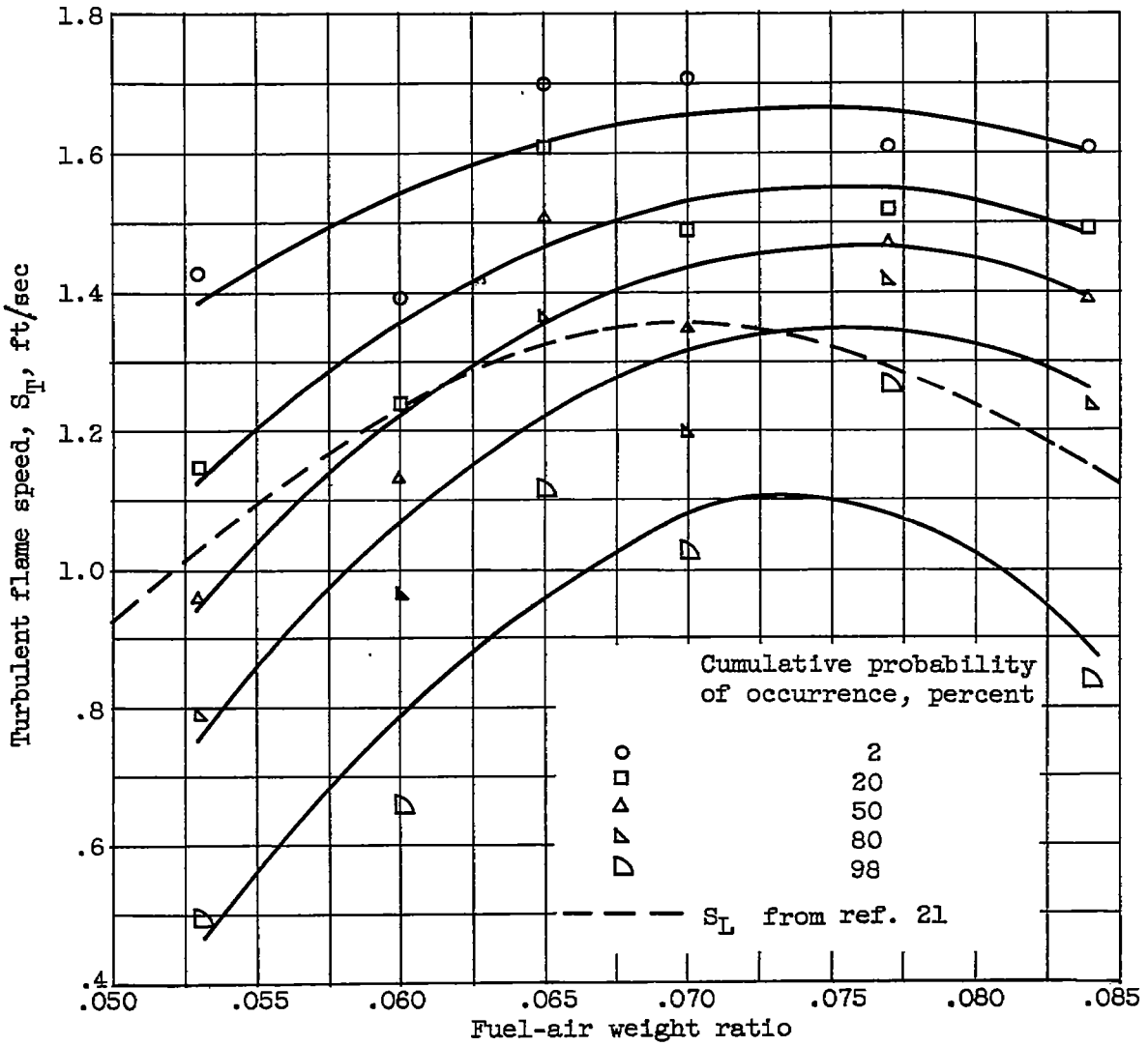

(c) Grid: 0.0313-inch diameter, 0.156-inch mesh.

Figure 25. - Concluded. Turbulent flame speed as function of fuel-air ratio with cumulative probability of occurrence as parameter. Mean stream velocity, 70 feet per second; stream static pressure, 1 atmosphere; static temperature, 85° F.

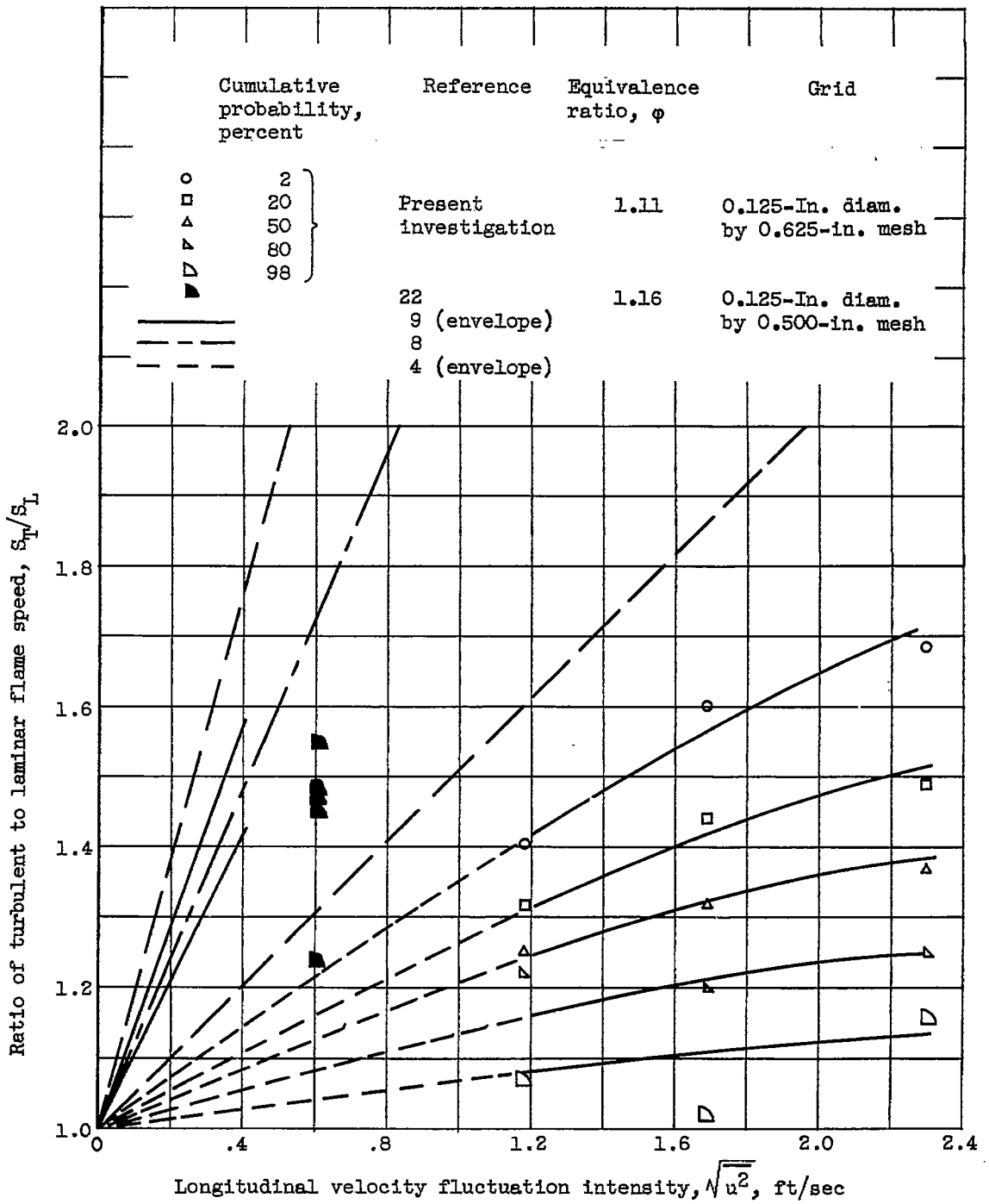

(a) Free-jet data. Propane-air ratio, 0.070.

Figure 26. - Comparison of turbulent flame-speed data with those of other investigations.

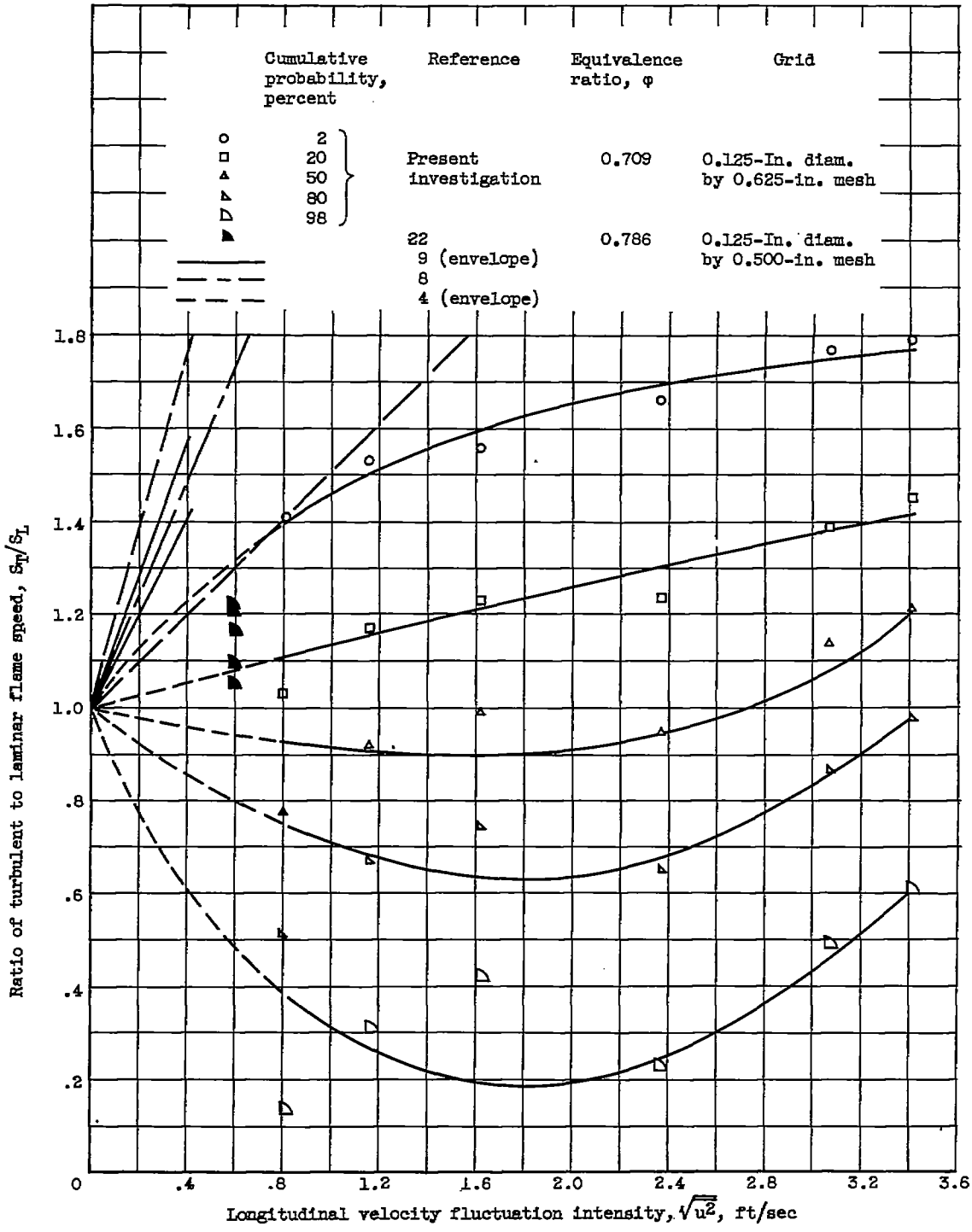

(b) Enclosed-tunnel data. Propane-air ratio, approximately 0.045.

Figure 26. - Concluded. Comparison of turbulent flame-speed data with those of other investigations.

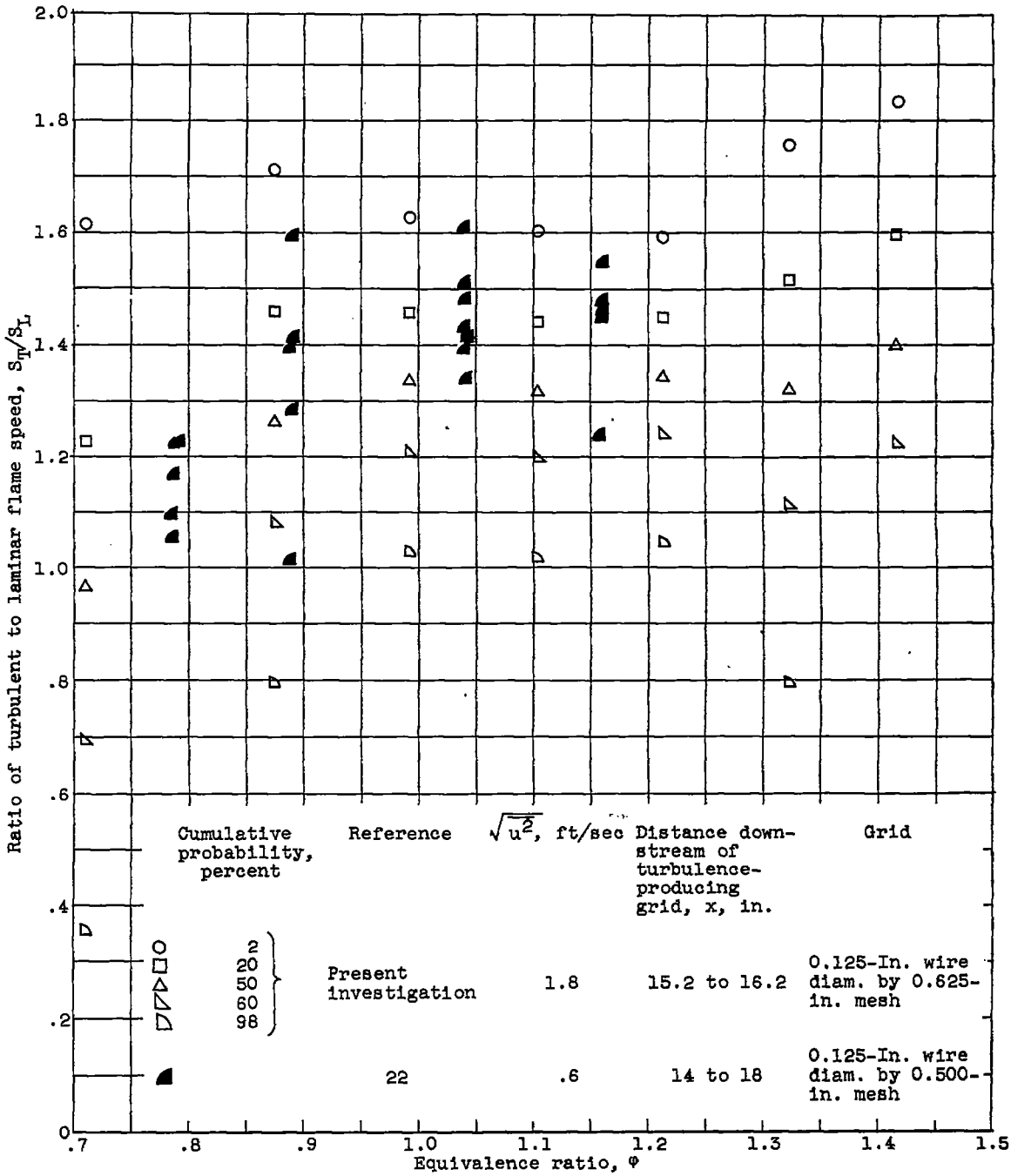

Figure 27. - Comparison of turbulent flame-speed data with those of reference 22.

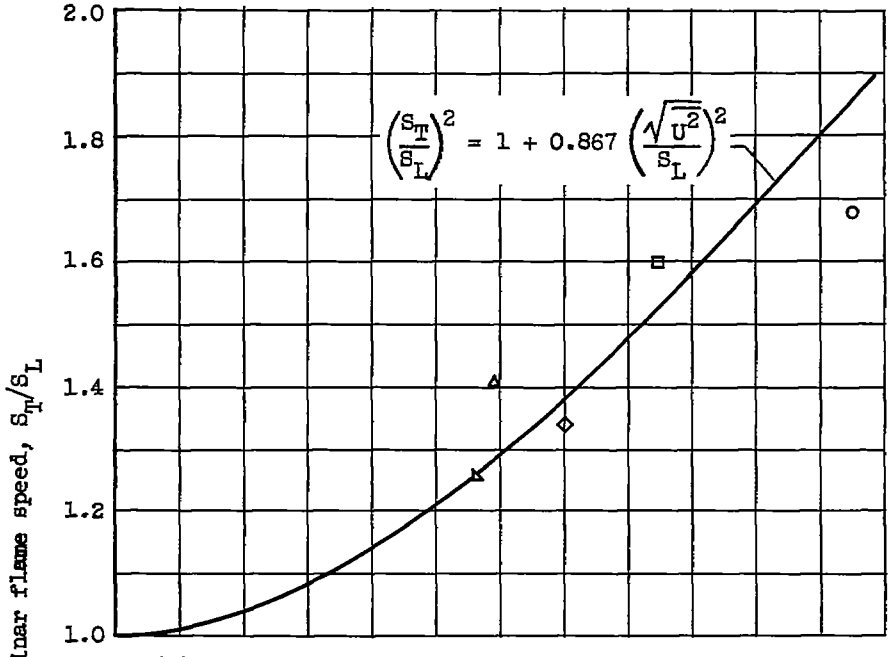

(a) Cumulative probability of occurrence, 2 percent.

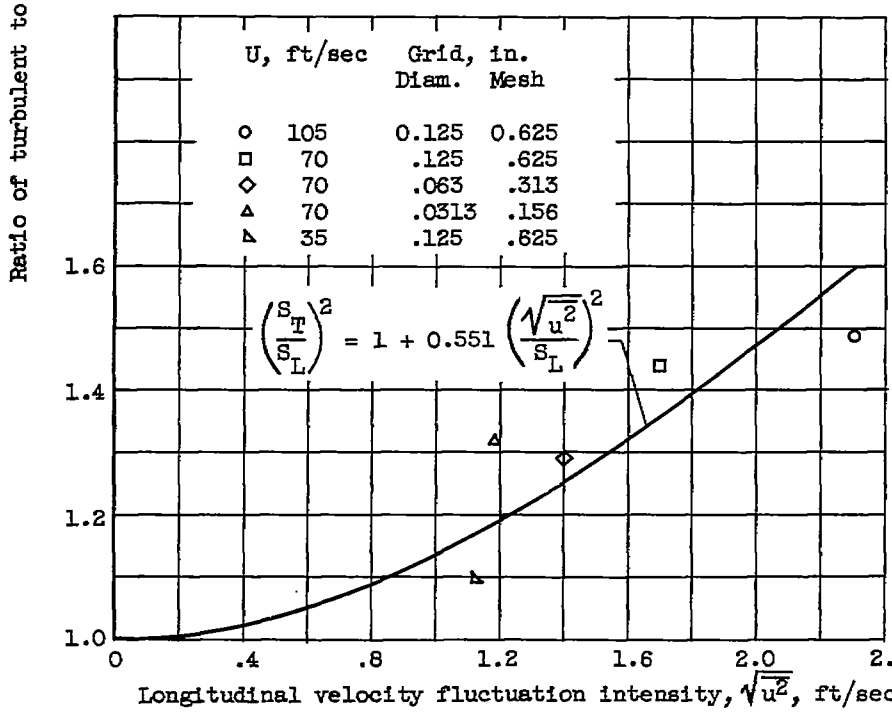

(b) Cumulative probability of occurrence, 20 percent.

Figure 28. - Comparison of turbulent flame-speed data with theory of reference 26. Fuel-air weight ratio, 0.07.

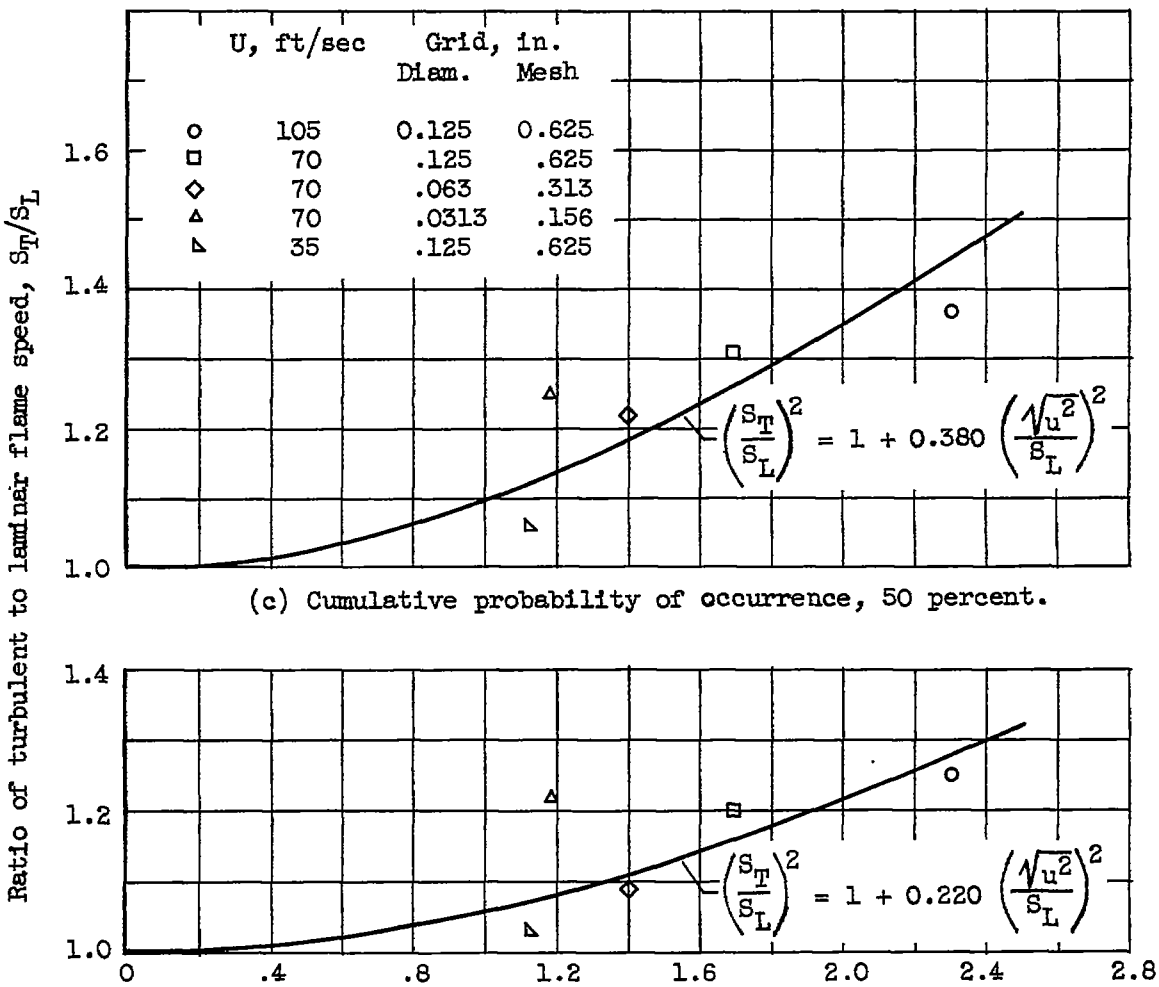

(c) Cumulative probability of occurrence, 50 percent.

(d) Cumulative probability of occurrence, 80 percent.

Figure 28. - Concluded. Comparison of turbulent flame-speed data with theory of reference 26. Fuel-air weight ratio, 0.07.

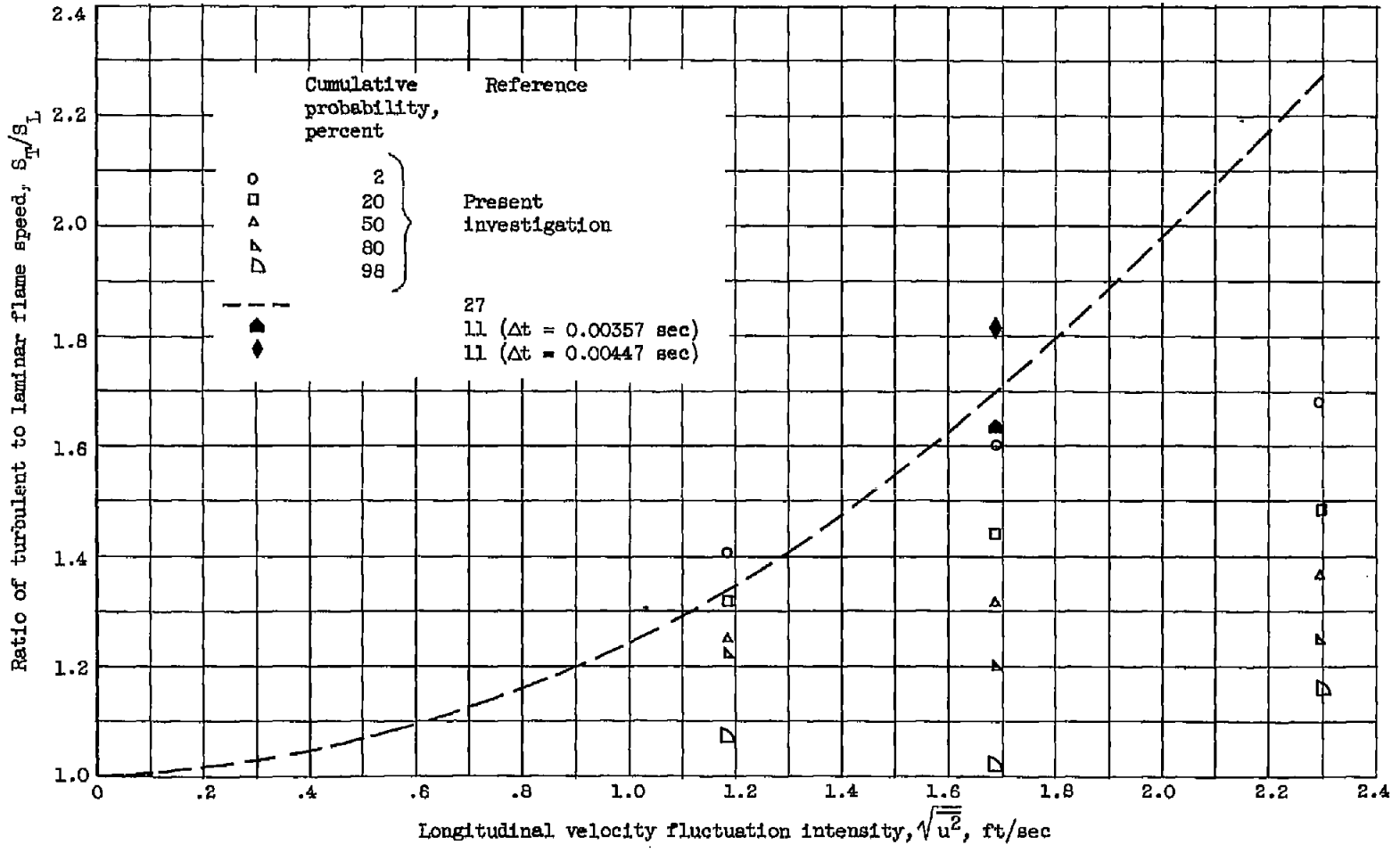

Figure 29. - Comparison of turbulent flame-speed data with theories of references 11 and 27. Propane-air weight ratio, 0.07; stream static pressure, 29.3 inches of mercury absolute; temperature, 545° R; grid: 0.125-inch wire diameter, 0.625-inch mesh.

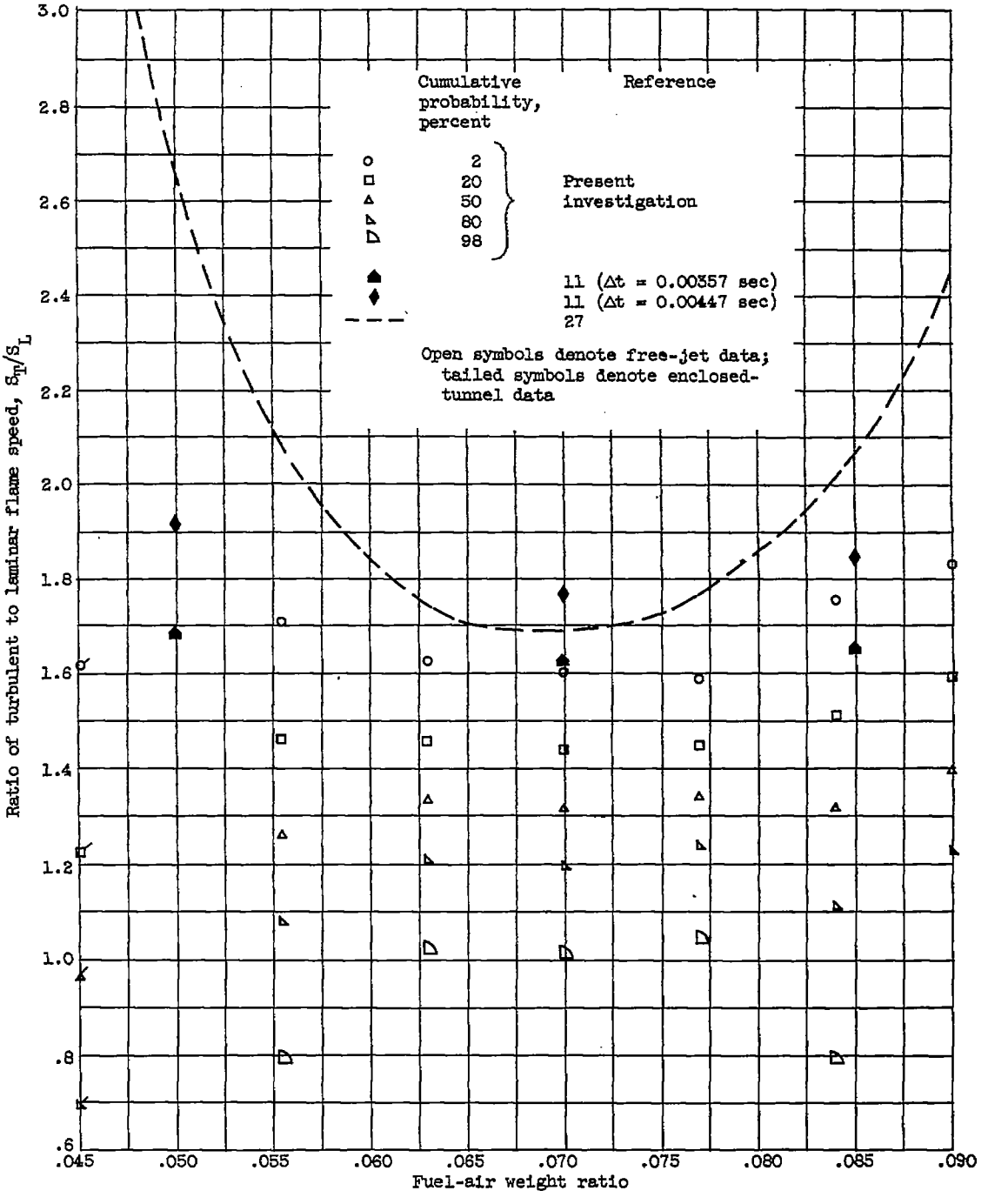

(a) Grid: 0.125-inch wire diameter, 0.625-inch mesh.

Figure 30. - Comparison of turbulent flame-speed data with theories from references 11 and 27.

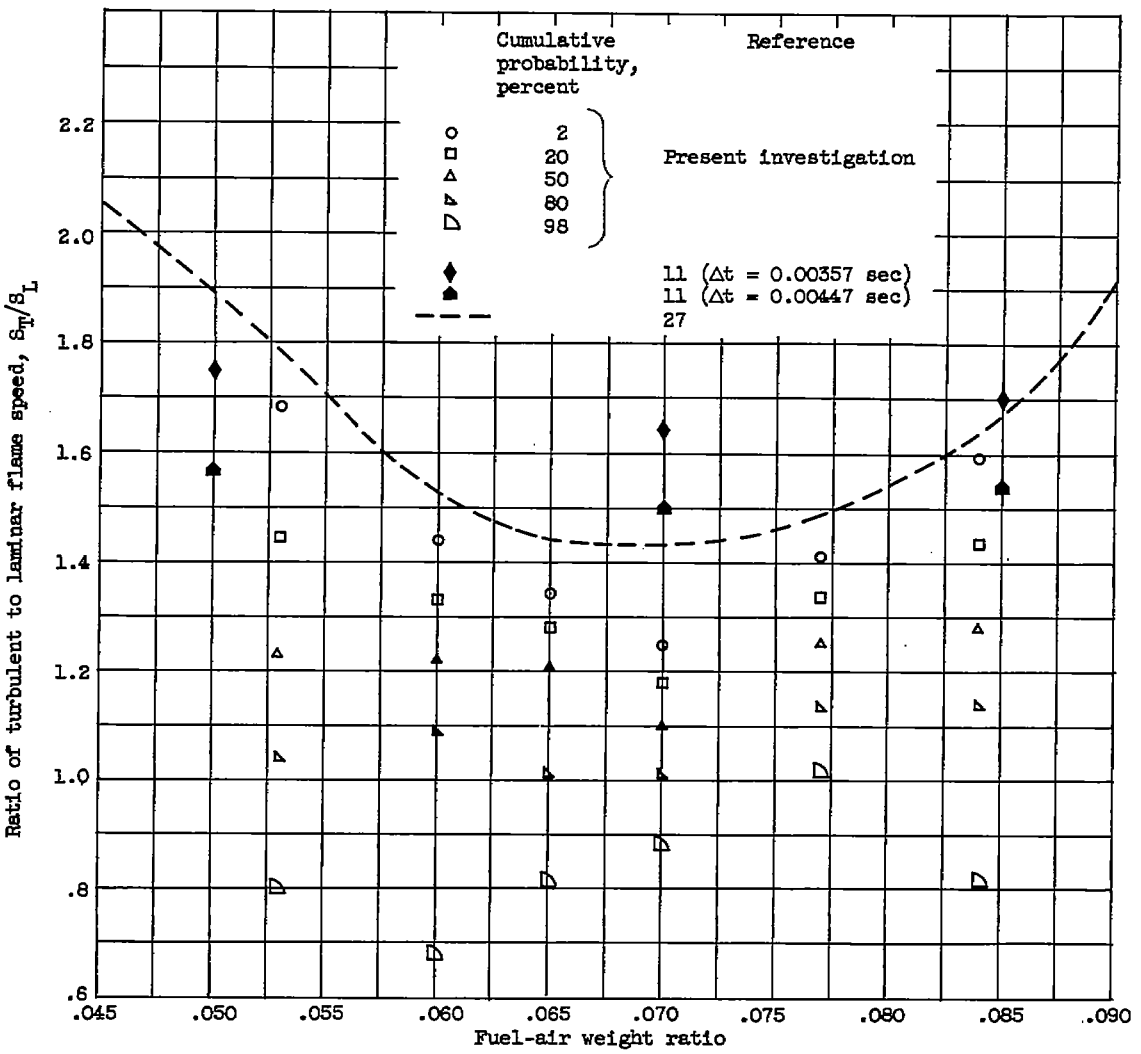

(b) Grid: 0.063-inch wire diameter, 0.313-inch mesh.

Figure 30. - Continued. Comparison of turbulent flame-speed data with theories from references 11 and 27.

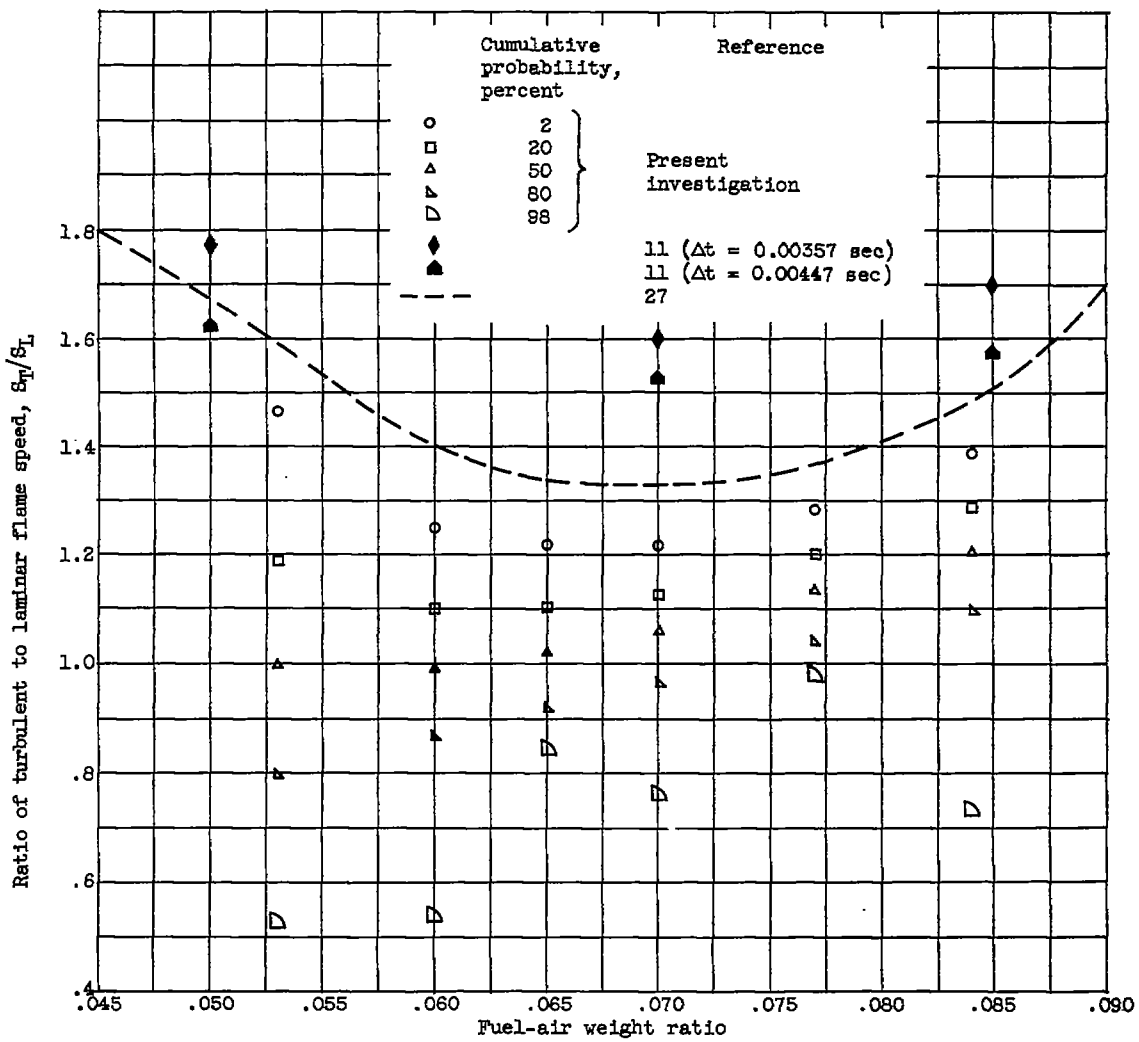

(c) Grid: 0.0313-inch wire diameter, 0.156-inch mesh.

Figure 30. - Concluded. Comparison of turbulent flame speed data with theories from references 11 and 27.

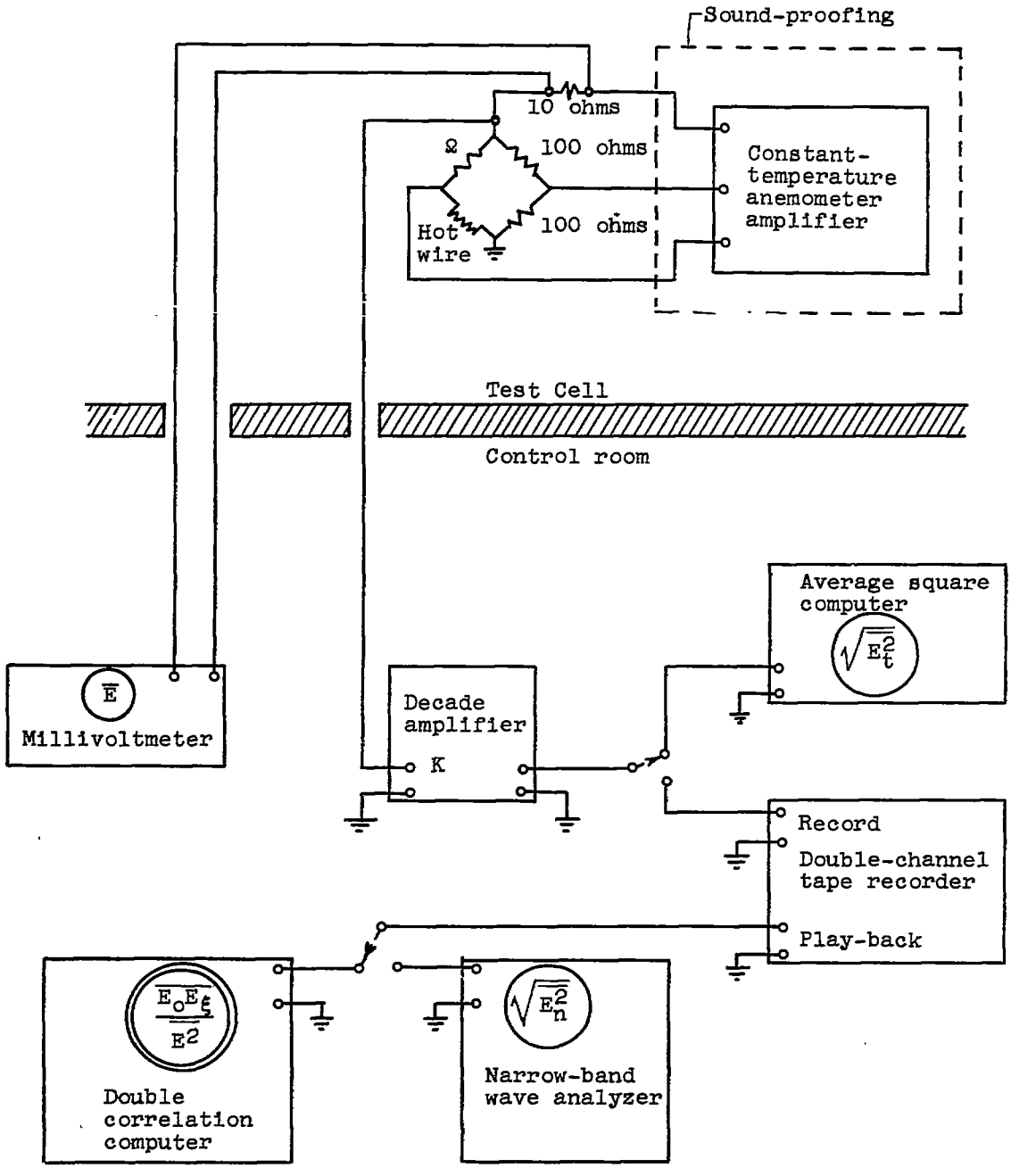

Figure 31. - Hot-wire anemometer and auxiliary instrumentation.

NACA-Langley - 7-8-55 - 1000